Development and Application of Optical Diagnostics of Alkali Vapours for Solid Fuel Combustion

Leffler, Tomas

2016

Citation for published version (APA):
Leffler, T. (2016). *Development and Application of Optical Diagnostics of Alkali Vapours for Solid Fuel Combustion*. [Doctoral Thesis (compilation), Combustion Physics]. Lund University.

Total number of authors:
1

Development and Application of Optical Diagnostics of Alkali Vapours for Solid Fuel Combustion

TOMAS LEFFLER
DEPARTMENT OF PHYSICS | FACULTY OF ENGINEERING | LUND UNIVERSITY
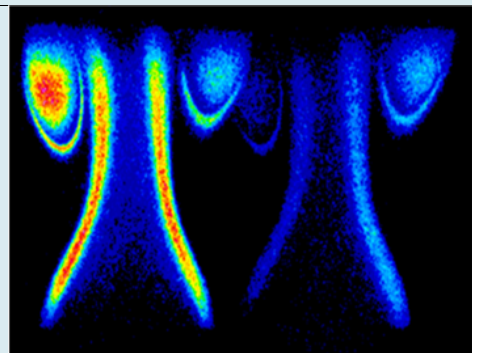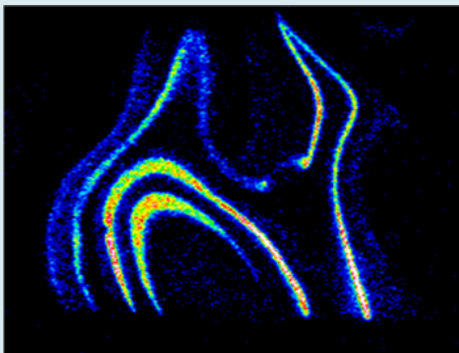
Development and Application of Optical Diagnostics of Alkali Vapours for Solid Fuel Combustion

Tomas Leffler

LUND
UNIVERSITY

Organization	Document name
LUND UNIVERSITY Division of Combustion Physics Department of Physics P. O. Box 118, SE-221 00 Lund, Swden	Doctoral disertation
	Date of issue 2016-12-02
Author(s) Tomas Leffler	Sponsoring organization

Title and subtitle
Development and Application of Optical Diagnostics of Alkali Vapours for Solid Fuel Combustion

Abstract

Background:

High amounts of alkali in the fuel, such as potassium and sodium in combination with high amounts of chlorine increase the chances of high-temperature corrosion, deposit growth and slagging and fouling. These risks need to be reduced to avoid losses in revenue due to unplanned stops and costs related to increased maintenance.

Aims:

This research targets the development of a new cell to produce calibration spectra of good quality that render accurately-determined alkali chloride concentrations. Similarly, it aims to develop new measurement techniques that can be used to determine the concentration and formation of alkali.

Methods:

UV absorption measurement on sublimated vapour from potassium chloride under well-defined conditions, which subsequently can be converted into an accurate calibration spectrum. Differential Absorption LIDAR technique adapted to measurements in the combustion environment using one optical access port. Laser-induced Photofragmentation Fluorescence imaging for formation studies of alkali compounds.

Results:

This work has resulted in a calibration cell able to provide alkali vapour of well-controlled conditions and Laser-induced Photofragmentation Fluorescence imaging set-up for the formation studies of alkali compounds. It has been shown in the laboratory environment that the Differential Absorption LIDAR technique can be used for alkali chloride measurements.

Discussion:

Prospectively the work aims at contributing to the development of more efficient combustors with low levels of emission and reduced operational problems and also increase the academic knowledge of alkali compound formation during biomass combustion.

UV Absorption Spectroscopy; Alkali Vapour Pressure; KCl; KOH; NaCl; NaOH; high-temperature corrosion; Laser-induced Photofragmentation Fluorescence; slagging; fouling; reduced maintenance cost

Classification system and/or index terms (if any)	
Supplementary bibliographical information	Language English
ISSN and key title 1102-8718	ISBN 978-91-7753-040-4
Recipient's notes	Number of pages 211	Price
	Security classification	

Development and Application of Optical Diagnostics of Alkali Vapours for Solid Fuel Combustion

Doctoral Thesis

Tomas Leffler

Division of Combustion Physics
Department of Physics

Lund, Sweden
December 2016

LUND
UNIVERSITY

Tomas Leffler
Division of Combustion Physics
Department of Physics
Lund University
P.O. Box 118
SE-221 00 Lund, Sweden

Contents

Abstract

Background:

High amounts of alkali in the fuel, such as potassium and sodium in combination with high amounts of chlorine increase the chances of high-temperature corrosion, deposit growth and slagging and fouling. These risks need to be reduced to avoid losses in revenue due to unplanned stops and costs related to increased maintenance.

Aims:

This research targets the development of a new cell to produce calibration spectra of good quality that render accurately-determined alkali chloride concentrations. Similarly, it aims to develop new measurement techniques that can be used to determine the concentration and formation of alkali.

Methods:

UV absorption measurement on sublimated vapour from potassium chloride under well-defined conditions, which subsequently can be converted into an accurate calibration spectrum. Differential Absorption Light Detection and Ranging technique adapted to measurements in the combustion environment using one optical access port. Laser-induced Photofragmentation Fluorescence imaging for formation studies of alkali compounds.

Results:

This work has resulted in a calibration cell able to provide alkali vapour of well-controlled conditions and Laser-induced Photofragmentation Fluorescence imaging set-up for the formation studies of alkali compounds. It has been shown in the laboratory environment that the Differential Absorption Light Detection and Ranging technique can be used for alkali chloride measurements.

Discussion:

Prospectively this work intends to contribute to the development of more efficient combustors with low levels of emission and reduced operational problems as well as increase the academic knowledge of alkali compound formation during biomass combustion.

About the Author

My career in the combustion field started directly after completing a University Certificate in Control and Maintenance at the Royal Institute of Technology in Stockholm, Sweden. I worked nearly 17 years at the power plant owned by Karskär Energi AB (KEAB), where I gained skills pertaining to the operation of the power plant, which consisted of the following units: a steam boiler of 540 MW_{th} (megawatt, thermal) combusting oil combined with 70 MW_{th} biomass, flue gas condensation of 20 MW_{th}, condense turbine of 125 MW_e (megawatt, electrical), back-pressure turbine of 50 MW_e, heat water boiler 120 MW_{th}, two heat pump units of 14 MW_{th} each and an electrical boiler of 40 MW_e. During my employment at the power plant I finalized my Master of Science in Applied Physics and Electrical Engineering, majoring in Measurement Technology.

Employment at Vattenfall AB as a research engineer ensued, and during the space of eight years I saw myself involved in a variety of research projects that called for different types of measurement concerning deposit growth, corrosion rates, temperatures, as well as concentrations of various flue gas components and alkali metal chlorides. The alkali measurements were carried out with a self-developed and patented instrument at Vattenfall AB. The In-situ Alkali Chloride Monitor measures alkali chlorides in the flue gas and is used in various internal and external power plants and waste incinerators. The further development of this instrument within Vattenfall AB was something that caught my interest and this is what I worked the longest with. It was when ChlorOut AB, a subsidiary company of Vattenfall AB, signed a partnership agreement with a boiler manufacturer that the idea for an industrial PhD programme was born.

The justification for undertaking this programme was two-pronged. Firstly, the inventor of the In-situ Alkali Chloride Monitor transferred to other tasks within Vattenfall AB and was no longer available in the same way as before. Secondly, despite extensive practical knowledge and field experience, I realized that my theoretical knowledge in the area was limited. This led me to contact my manager at the time, Lennart Gårdman, and the CEO of ChlorOut AB, Magnus Berg, to enquire about the possibility of taking the research of the In-situ Alkali Chloride Monitor to doctoral level.

Once the partnership agreement with the boiler manufacturer was in place, it was easier to provide a rationale for an industrial PhD programme and I felt motivated to take up

the challenge. I believe it is in my nature to accept challenges; nothing is impossible until it has been tried out. My thoughts and ideas around this PhD programme have revolved around a pivot that is academic, applied and innovative in nature.

Populärvetenskaplig sammanfattning

Energikris, tillgång på bränsle, bränslepriser, lagar och miljöpåverkan är faktorer som gjort att förbränningen i våra kraftvärmeverk har styrts om från fossila bränslen såsom olja och kol till förbränning av biomassa. Biomassa är ett vitt begrepp och kan vara allt från skogsavfall, energiskog och jordbruksavfall till industriavfall, delar av innehållet i hushållsavfall och liknande. Den ökade förbränningen av dessa biobränslen har medfört att kraftvärmeverken har fått olika typer av problem i sina anläggningar. Det kan vara allt ifrån hårda och mjuka beläggningar på värmeöverförande ytor, igensättningar och högtemperaturkorrosion på överhettare, korrosion på eldstadsväggar till sintrade bäddar i fluidbädd pannor. Många av dessa problem medför långa oplanerade driftstopp samt utbyte av eldstadsväggar och överhettare vilket medför höga kostnader. Alkaliklorider av kalium och natrium har i tidigare forskning identifierats vara orsaken till ovan nämnda problem och dessa ämnen är därför av intresse i detta arbete. Ty de utgör den bidragande orsaken till korrosion och beläggningar i pannan. För att sätta in bästa möjliga motåtgärd mot bildning av dessa kemiska ämnen är det önskvärt om dessa kan kvantifieras med lämpliga mätinstrument. Ett sådant mätinstrument, In-situ Alkali Chloride Monitor har utvecklats på Vattenfall Research and Development AB i Älvkarleby och kan nu användas för minimering av alkaliklorider. Exempelvis genom att kombinera olika typer av bränsleblandningar alternativt ge en styrsignal som kan användas vid dosering av additiv som reducerar alkaliklorider i rökgaserna och därmed reducerar problemen i anläggningen.

Målsättningen med den utförda forskningen har varit att ge den en akademisk grundläggande-, industriell tillämpad- och en innovativ prägel. Den bakomliggande orsaken till det är mina erfarenheter som forskningsingenjör på Vattenfall AB.

Den grundläggande akademiska prägeln på avhandlingen utgörs av det utvecklingsarbete som lagts ned på framtagningen av en ny kalibreringscell för mätning av kaliumklorid. Här har termodynamiska resultat som tagits fram under årens lopp av olika forskare världen över varit behjälpliga samt egna erfarenheter för att designa cellen. Jag hoppas att den utvecklade cellen och de resultat som produceras i den ska vara till gagn för andra forskare i deras strävan att föra utvecklingen vidare. Ett konkret exempel på det är den gedigna undersökning som lagts ned i detta arbete för att undersöka hur absorptionstvärsnittet för kaliumklorid beror av temperaturen. Detta är av stor vikt för

att kunna beräkna rätt kaliumklorid koncentration i en rökgas vars temperatur är i ständig förändring.

Arbetets industriella prägel karakteriseras av försök att införa förbättringar för instrumentet med redan befintlig teknik. Exempelvis ny optik i form av paraboliska speglar i stället för linser vilket medför att man undviker brytningsfel och medför mindre problem vid upplinjeringen under installation och intrimning av instrumentet. Genom försök i en forskningspanna på Chalmers Tekniska Högskola samt fullskaleförsök i en kommersiell panna har det visats att en In-situ Alkali Chloride Monitor är ett utmärkt mätinstrument för att avgöra ett bränsles benägenhet att bilda beläggningar och orsaka korrosion i en panna. I avhandlingen ges också flera exempel på hur detta instrument kan användas i olika typer av pannor vid förbränning av olika bränslemixar av biobränslen.

Den innovativa prägeln i detta arbete ges av de undersökningar som genomförts med pulsat laserljus av våglängd 193 nm för att slå sönder molekyler av kalium- och natriumklorid med samtidig excitation av de frigjorda kalium- och natriumatomerna. Detektion av ljus från de exciterade atomerna möjliggör detektion av alkaliklorider och denna metod, *Laser-induced Photofragmentation Fluorescence*, har använts vid studier i laboratorieflammor. Tekniken kan med fördel användas för att studera var formationen av kalium- och natriumklorid sker vilket är till nytta vid modellering av förbränningsprocessen. Genom att montera ett stereoskop på kameraobjektivet delas bilden med signal från alkalikloriderna upp i två lika stora delar och med lämpligt valda filter går det att detektera dessa två komponenter såsom kalium och natrium samtidigt. Det har också visats i avhandlingsarbetet att *Light Detection and Ranging* tekniken och då främst i den form som benämns *Differential Absorption Light Detection and Ranging* har potential för koncentrationsmätningar av kaliumklorid i rökgaser. Denna teknik möjliggör rumsupplöst mätning i bakåtriktningen för en utsänd laserstråle och kan med fördel användas då det bara finns en öppning tillgänglig för optiska mätningar i en panna.

List of Papers

I. **T. Leffler,** C. Brackmann, A. Ehn, B. Kaldvee, M. Aldén, M. Berg and J. Bood. *Range-resolved Detection of Potassium Chloride Using Picosecond Differential Absorption LIDAR.* **Applied Optics. 2015. 54(5): 1058-1064.**

II. **T. Leffler,** C. Brackmann, M. Berg, Z. S. Li and M. Aldén. *Online Alkali Measurement for Fuel Quality Control in Biomass-operated Boilers.* **Industrial Combustion. Journal of the International Flame Research Foundation, article number 201601, March 2016.**

III. **T. Leffler,** C. Brackmann, M. Aldén and Z. S. Li. *Laser-induced Photofragmentation Fluorescence Imaging of Alkali Compounds in Flames.* **Accepted for publication in Applied Spectroscopy.**

IV. **T. Leffler,** C. Brackmann, M. Berg, M. Aldén and Z. S. Li. *Developments of an Alkali Chloride Vapour-generating Apparatus for Calibration of Alkali-measuring Devices.* **Submitted to Review of Scientific Instruments.**

V. **T. Leffler,** C. Brackmann, W. Weng, Q. Gao, M. Aldén and Z. S., Li. *Experimental Investigations of Potassium Chemistry in Premixed Flames.* **To be Submitted to Fuel.**

Contributions to the Papers

Paper I

Paper I investigates the possibility of using the Differential Absorption Light Detection and Ranging (DIAL) technique for alkali chloride measurements that can be utilized when only one optical access is available; for example, in a boiler at a power plant. Two experimental configurations of DIAL are considered and the In-situ Alkali Chloride Monitor instrument is used as a reference instrument for the alkali measurement.

I was responsible for the construction and design of the furnace used in the combined absorption measurements with DIAL and IACM, the IACM measurements and the evaluation of the IACM data. B. Kaldvee, C. Brackmann and A. Ehn were responsible for the DIAL and double-pulse DIAL measurements and the evaluation of the data from those two measurements. J. Bood wrote the first draft based on a conference paper that was submitted to the 6th European Combustion Meeting ECM 2013 in Lund, Sweden. I took over as the corresponding author and together with C. Brackmann and A. Ehn we finalized the paper followed by revision by the co-authors.

Paper II

Paper II describes the uses of the In-situ Alkali Chloride Monitor as a tool for online fuel quality control related to alkali chlorides (such as potassium and sodium chlorides). It shows that the In-situ Alkali Chloride Monitor can be used in co-combustion to optimize the fuel mixture to minimize alkali chloride formation and induced problems with corrosion.

I was responsible for the IACM measurements, the analysis of the data and the writing of the paper, which was then reviewed by C. Brackmann and the other co-authors prior to submission. This paper was first presented at the 10th European Conference on Industrial Furnaces and Boilers in Porto, Portugal in April 2015.

Paper III

Paper III deals with measurements of alkali compounds in laboratory flames by means of absorption spectroscopy and Laser-induced Photofragmentation Fluorescence imaging. This research uses an ArF Excimer laser, which provides pulses of wavelength 193 nm, to photofragment the KCl, NaCl and KOH molecules in the flame and post-flame region of premixed laminar one-dimensional methane-air flames. Emphasis is made on the imaging capabilities of the Laser-induced Photofragmentation Fluorescence technique. In addition, the approach for quantitative concentration measurements is addressed.

I was accountable for the planning and execution of the experiments; the data was evaluated in close collaboration with C. Brackmann. I wrote the first draft of the manuscript and C. Brackmann revised it followed by revision by the remaining co-authors.

Paper IV

Paper IV describes the development, design and tests of a sealed cell for calibration of optical alkali-measuring devices –in this case, the In-situ Alkali Chloride Monitor. This configuration allows for determination of KCl absorption cross-sections under well-controlled conditions and calibration of the In-situ Alkali Chloride Monitor, which is crucial for its accurate operation.

The idea came from my supervisor, Z. S. Li. I designed and developed the calibration cell in close collaboration with Scientific-Lab Glass AB in Lund. All the laboratory tests and measurements were carried out by me and the data was evaluated in close collaboration with C. Brackmann. I wrote the manuscript with support from C. Brackmann followed by revision by the co-authors.

Paper V

Paper V investigates the flame chemistry of alkali compounds in alkali-seeded premixed laboratory flames burning methane-air mixtures at different equivalence ratios. Laser-induced Photofragmentation Fluorescence and absorption measurements are used for measurements of potassium chloride and potassium hydroxide concentrations, while diode-laser absorption spectroscopy is employed for potassium atom measurements. Rayleigh scattering is used to measure temperatures in the flame.

The experiments were planned, conducted and the data evaluation was carried out in close collaboration with C. Brackmann. Q. Gao was responsible for the diode-laser absorption measurements. C. Brackmann was responsible for writing the manuscript.

Unpublished material

The results presented in Subchapter **4.7** stem from different field measurement campaigns conducted by me. These results are exclusive to ChlorOut AB, which means that they are not available in the public domain (e.g. scientific journals).

I held responsibility for the planning and execution of the experiments, the evaluation of the data and the preparation of the related reports, all of which was checked by my supervisors at ChlorOut AB.

Related work

Paper A

T. Ekvall, K. Andersson, **T. Leffler** and M. Berg. *K-Cl-S Chemistry in Air and Oxy-Combustion Atmospheres.* **Proceedings of the Combustion Institute (2016)**

Abbreviations, Acronyms and Symbols

Alkali	Potassium (K) and sodium (Na)
BFB	Bubbling Fluidized Bed
CFB	Circulating Fluidized Bed
DIAL	Differential Absorption LIDAR
DOAS	Differential Optical Absorption Spectroscopy
ELIF	Excimer Laser Induced Fluorescence
FTIR	Fourier Transform Infrared Spectroscopy
IACM	In-situ Alkali Chloride Monitor
LIBS	Laser-induced Breakdown Spectroscopy
LIDAR	Light Detection and Ranging
LIF	Laser-induced Fluorescence
MW_{th}	Megawatt, thermal
MW_e	Megawatt, electrical
OPA	Optical Parametric Amplifier
OPG	Optical Parametric Generator
PES	Potential Energy Surface
PF	Pulverised Fuel
LI-PFF	Laser-induced Photofragmentation Fluorescence
RFG	Recycled Flue Gas
SMA	SubMiniature Version A
SNCR	Selective Non-Catalytic Reduction
Φ	Fuel-air equivalence ratio
λ	Air-fuel equivalence ratio

1 Introduction

The introduction chapter provides an overview of the background, motivation and outline of this thesis. The background subchapter briefly describes the alkali metal-related problems that can arise during the combustion of a variety of biomass fuels. The motivation subchapter details the reasons underpinning this research. Finally, the outline subchapter describes the different chapters in this thesis.

1.1 Background

Environmental issues, legislation on emissions, cost, availability and sustainable energy supply demands have increased the use of renewable biomass fuels to produce electricity and district heat in power plants [1, 2]. Renewable fuels such as herbaceous material (straw and grass), agricultural by-products (pits, shells and hulls, e.g. from almonds, olives and palm kernels), demolition wood, waste and forest residues have high contents of alkali metals and chlorine [3]. These fuels tend to form gas-phase alkali chlorides such as potassium chloride (KCl) and sodium chloride (NaCl) in the flue gas. KCl and NaCl, when formed, for example during combustion in a CFB boiler, are the main culprits of bed agglomeration, superheater corrosion and deposit formation [4-6].

The different release pathways for potassium (K), chlorine (Cl) and sulphur (S), which among others have been studied by Johansen et al. [7] during devolatilization and combustion stages and, subsequently, the char burnout stage, are the following: organic K in the fuel released as K(g) during devolatilization and combustion stages and as K(g), potassium hydroxide(g) (KOH(g)) and potassium sulphate(g) (K_2SO_4(g)) in the char burnout stage. The inorganic K (KCl(s)) is released as KCl(g) during the devolatilization and combustion stages as well as in the char burnout stage and also as K salt(g). Organic Cl is released as HCl(g) in the devolatilization and combustion stages while the inorganic Cl (metal chlorides (s)) is released as HCl(g) and metal chlorides(g) in the devolatilization and combustion stages. Inorganic as well as organic Cl are both released as metal chlorides(g) during the char burnout stage. Organic S is released as SO_2(g) in the devolatilization and combustion stages and the same applies during the char burnout

stage. Inorganic S (metal sulphates(s)) is released as $SO_2(g)$ in the devolatilization and combustion stages and as metal sulphates(g) and $SO_2(g)$ in the char burnout stage. For further details, refer to the above-mentioned authors. During biomass combustion, K forms mostly gas-phase KCl and KOH. High content of Cl favours the formation of KCl [8-11]. The alkali, chlorine and sulphur are closely linked via chemical reactions.

High-temperature corrosion, slagging and fouling decrease the operational time, and increase maintenance costs for plant owners [5]. This type of problems can be avoided with the help of an instrument that measures the gas-phase alkali chloride concentration in the flue gas [8]. Such an instrument can be used to control the injection of a sulphate-containing additive [10, 11] or in co-combustion, mixing a fuel rich in alkali and chlorine with a sulphur-containing fuel to reduce the gas-phase concentration of KCl in the flue gas [13]. Comparing additives Kassman et al. showed that the performance of ammonium sulphate was significantly better than that of elemental sulphur for suppression of alkali chloride formation [9]. The impact of co-combustion has for example been demonstrated in an investigation of the In-situ Alkali Chloride Monitor (hereafter IACM) for online fuel quality control in Paper II [12].

Initially the alkali concentration in the flue gas was determined by means of different sampling systems developed separately by British Coal [13] and the Technical Research Centre of Finland [14]. Hald [15] developed the technique further by including the total amount of chlorine. Additional research has moved towards the development of online measurement of gas-phase alkali metals such as K and sodium (Na) in the flue gas. Monkhouse [16] wrote a thorough review article on different online spectroscopic and spectrometric methods for the determination of alkali metal species in the flue gas. Especially the Excimer Laser-induced Fluorescence (ELIF) technique has been used in Circulating Fluidized Bed (CFB) boilers during coal combustion [17, 18], co-combustion with biomass [19] and in gasification [20] for measurements of KCl/KOH and NaCl/NaOH. He et al. [21] used the Laser-induced Breakdown Spectroscopy (LIBS) for quantitative measurements of Na and K released from burning coal particles during oxy-fuel conditions. Sorvajärvi et al. [22] developed the photofragmentation technique further and made it possible to measure the individual components of K, KCl and KOH. See **Figure** 1.1 for a qualitative look of the absorbance spectrum of KCl, NaCl, KOH and NaOH. This Figure also shows that KOH and NaOH interfere in the region where KCl and NaCl are being evaluated by the IACM instrument –see **Figure** **2.2**. However, as can be observed in **Figure** 1.1, at wavelength 320 nm the hydroxides present an absorption feature whereas the chlorides lack such feature.
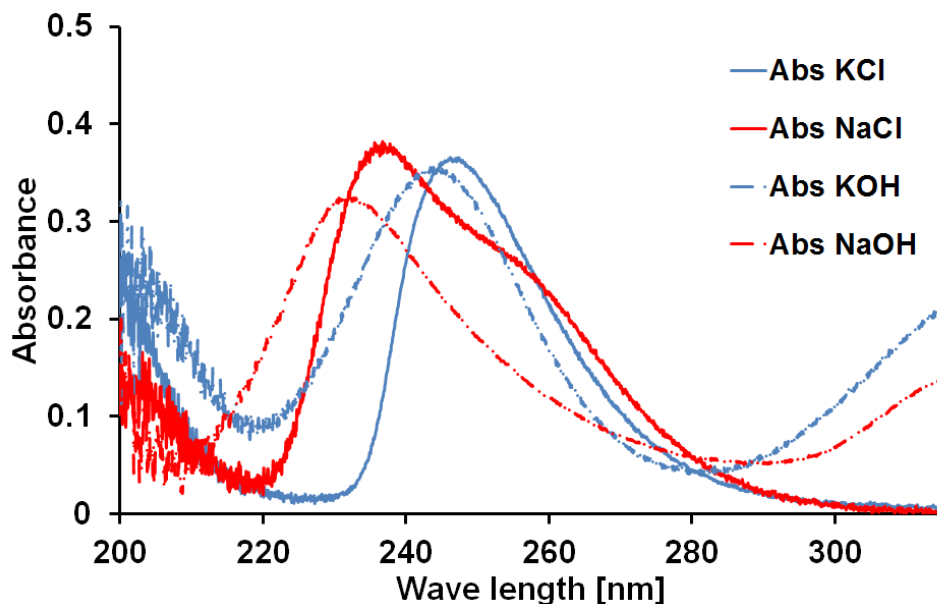
Figure 1.1. Diagram showing the qualitative look of the absorbance spectra of KCl, NaCl, KOH and NaOH.

A non-optical method worth mentioning is surface ionization (SI), which offers the possibility to measure alkali metals (K and Na) in gas-phase and on particles [23]. The Differential Optical Absorption Spectroscopy (DOAS) technique is used by the IACM [8, 24]. This instrument was developed by Christer Forsberg (former Andersson) at Vattenfall Research and Development AB to measure alkali chlorides at high temperatures in the flue gas.

This thesis is organised as follows: a fundamental part (academic), an industrial part (applied) and finally a developing part (innovative) with focus on the IACM instrument and alkali metal measurements in the flue gas. Fundamentally, this work contributes to the field with generic studies of quantitative measurements of alkali compounds in laboratory flames, which can be used to validate chemical models. It also increases fundamental knowledge on spectroscopic quantities, such as the UV absorption cross-section of KCl. Industrially, this research has taken the IACM instrument one step forward, making it more versatile and facilitating a more thorough calibration routine for KCl measurements. The removal of the spherical- and chromatic aberrations by means of parabolic mirrors, which makes the alignment procedure during installation significantly easier and the precision and accuracy of the IACM instrument much better during operation and calibration, is also a step in that direction. The developed version

has been employed for measurements of KCl in oxy-fuel combustion. The innovative part includes the development of Differential Absorption Light Detection and Ranging technique, which has been tested successfully on KCl vapours generated in a furnace in the laboratory [25]. Finally, an innovative technique for simultaneous imaging of KCl and NaCl by Laser-induced Photofragmentation Fluorescence has been developed together with an approach for quantitative concentration measurements, which allows for formation studies in flue gas.

1.2 Motivation

During the last 15 years Vattenfall AB has employed the IACM instrument in a number of biomass-firing boilers as a tool for alkali detection and in a series of research projects. These were aimed at increasing the knowledge on formation and mitigation of the effects of high-temperature corrosion, deposit growth, and slagging and fouling caused by high amounts of alkali and chlorine in the fuel. The alkali chloride measurements were carried out in a variety of boilers, such as CFB, BFB, PF and grate-fired boilers of various sizes, and during combustion of different kinds of biomass fuel, such as wood chips, agricultural by-products, waste and forest residues.

In this thesis alkali chlorides are referred to as KCl in relation to biomass combustion and as NaCl in the context of combustion of household waste. These chlorides can cause corrosion and deposits in various parts of a boiler, for example on fire walls, superheaters and economizers, and this can lead to unplanned stops. These disruptions are associated with high maintenance costs and reduced revenues for the sale of district heating and electricity for the boiler owners.

To help field professionals and researchers handle the above-mentioned challenges, a deeper understanding of the formation process of alkali compounds consisting of chlorine and sulphur is needed. This could be achieved by using an alkali-measuring device such as the IACM instrument, as it can help determine which fuel mixtures are best avoided. An additional motivation was to explore the possibilities for other alkali detection techniques.

Over the years a lot of practical experience has been amassed from work with the IACM instrument during field measurements as well as during calibration in the laboratory. All this practical knowledge and experience, which has generated ideas to improve the measurements and optimize the instrument design in favour of more accurate

measurements and enhanced calibration routines, has not only thrust forward this research but also constitutes my personal motivation.

1.3 Outline of this thesis

The Methodology Chapter describes the theory, physical phenomena and measurements techniques that underpin this research. The Equipment Chapter offers a short description of the equipment used while the different experiments were carried out. The Results Chapter highlights the outcomes and describes how and where the experiments were performed. The Results Chapter ends with a subchapter describing field measurements with the IACM instrument. The Summary, Conclusion and Outlook chapters provide a summary of the work performed, the main conclusions and the outlook of this thesis.

2 Methodology

The Methodology Chapter briefly discusses the theories and techniques behind the work carried out on alkali species detection in a furnace, laboratory flames and on KCl vapour in a calibration cell. Subchapter **2.1** describes general characteristics of light scattering and introduces the Rayleigh scattering technique used for temperature measurements in different alkali-seeded laboratory flames. Subchapter **2.2** briefly discusses the Laser-induced Photofragmentation Fluorescence technique. Subchapter **2.3** deals with absorption and explains the Beer-Lambert law, which establishes the theoretical relationships to calculate the concentration of the species of interest. Subchapter **2.3** is divided into the following subchapters: **2.3.1**, introducing the absorption characteristics of KCl; **2.3.2**, describing the DOAS technique used for line-of-sight measurements; **2.3.3**, detailing the evaluation of the KCl concentrations by means of the IACM instrument based on the DOAS technique; and **2.3.4** describes the Differential Absorption Light Detection and Ranging technique for spatially-resolved KCl measurements. Subchapter **2.4** includes three sections that calculate the vapour pressure for KCl with different methods. The first subchapter describes a method where the KCl vapour pressures from experimental data are used to fit the constants in the Antoine equation to calculate KCl vapour pressure at arbitrary temperatures. The last two subchapters deal with the Clausius-Clapeyron equation and the HSC chemistry 7.1 program for vapour pressure calculations for comparison with the analytical results given by the Antoine equation. Subchapter **2.5** introduces basic terminology and quantities related to combustion: the global reaction for stoichiometric combustion, the fuel-air equivalence ratio Φ, and the air-fuel equivalence ratio λ.

2.1 Light scattering

Scattering is a phenomenon of light interacting with matter, which can be typified into elastic and inelastic. During an elastic scattering process there is no energy exchange between the incident light and the scattering molecule or particle while the opposite occurs in an inelastic scattering process. In an inelastic scattering process, the photon energy of the scattered light may increase or decrease. An example of this type of scattering would be Raman scattering involving interaction and energy transfer with molecular vibrational and rotational levels [26]. Elastic scattering can further be divided into Rayleigh- and Mie scattering. Rayleigh scattering occurs with molecules or small particles when $d/\lambda \ll 1$ [27], where d is the particle diameter and λ is the wavelength of the incident light. Mie scattering occurs when light interacts with particulate matter when the condition $d/\lambda \ll 1$ does not hold. In this work the Rayleigh scattering has been used to measure the temperature profile in the laboratory flames. Zhao and Hiroyasu [28] review different applications using Rayleigh scattering as a diagnostic tool in combustion.

The Rayleigh [29] scattering signal, I_{Ray}, given by Eq. **(2-1)** [30] is proportional to the total gas number density, N, in the probe volume of interest.

$$I_{Ray} = E_0 \cdot C \cdot N \cdot \Omega \cdot L \cdot \left(\frac{d\sigma_{Ray}}{d\Omega}\right) \tag{2-1}$$

Where I_{Ray} is the Rayleigh signal intensity, E_0 is the laser energy, C is a calibration constant including the quantum efficiency of the detector and the optical system, Ω is the solid angle of the collection optics, L is the length of the scattering volume and $d\sigma_{Ray}/d\Omega$ is the differential Rayleigh scattering cross-section. Using Eq. **(2-1)** for measurements of a gas mixture of known composition at temperatures T_{ref} and T allows T to be determined by Eq.**(2-2)** [30].

$$\frac{T}{T_{ref}} = \frac{\sigma_{Ray}}{\sigma_{ref}} \cdot \frac{I_{ref}}{I_{Ray}} \tag{2-2}$$

The reference signal I_{ref} is often measured in N_2 or air at room temperature (see **Figure 2.1a**). This method assumes that the gas behaves as an ideal gas, which leads to the expression $T \sim 1/N$, where N is the number density [molecules/m^3] and T is the

temperature [K]. This technique has been used in this work to measure flame temperature at different equivalence ratios. **Figure 2.1b** shows the Rayleigh scattering from a methane-air flame, $\Phi = 0.9$, seeded with a trace amount of 1 M KCl liquid solution. The continuous laser sheet in **Figure 2.1a** presents an evenly-distributed temperature across the burner and its sides, which causes the molecules in the region to be evenly scattered, subsequently rendering a strong Rayleigh scattered signal. The discontinuity in the laser sheet in **Figure 2.1b** is caused by the temperature difference between the centre of the burner and its sides, which generates a low molecular density in the centre and a high molecular density at the sides. The difference in density between the centre of the burner and its sides creates a weak Rayleigh scattered signal in the centre and a strong Rayleigh scattered signal on each side of the centre of the burner. The two white arrows in **Figure 2.1b** indicate an increased scattering signal, which is caused by condensation and nucleation of KCl molecules.
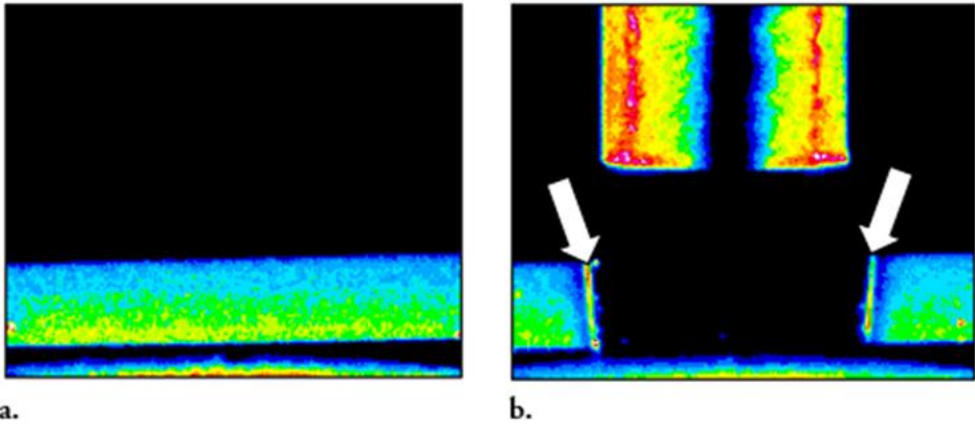

Figure 2.1a. Rayleigh scattering at room temperature. **b**. Rayleigh scattering in a methane-air flame at $\Phi = 0.9$, seeded with 1 M KCl. The scattered signal from the top part in figure b comes from the flame stabilizer located 30 mm above the burner.

2.2 Laser-induced Photofragmentation Fluorescence (LI-PFF)

Photofragmentation-Laser Induced Fluorescence is a technique that can be utilized for detection of numerous trace gases in the absence of bonding excited states in the molecule of interest to probe, which then lack fluorescence [31]. The photofragmentation-fragment detection technique is thus commonly used for analyte molecules that are not suitable for direct spectroscopic detection or for detection of classes of compounds, which share a common functionality such as -Cl, -Br, -I, $-NO_2$, $-NH_2$ and -PO, and which is targeted for detection, as per Simeonsson and Sausa [32]. The technique is based on the excitation of a molecule of interest with laser photons of sufficient energy to bring the molecule from its ground state into an unbound excited state with subsequent fragmentation into two parts due to the absorbed energy. The part that is targeted can subsequently be detected by spontaneous emitted fluorescence when the fragment is in an excited state, or actively probed by absorption [33], Laser-induced Fluorescence [34] (LIF) or Photoionization (PI) [32].

In detection of alkali compounds such as KCl, KOH, NaCl and NaOH excited alkali fragments are generated, only one laser is needed for photofragmentation, and the method is hereafter named Laser-induced Photofragmentation Fluorescence (LI-PFF). In the experiments carried out laser radiation of wavelength 193 nm generated by an ArF Excimer laser was formed into a laser sheet and focused into the probe volume to dissociate alkali compound molecules under investigation and to excite the target fragment, K or Na, leading to subsequent detection of fluorescence light. The detection system is localized near the probe volume and is perpendicular to the laser sheet. The fluorescence light emitted from fragments leaving their excited state was recorded by means of an intensified CCD camera. In this work the detection wavelengths were 766 and 589 nm, which correspond to the fluorescence light from excited K and Na, respectively. This technique has previously been characterised for gas-phase alkali chlorides by Oldenborg and Baughcum [35]. Quenching studies of fluorescence from $Na(3^2P)$ and $K(4^2P)$ atoms following photodissociation of NaCl and KCl at a wavelength of 193 nm with this technique have been made by Hartinger et al. [36]. They have also performed in-situ measurements of gas-phase Na in a fluidized bed reactor [37]. Simultaneous detection of NaCl and NaOH has been achieved by Chadwick and Domazetis [38] in a reactor simulating the condition in a coal gasification system.

2.3 Absorption

Extinction (absorption plus scattering) constitutes the physical phenomenon where light of intensity, I_0, at a specific wavelength, λ, interacts with molecules or atoms and loses a part of its intensity, which becomes I when propagating through a medium. A part of this intensity loss can be owed to elastic and inelastic scattering, as described in Subchapter **2.1**. Another part of this intensity loss results from absorption by molecules or atoms that have been brought from their ground state to an excited state. The energy difference, $\Delta E = hc/\lambda$, between the ground state and the excited state is well defined, h = Plank constant, c = speed of light and λ is the wavelength of the used light to excite the molecules or atoms of interest. This intensity loss can be transformed into absorbance by means of Beer-Lambert law, which provides a linear relationship between the absorbance and the concentration of the absorbing species of interest. Absorption has occurred once light of intensity I_0 at a species-specific wavelength has passed through a volume of length l [cm] and within that specific volume interacts with n [molecules/cm³], which have a desired absorption cross-section σ [cm²/molecules] and leaves the volume with reduced intensity I. The named variables, A, I, I_0, σ, l and n are all included in the Beer-Lambert law, which gives a linear relationship between absorbance, A and concentration –see Eq. **(2-3)**. Strong gives a theoretical basis of the law [39]:

$$A = -ln\frac{I}{I_0} = \sigma \cdot l \cdot n \qquad\qquad (2\text{-}3)$$

2.3.1   The absorption of KCl

This section presents general information about KCl absorption in the UV wavelength region used for absorption measurements by the IACM instrument, for KCl excitation during the DIAL measurements, and for KCl detection with Laser-induced Photofragmentation Fluorescence.

Figure 2.2 shows an absorbance spectrum of KCl vapour in the developed calibration cell. It can be seen that KCl has two major absorption regions: 200 – 225 nm and 230 – 300 nm. Davidovits and Brodhead [40] offer an explanation for the two absorption features shown in **Figure 2.2**. The first absorption band between 200 – 225 nm originates from the following dissociation process:

$$KCl + h\nu_2 \rightarrow K^*(^2P) + Cl(^2P_{3/2}) \qquad\qquad \text{(2-4)}$$
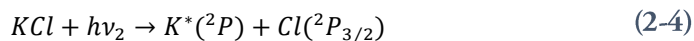
Observations of emissions from excited alkali atoms by means of UV photodissociation of the parent alkali halides was first made by Terenin [41].

The photon energy from the light source responsible for this transition is sufficient to split the KCl molecule into Cl and K atoms and subsequently excite the K atom to K* –see **Figure 2.3**. This transition is used in the LI-PFF experiments utilizing ArF Excimer laser radiation of wavelength 193 nm.

The second absorption band between 230 – 300 nm originates from the process given by Eq. **(2-5)**, where *KCl* is in its ionic $^1\Sigma^+$ ground state:

$$KCl + h\nu_1 \rightarrow K(^2S) + Cl(^2P_{3/2}) \qquad\qquad \text{(2-5)}$$
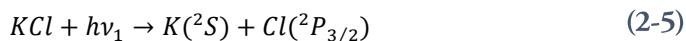
The energy from the light source in this transition is just enough to split the KCl molecule into atoms of K and Cl at ground state –see **Figure 2.3**. This transition is used by the IACM instrument.

Rather than showing fine absorption structures, the absorption spectrum in **Figure 2.2** presents only broadband structures, indicating that the KCl molecule does not have any stable excited vibrational states, only dissociative states [42] –see **Figure 2.3**. This feature is used in the LI-PFF technique described in Subchapter **2.2**, where the KCl molecule is dissociated as per Eq. **(2-4)** and the fluorescence from the excited alkali metal fragment is detected. The broadband absorption feature within the limited region between a and b (blue segment of the absorbance spectrum in **Figure 2.2**) is utilized by the IACM instrument to calculate the KCl concentration in biomass combustion. Absorption measurements performed on KCl are relying on thoroughly determined absorption cross-section, as carried out in Paper IV.

To calculate the KCl concentration by means of the DIAL technique two different excitation wavelengths are needed –off and on KCl resonance, respectively. The wavelengths λ = 235 nm was chosen to represent off resonance and λ = 247 nm was chosen to represent on resonance as indicated in **Figure 2.2** –see Paper I for details.

Further information about production, detection, thermodynamic properties, optical spectra and cross-section of alkali halide vapours is available from the text book *Alkali Halide Vapors, Structure, Spectra and Reaction Dynamics* [43].
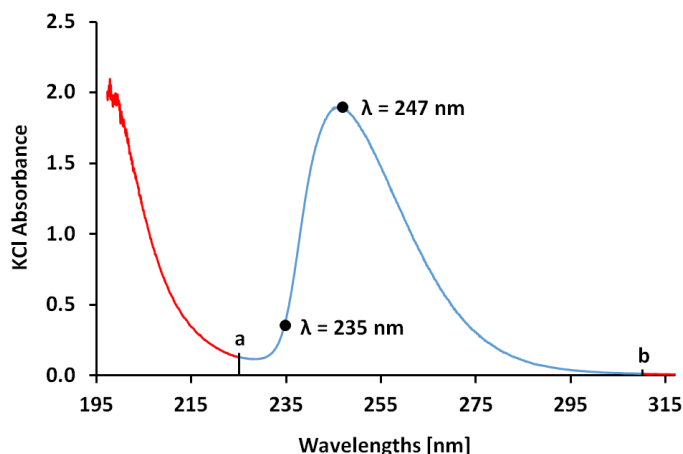
Figure 2.2. Absorbance spectrum of KCl with the excitation wavelengths, $\lambda = 235$ nm (off) and $\lambda = 247$ nm (on) for the DIAL measurements and the evaluation region, marked blue for KCl between the wavelengths, $\lambda = 225$ nm and $\lambda = 310$ nm used by the IACM instrument. The absorbance spectrum was obtained from experimental measurements.
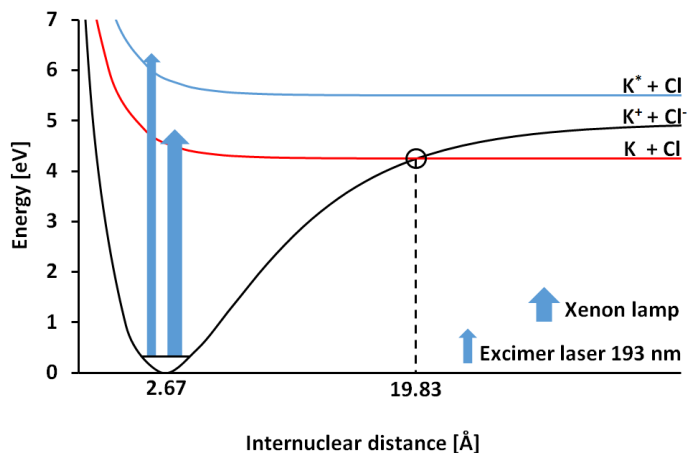
Figure 2.3. Potential Energy Surface (PES) for the KCl molecule showing bond length, energy levels and type of light sources used in the experiments.

2.3.2 Differential optical absorption spectroscopy (DOAS)

DOAS is an in-situ technique utilizing a broadband light source for line-of-sight absorption measurements in the atmosphere [44] and subsequently adapted for flue gas measurements [45-47] in a boiler. This technique was originally developed to overcome the problem with unknown light extinction from different sources, which needs to be known in order to correctly calculate the trace gas concentration of interest. This technique is based on the notion that extinction caused by Rayleigh and Mie scattering, turbulence and absorption by other trace gases, shows smooth and broad spectral features –compare I_0 with I_0' in **Figure 2.4**.
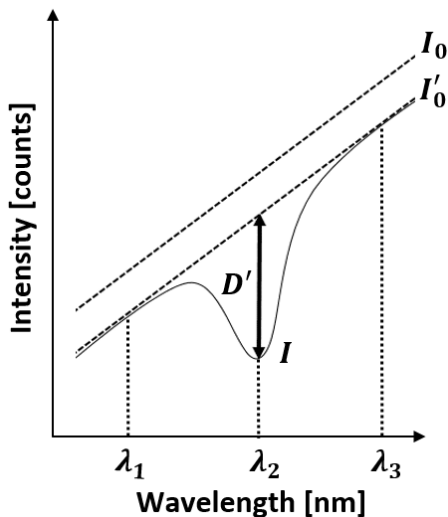
Figure 2.4. Schematic of the spectral evaluation of the DOAS technique where the differential absorbance D' is derived from the fitted low order polynomial I_0' and transmitted intensity I at resonance wavelength at λ_2.

The I_0' spectrum is a fitted low-order polynomial of degree 1 - 6 to the I spectrum where the absorption feature at λ_2 has been omitted. This technique makes it possible to make use of the Beer-Lambert law –see Eq. **(2-6)** to calculate the concentration.

$$D' = ln\frac{I_0'}{I} = \sigma' \cdot l \cdot n \tag{2-6}$$

Where D' is the differential absorbance, I is the intensity received by the detector, I_0' is the intensity of the fitted spectrum, σ' [cm^2/ molecules] is the differential absorption cross-section, l [cm] is the path length at the measuring location and n [molecules/cm^3] is the number density of the absorbing species. The name differential absorbance comes from the fact that Eq. **(2-6)** uses I_0' rather than I_0. The separation of broad- and narrowband spectral features is the key concept underpinning the DOAS technique where the fitted I_0' spectrum acts as a new reference spectrum. The interested reader is referred to the text book *Differential optical absorption spectroscopy: principles and applications* [48].

2.3.3 In-situ Alkali Chloride Monitor (IACM) measurements

This section describes the manner in which the IACM instrument determines the concentration of KCl. When installed in a combustion boiler the IACM instrument is preferably located near the superheater in a temperature region of $650 - 1000$ °C, where the measuring path length can range between $1 - 15$ m depending on the alkali and chlorine content in the fuel mixture combusted. When the IACM instrument is situated in a low-temperature region (around 700 °C) and the fuel mixture contains high amounts of alkali and chlorine, extra caution should be exercised. This is because the KCl vapour pressure at this temperature is rather low and partial condensation of KCl on cold surfaces can occur, resulting in measurement of the saturated concentration of KCl by the IACM instrument. Once an IACM instrument has been installed, it is fine-tuned to match a reference spectrum obtained in the laboratory during instrument configuration in spectral regions where no absorption occurs. The next step is to collect a background spectrum where the light from the transmitter is blocked. This is done to compensate for the electronic noise in the detector and light coming from the measuring chamber, i.e. the flue gas duct. The determination of the KCl concentration from a measured spectrum is carried out in the following way. Step one: the background spectrum is subtracted from the measured and reference spectrum –see **Figure 2.5a**. Step two: a spline is fitted to the transmittance spectrum obtained by forming the ratio between the measured and reference spectrum –see **Figure 2.5b**. Step three: the transmittance spectrum is normalized by dividing it with the fitted spline in step two – see **Figure 2.5c**. Step four: calculation of the natural logarithm of the normalized spectrum obtained in step three –see **Figure 2.5d.** Step five: a least-square fit between a calibration spectrum for KCl and the spectrum obtained in step four is carried out to

determine the KCl concentration in the flue gas –see **Figure 2.5e**. The KCl concentration is evaluated in the wavelength region 225 – 310 nm.
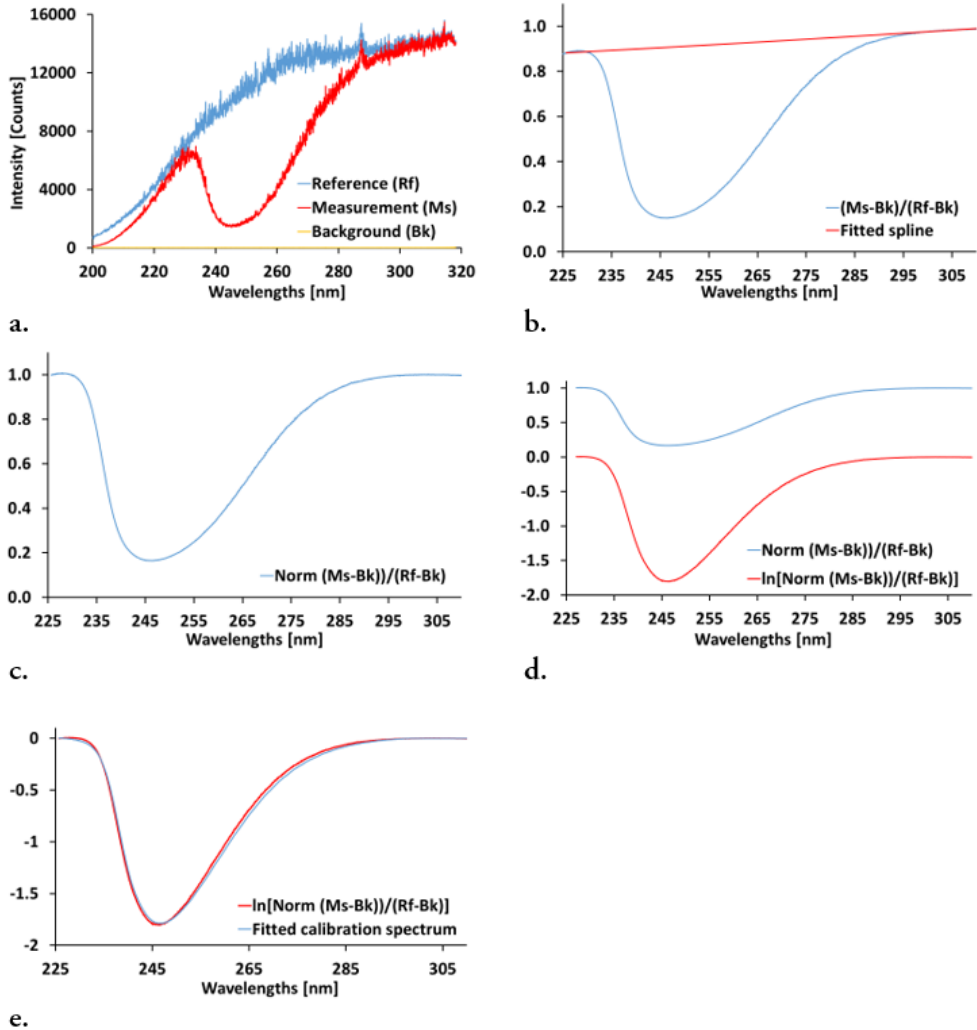
Figure 2.5. The different steps in the evaluation procedure to calculate the KCl concentration by the IACM instrument. **a**. The reference (Rf), measurement (Ms) and background (Bk) spectra. **b**. The calculated transmittance spectrum (blue) with its fitted spline (red). **c**. The transmittance spectrum normalized against its fitted spline spectrum. **d**. The normalized transmittance spectrum (blue) and the resulting natural logarithm (red). **e**. The natural logarithm of the normalized transmittance spectrum (blue) with the least square fitted KCl calibration spectrum (red) to determine the KCl concentration.

2.3.4 Differential Absorption LIDAR (DIAL)

Differential Absorption Light Detection and Ranging (DIAL) is a laser-based optical measuring technique developed for the measurement of trace gases remotely in the atmosphere. This technique has been tested together with the DOAS technique in the laboratory for KCl measurements in the context of this study. The DOAS technique provides line-of-sight measurements, which results in an average concentration over the measuring path length and requires two optically accessible ports. The DIAL technique can provide spatially-resolved measurements using only one optically accessible port. These two advantages make it a suitable candidate to become a measurement technique where only one optically accessible port is available, i.e. a flue gas duct in a power plant –see **Figure 2.6**.

The Lidar system can be built up with the following parts: a transmitter; a pulsed laser where the spatial resolution of the LIDAR measurement is determined by the pulse duration; a receiver containing collecting optics; and a detector, which could be a photomultiplier tube (PMT) or a streak camera. A LIDAR measurement is performed in the following way: short pulsed laser light is sent out from the transmitter towards the region of interest at a distance, R. The laser light interacts with the object under investigation and a part of the light is scattered in the opposite direction, collected in the optics of the receiver and subsequently registered by the detector and amplified.

The presentation of the measured LIDAR signal in the region of interest is delayed in time, t, seconds relative to the laser pulse. The time delay, t, can be calculated with the relationship $t = 2R/t$ seconds because the backscattered light needs to travel the distance $2R$ before it reaches the detector. R is the distance to the region of interest in metres and c is the speed of light in m/s. Time-resolved measurements give the spatial resolution along the laser beam, which is determined by the laser pulse duration and the temporal resolution of the detector.

The power of the backscattered signal can be calculated with Eq. **(2-7)** [49]:

$$P(R) = P_0\eta \left(\frac{A}{R^2}\right)\left(\frac{c\tau}{2}\right)\beta(R)exp\left[-2\int_0^R \alpha(r)dr\right] \qquad \text{(2-7)}$$

Where $P(R)$ is the backscattered signal from the region of interest at a distance R from the receiver. P_o is the average power of the laser pulses, η is the receiver efficiency, A is

the area of the receiving optics, R is the distance to the region of interest, c is the speed of light, τ is the laser pulse duration, β is the backscattered coefficient of the atmosphere and α is the extinction coefficient of the atmosphere at a distance R from the receiver.

The DIAL technique requires carrying out two LIDAR measurements on the backscattered light from a species of interest at a wavelength λ_{on} of larger absorption cross-section and another one at a wavelength λ_{off} of smaller absorption cross-section, thereafter taking the ratio between the strong and weak LIDAR signal. The ideal DIAL equation Eq. **(2-10)** has been derived with the following equations: Eq. **(2-7)**, Eq. **(2-8)**, Eq. **(2-9)** and two assumptions about the atmospheric coefficients for extinction, α and backscatter, β. Where the extinction coefficient, α, for both wavelengths is assumed to be entirely due to the trace gas under investigation and the backscattered coefficient, β, is assumed to be identical for both wavelengths in this simplified case. After some algebraic calculations and two assumptions about α and β the LIDAR signals with λ_{on} and λ_{off} result in the simplified relationship –see Eq. **(2-10).** The interested reader can find the details about the equations and assumptions used in this section in the book *Lidar, Range-Resolved Optical Remote Sensing of the Atmosphere* [49], where they have been sourced from.

$$\Delta\alpha = N\Delta\sigma \qquad\qquad \textbf{(2-8)}$$

$$\Delta\sigma = \sigma(\lambda_{on}) - \sigma(\lambda_{off}) \qquad\qquad \textbf{(2-9)}$$

$$N(R) = \frac{1}{2\Delta\sigma}\left[\frac{d}{dR}ln\left(\frac{P(R,\lambda_{on})}{P(R,\lambda_{off})}\right)\right] \qquad\qquad \textbf{(2-10)}$$

In Eq. **(2-10)** *N(R)* is the number density of the absorbing species of interest, $\Delta\sigma$ is the difference in absorption cross-section between λ_{on} and λ_{off} of the absorbing species of interest, R is the distance and *P(R)* is the power received from the range, R for λ_{on} and λ_{off}.

A hypothetical DIAL set-up for KCl measurements in flue gases where only one optical port is available is described in **Figure 2.6**. Since flue gas measurements are non-stationary, a double-pulse LIDAR set-up is a necessary condition to create the two DIAL wavelengths, λ_{on} and λ_{off}, on and off resonance, respectively. The hypothetical set-up can include the following components: a mode-locked picosecond Nd:YAG laser with

the fundamental radiation of 1064 nm that pumps an external amplifier, which converts the fundamental wavelength to the third harmonic wavelength of 355 nm. The third harmonic wavelength is fed to two Optical Parametric Generator/Amplifier (OPG/OPA) systems that generate the two excitation wavelengths of 247 nm and 235 nm on and off KCl resonance, respectively. These two pulsed beams are co-linearly aligned via different mirrors and separated in time before they end up in the flue gas duct. The backscattered laser light from the wavelengths 247 nm and 235 nm is collected in a spherical mirror mounted on a translation stage, which permits adjusting the focal plane on the detector. The collected light from the two different wavelengths are directed via a smaller planar mirror in front of the spherical mirror towards the detector. The signal from the detector is collected by a standard computer via a data acquisition card before the KCl concentration is calculated. More details about this set-up used in a laboratory environment can be read in Paper I [25]. This experimental set-up was used for Rayleigh temperature measurements [50] and ammonia detection [51], which are also highly relevant in a combustion context.
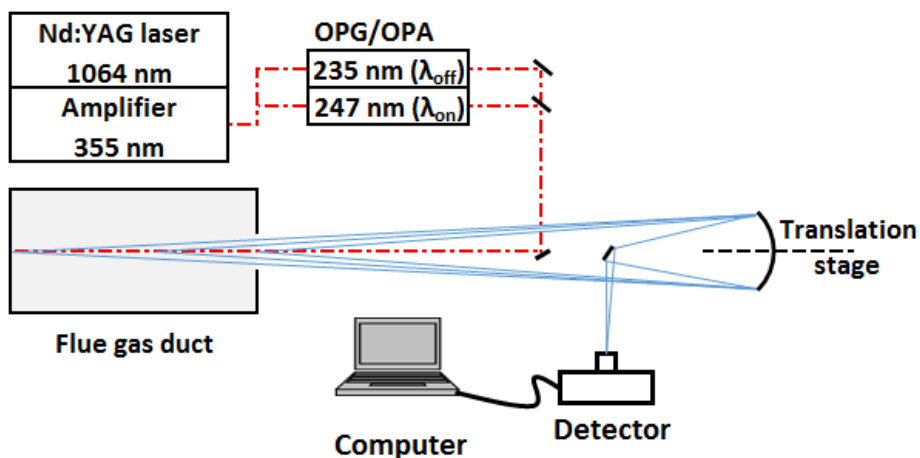

Figure 2.6. A principle schematic of a hypothetical DIAL measurement set-up configured for measurements in a flue gas duct.

2.4 Vapour Pressure of Potassium Chloride

Part of this work has been centred on the determination of KCl vapour pressures in order to obtain accurate calibration spectra in a cell. The vapour pressures of sublimated

KCl can be determined by different methods such as direct pressure measurement [52], mass-spectrometry in combination with effusion [53], pure effusion [54] and the use of different thermodynamic equations to calculate the vapour pressure [55]. Another method consists in using data from the literature, and adapting a proper equation to those data, which is what was done in this case. The experimental data selected from the literature [53] were used to determine the coefficients in the Antoine equation used for the purposes of this research. Vapour pressure calculations that were made by means of the Clausius-Clapeyron equation and the commercial software HSC Chemistry 7.1 were compared to the values calculated with the Antoine equation.

2.4.1 The Antoine equation

The Antoine equation, Eq. (2-11), was used to calculate the vapour pressure for experimental KCl temperatures investigated in this research and subsequently used to determine the KCl concentration in the calibration cell.

$$ln\, p = A - \frac{B}{C + T} \tag{2-11}$$

Where p [Pa] is the vapour pressure, T [K] is the temperature and A, B and C are coefficients specifically determined from the experimental data selected from the literature [53], optimised in Excel using the LINEST function.

2.4.2 The Clausius-Clapeyron equation

The thermodynamic Clausius-Clapeyron equation, Eq. (2-12), is an approximation where it has been assumed that the vapour volume is much larger than the solid volume, ΔH_{sub} is constant over the temperature region $569 - 766\,°C$ and the vapour behaves as an ideal gas [56]. This equation has been used to calculate different vapour pressures of KCl based on data from a best fit from the literature [54].

$$p_2 = p_1 \exp\left(-\frac{\Delta H_{sub}}{R}\left(\frac{1}{T_2} - \frac{1}{T_1}\right)\right) \tag{2-12}$$

In Eq. **(2-12)** ΔH_{sub} is the sublimation enthalpy, R is the universal gas constant, p_1 and T_1 are the pressure and temperature, respectively, at state 1, chosen from the best fit from the literature, T_2 is the temperature at state 2 and p_2 is the calculated vapour pressure at state 2.
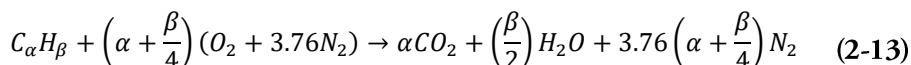
2.4.3 The HSC chemistry software

HSC chemistry 7.1 is a commercially available software from Outotec Oy in Finland. This software [55] uses 12 different databases and thermodynamic equations to calculate different properties such as vapour pressure. The vapour pressure calculations carried out for KCl in this thesis with the Antoine equation were subsequently compared with those calculated with the Clausius-Clapeyron equation and the HSC software.

2.5 Combustion Stoichiometry

A part of the experiments, specifically absorption and LI-PFF measurements, took place in a modified laboratory burner, Perkin-Elmer, normally used for atom absorption spectroscopy. The burner combusted a mix of methane (CH_4) and air (oxygen (O_2) and nitrogen (N_2)).

The global reaction equation for stoichiometric combustion of a hydrocarbon $C_\alpha H_\beta$, with air into CO_2 and H_2O as combustion products is given by Eq. **(2-13)**.

$$C_\alpha H_\beta + \left(\alpha + \frac{\beta}{4}\right)(O_2 + 3.76 N_2) \rightarrow \alpha CO_2 + \left(\frac{\beta}{2}\right)H_2O + 3.76\left(\alpha + \frac{\beta}{4}\right)N_2 \quad \textbf{(2-13)}$$

In the case of methane, CH_4, the proportions between fuel and air become 1:9.52 for a stoichiometric combustion.

The relation between fuel and oxidizer in premixed combustion is expressed using the equivalence ratio Φ, defined by Eq. **(2-14)**, which was used to calculate the proportion between CH_4 and O_2 during the different flame studies. The nominator in Eq. **(2-14)** contains the ratio between the CH_4 and O_2 to achieve the equivalence ratio of interest

while the denominator contains the ratio between the fuel and air during stoichiometric combustion as defined by Eq. **(2-13)**.

$$\Phi = \frac{\left(\frac{Fuel}{O_2}\right)_{mix}}{\left(\frac{Fuel}{O_2}\right)_{stoic}} \qquad\qquad \textbf{(2-14)}$$

A Φ value greater than 1 refers to a rich fuel mixture, or excess of fuel, whereas a Φ value less than 1 is referred to as lean fuel mixture, or deficit of fuel. An alternative parameter, which relates to the numerator, air-to-fuel ratio in Eq. **(2-14)**, to the denominator, air-to-fuel stoichiometric ratio in Eq. **(2-14)**, instead of the opposite for Φ, is the excess air quantity, designated lambda (λ), which is used by combustion engineers –see Eq. **(2-15)**.

$$\lambda = \frac{1}{\Phi} 100\% \qquad\qquad \textbf{(2-15)}$$

In a practical large-scale combustion furnace/boiler the λ value depends on the size of the fuel particles and on the type of fuel and on how it is combusted: oil and gas have a λ in the region of $1.05 - 1.1$, wood has a λ in the region of $1.2 - 1.35$, waste has a λ in the region of $1.5 - 1.6$, to mention a few [57]. Combustion is thus globally carried out at slightly lean conditions. The impact of Φ on KCl formation has been investigated in premixed CH_4-air flames and is discussed in Paper V.

3 Equipment

3.1 Lasers

Three different types of pulsed lasers (Light Amplification by Stimulated Emission of Radiation) were used to perform the experiments: an Excimer laser, a Nd:YAG laser, and a short-pulse laser system consisting of a Nd:YAG laser pumping tuneable optical parametric generator units (OPGs).

In the LI-PFF experiments an ArF Excimer laser Compex 102 from Lambda Physik was used. This is a multicomponent Excimer laser where the active medium is a mix of a rare gas [Argon (Ar), Krypton (Kr), Xenon (Xe)] and a halogen gas [Fluorine (F_2) or Chlorine (Cl_2)], depending on the desired output wavelength. In this particular case the following gas mix was used: 100 mbar, F_2 in Helium (He) (5% F_2 / 95% He mixture), 160 mbar Ar, 2340 mbar Ne (Neon) and 400 mbar He, which provided a wavelength of 193 nm and a pulse duration of 25 ns. The name Excimer comes from the **exci**ted state di**mers** of (ArF)* from which lasing occurs.

The Rayleigh scattering thermometry measurements were carried out with a Brilliant B laser from Quantel at a wavelength of 532 nm. This is a Nd:YAG (**N**eo**d**ymium : **Y**ttrium - **A**luminium - **G**arnet) solid state laser that emits at: 1064 nm and at wavelengths 532, 355, 266, and 213 nm through second, third, fourth and fifth harmonic generation, respectively. This laser is able to provide a pulse of 850 mJ at 1064 nm with a pulse duration of 4-6 ns. The second harmonic at 532 nm was employed in temperature measurements by Rayleigh scattering in flames.

The picosecond laser system [25] is built up by the following components –see **Figure 3.1**): a mode locked Nd:YAG laser with picosecond pulses that feeds an external amplifier with the radiation of 1064 nm (fundamental wavelength). The amplifier thereafter provides two Optical Parametric Generator/Amplifier (OPG/OPA), a tuneable system in the wavelength range of 219 – 2300 nm with radiation of 355 nm (third harmonic wavelength). The two wavelengths used to probe the KCl molecule on and off resonance were 247 and 235 nm, respectively –see **Figure 2.2**. Pulse energies in

the range of 0.3 – 1 mJ were used at the time the experiments were carried out. The generated pulses had a duration of 80 ps, with a repetition rate of 10 Hz and a beam width of 12 mm.
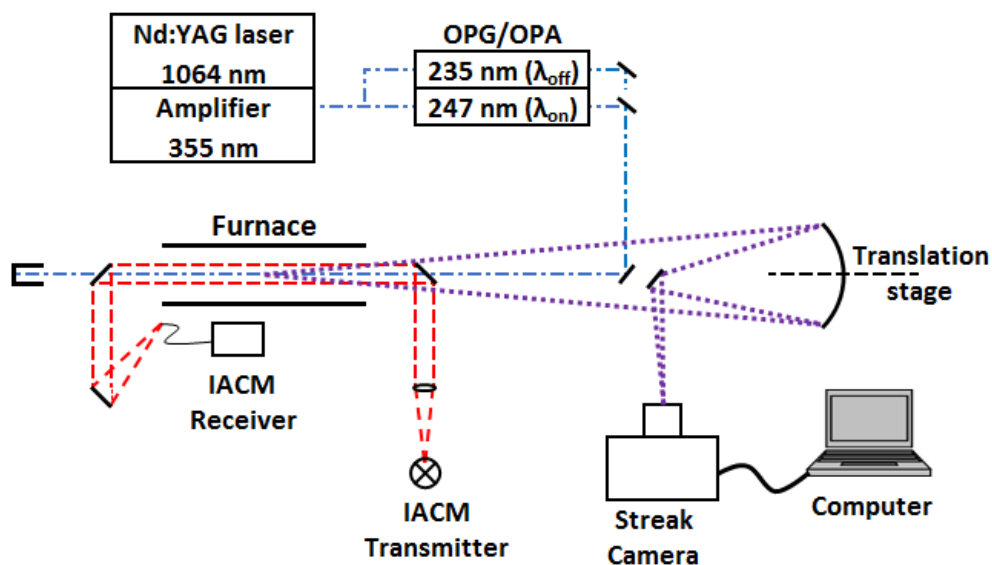

Figure 3.1. The experimental set-up for DIAL and IACM measurements used in Paper I. The blue (dashed dot) line indicates the beam path for the 235 nm λ_{off} and the 247 nm λ_{on} off and on KCl resonance, respectively used during the DIAL measurements. The red (dashed) line shows the beam path for the KCl measurements with the IACM instrument. The purple (doted) line shows the backscattered light used to determine the KCl concentration by means of DIAL measurements.

3.2 2-D Imaging

The basic principle to carry out 2-D imaging diagnostics is to create a laser sheet with the proper geometric dimensions using different optical components such as cylindrical- and spherical lenses, which are focused into the probe volume. The signal obtained from the species of interest is collected perpendicular to the focused laser sheet in the probe volume through the collecting optics of the camera and recorded on a 2-D Charge Coupled Device (CCD) chip. The collected signal could be light scattered from molecules, Rayleigh scattering, or fluorescence from photofragmented molecules. In this work Laser-induced Photofragmentation Fluorescence- and Rayleigh temperature measurements were carried out on alkali metal species in laboratory flames at different

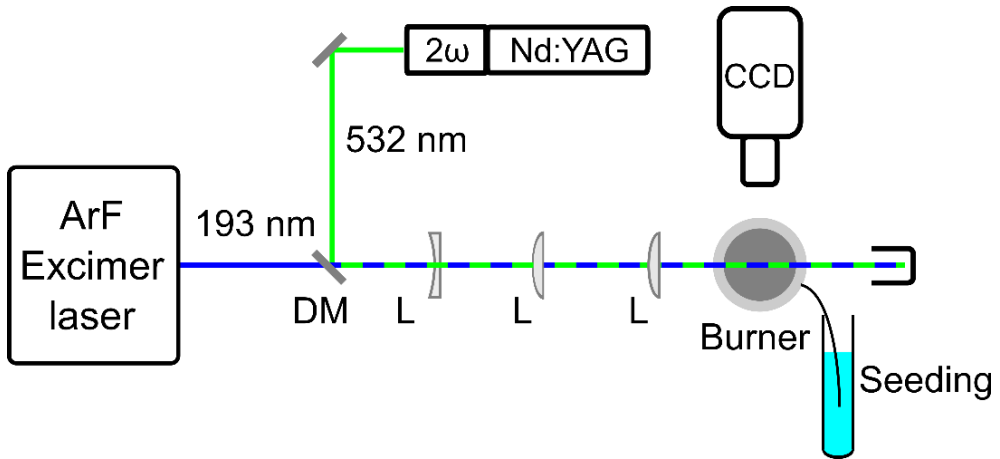equivalence ratios and the arrangement for these experiments is shown schematically in **Figure 3.2.**

Figure 3.2. Experimental set-up for 2D Laser-induced Photofragmentation Fluorescence and Rayleigh scattering thermometry measurements where DM is a dichroic mirror and the first L is a concave lens and the other two L are plano-convex lenses.

3.3 IACM instrument

3.3.1 Operation principle and set-up

The IACM instrument [8] is an alkali-measuring device developed at Vattenfall Research and Development AB and patented in different European countries [24]. This optical instrument utilizes broadband UV light to measure the sum of alkali chlorides, KCl and NaCl, in flue gas. The alkali concentration is determined with the DOAS technique, where the Bear-Lambert law provides a linear relationship between the absorbance and the concentration –see Subchapter **2.3**. It also has an additional feature: the possibility to measure sulphur dioxide (SO_2), which has absorption in the spectral region 290 – 310 nm. When the instrument is utilized in pure biomass combustion the alkali chlorides are represented as KCl and when it is used in combustion of municipal waste the alkali chlorides are represented as NaCl [8, 12]. When the fuel mixture contains both K, Na and Cl the alkali chlorides are represented as the sum of KCl and NaCl. This instrument has been used both in measurements carried out in the field and in laboratory conditions. The IACM instrument includes the following parts (see **Figure**

3.3): UV light from a broadband source is collimated through a plano-convex fused silica lens. The collimated light is transmitted through a measuring volume, i.e. a flue gas duct or a calibration cell, and reflected in a spherical mirror of enhanced alumina coating on the opposite side. The reflected light is projected onto the end of the optical fibre mounted in a fibre holder and subsequently guided through the optical fibre to the other end, where a spectrometer is connected. The data from the spectrometer is transmitted via Bluetooth connection to a standard computer for evaluation.
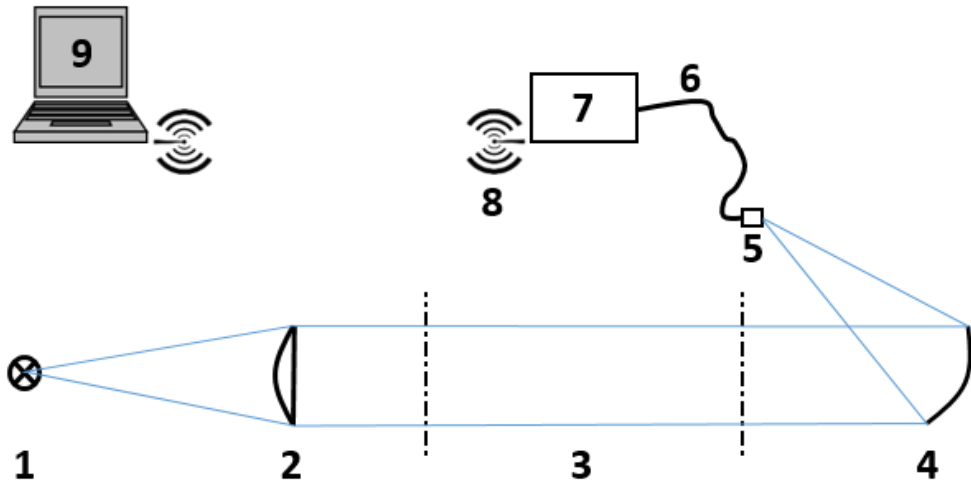

Figure 3.3. The IACM instrument optical set-up. **1**. broad band light source, high pressure xenon lamp; **2**. plano-convex UV grade fused silica lens; **3**. measurement region i.e. flue gas duct or calibration cell; **4**. collecting spherical mirror of enhanced alumina coating; **5**. fibre holder; **6**. optical fibre; **7**. spectrometer; **8**. Bluetooth connection; and **9**. computer.

3.3.2   New optical set-up

An earlier version of the IACM instrument uses a lens to collimate the broadband UV light that is radiated from the xenon lamp and traverses the measuring region. The transmitted light is focused onto a spherical mirror and projected onto an optical fibre, which guides the transmitted light to a spectrometer. The lens and the spherical mirror in the IACM optical system will give rise to at least two types of aberrations: spherical (lens and mirror) and chromatic (lens). This can affect the performance and the alignment procedure during the installation of the IACM instrument. Spherical aberration is the phenomenon where light from the outer part of the lens or mirror is focused in a different point than that from the central part of the lens or mirror, which is close to the optical axis [58]. From a practical point of view this means that a small

bending, which could be caused by thermal expansion, can affect the alignment and subsequently the shape of the spectrum. This change in the spectrum can affect the evaluation of the KCl concentration and finally lead to a need to realign the IACM instrument. Chromatic aberration occurs when a lens has different refractive indices for different wavelengths. As a result of this, short wavelengths have their focus closer to the lens than longer wavelengths. This introduces an additional factor affecting the shape of the spectrum. The spherical- and chromatic aberrations can be removed by replacing the lens with a parabolic mirror, where the light source is placed in the focal point of the parabolic mirror and the collecting spherical mirror is replaced with a parabolic mirror. This improves and makes the IACM alignment procedure much more robust, resulting in more reliable measurements in the field and in the laboratory during calibration. In this new optical set-up, the xenon lamp has been replaced with a deuterium lamp to increase the intensity of the radiated light at shorter wavelengths. The new optical set-up includes the following parts (see **Figure 3.4**): The UV light from the deuterium lamp (1) is transmitted through an aperture (2) and collimated by a parabolic mirror (3). The collimated light passes through a second aperture (4) before it is transmitted through a measuring volume, i.e. a flue gas duct or a calibration cell (5) and is collected in a parabolic collimator (6) with a SubMiniature version A (SMA) connector for an optical fibre. The collected light is guided via the optical fibre (7) to the spectrometer (8). The data from the spectrometer is transmitted via Bluetooth connection (9) to a standard computer (10) for evaluation.
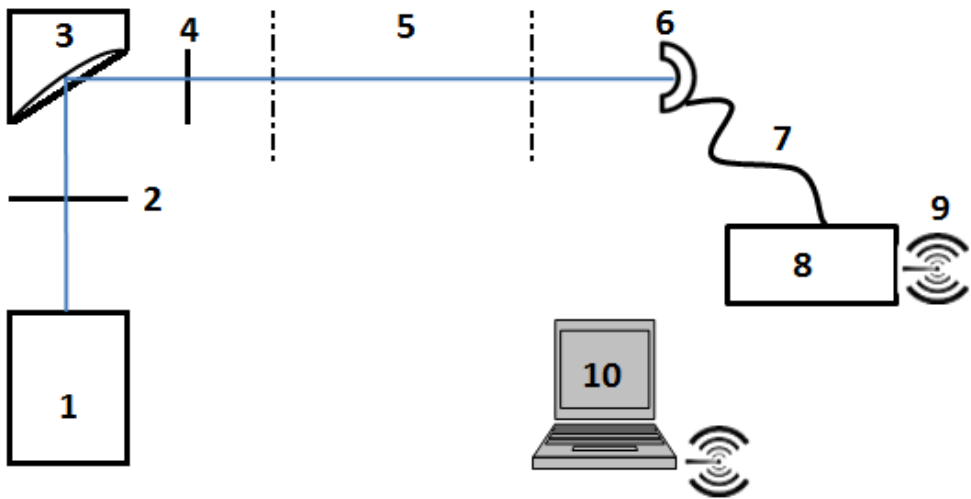

Figure 3.4. The IACM instrument with the new optical set-up. **1**. deuterium lamp; **2**. aperture; **3**. parabolic mirror; **4**. aperture; **5**. measuring place, i.e. flue gas duct or calibration cell; **6**. parabolic collimator with SMA connector for the optical fibre; **7**. optical fibre; **8**. spectrometer; **9**. Bluetooth communication unit **10**. Computer.
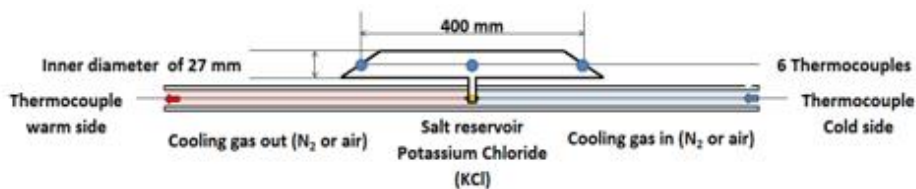
3.4 Calibration cell

One part of this thesis focuses on investigating the possibility to develop a new calibration cell for KCl concentration measurements utilizing the cold finger principle –see **Figure 3.5a** and **b**. From the outset in 2011 and up to the time of writing, various versions of the calibration cell were tested in laboratory conditions. The different development stages are visualized in Appendix A. During the development phase, conducted in close collaboration with Scientific Lab Glass in Lund AB, the calibration cell underwent several major changes. The first amendment involved using a furnace instead of a heating coil that was wrapped around the cell. This increased the homogeneity of the temperature over the measuring path length in the cell. A further improvement was made regarding the location and size of the salt reservoir, which was found to be either close to or far away from the cell centre. The cell length was also considered for betterment, and was extended from 200 mm to 400 mm to increase the absorption. Finally, improvements on how to control the salt reservoir temperature and subsequently the KCl vapour pressure in the cell were achieved. Three methods were tested: the first one used the heat from the furnace, the second one used a separate heat coil and the third one used a combination of heat from the furnace and air cooling. The last method proved to be the best one as it offered the advantage of keeping the measuring chamber and the salt reservoir at different temperatures.

The calibration cell was built up of a quartz tube with an outer and inner diameter of 30 and 27 mm, respectively. The ends of the quartz tube were cut at an angle of 45 degrees with a window made of quartz (SILUX® 3) fused at each end. The calibration cell has a length of 400 mm at its central line. A salt reservoir, containing around 2 g of crystalline KCl (EMSURE®, 1.04936.0500), was fused together with the calibration cell in the central part of the cell. The sealing of the calibration cell was carried out in the following two steps: in step one the pressure in the cell was brought down to a vacuum ($1.33 \cdot 10^{-4}$ Pa). In step two the calibration cell was filled with argon to a pressure of 100 Pa at room temperature before it was sealed.

The implementation of temperature control of the salt reservoir was made in the following way: two quartz tubes were used to form a double-jacket tube structure, which was fused together with the salt reservoir to achieve a well-controlled cooling and in such a way that the reservoir would be in the central position in the middle of the calibration cell –see **Figure 3.5a**. To keep the calibration cell in a centred and stable position in the middle of the furnace, three supporting legs were fused to the calibration cell –see **Figure 3.5b**. This design of the calibration cell enables a salt reservoir with precise and stable temperature control and subsequently a stable KCl concentration in the measuring chamber, which can be set on a preferred calibration temperature.

The thermocouples mounted on the calibration cell were calibrated before the absorption measurements took place. A calibrated thermocouple type K, with a length of 500 mm and a diameter of 3 mm and a handheld device (Pronto) to read the temperature was used.
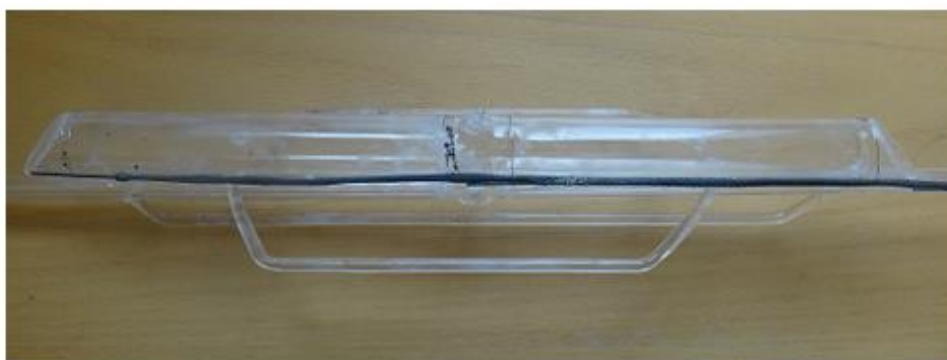
Figure 3.5a. A detailed sketch of the calibration cell. **b**. A photo of the calibration cell with its thermocouples for cell temperature measurement and temperature control of the cell temperature.

3.5 Furnace

In the initial design stage and during the development phase of the calibration cell there was no need for a furnace to carry out the experiment. The calibration cell was heated by a heating coil wrapped around the cell body. Thereafter, once it was decided to increase the cell length, and due to inhomogeneity in the temperature profile across the cell length, a commercial T-tube furnace was used. Results from the experiments performed on the calibration cell in the T-shaped furnace indicated that the furnace had an inhomogeneity in the temperature profile. A temperature survey over the distance

occupied by the calibration cell revealed a temperature difference of about 100 °C, which was deemed to be unsuitable. This would result in non-uniform distribution and condensation of KCl in the measuring chamber. As previously mentioned, the lowest temperature sets the vapour pressure and, subsequently, the KCl concentration. The worst-case scenario occurs when the salt reservoir temperature is higher than that in some local point in the measuring chamber because then KCl is transferred from the salt reservoir to the colder point and condensates in the measuring chamber. The reason for the temperature inhomogeneity was related to the way the heating elements were placed around the T-shaped ceramic pipe of the furnace. Therefore, it was decided to change the design for cell heating. It was also found that the lead time to heat up and cool down the furnace ceramic tube of alumina oxide could be decreased dramatically using a quartz tube instead. The first version of the newly-designed furnace had three heat spirals of wounded Kanthal D metal wires, placed parallel along the quartz tube surface and separated by 120 degrees. Each heating spiral was controlled manually by means of a variable transformer, which allowed to set the temperature. Unfortunately, after a long time and substantial testing of the furnace performance even this design had to be discarded due to inhomogeneity in the temperature profile. A temperature survey revealed a temperature difference of about 50 °C, which was still unsuitable. The temperature across the cell length should be homogeneous to achieve a constant KCl vapour density in the measuring chamber and, subsequently, a linear increase of the KCl concentration with increased path length, enabling the direct use of the Beer-Lambert law to attain a reliable calibration spectrum. Failing this, a non-linear relationship would be achieved where colder parts would render a higher concentration than warmer parts, with increased path length. The lowest cell temperature sets the upper limit on the salt reservoir temperature. It is important to maintain the salt reservoir as the coldest point of the system, otherwise unwanted condensation of KCl will occur at locations colder than the salt reservoir. The placement of the heating spirals was changed in the second version of the furnace design. Instead of being placed parallel along the quartz tube surface they were wrapped around the quartz tube, creating three independently-controlled heating zones. The two furnaces designs are shown in Appendix B.

The second version of the furnace was built with a 669.8 mm long quartz tube with an outer and inner diameter of 106 and 100 mm, respectively. The heating element was made of Kanthal D wire, which was cut from a cable reel in three pieces with an equal length of 15 m and a diameter of 1 mm. This type of wire has a resistivity of 1.733 Ω/m, resulting in a total resistance of 26 Ω in each heating element. This design gave the furnace a total power of 6 kW (3x2 kW) when 230 V is applied. The heating element

was made by manually winding the wires one by one around a steel rod to form spring-like elements. A stainless steel pipe was connected at the end of each heating element to make a low-ohmic contact between the heating element and the wires of the power supply. The three heating elements were wound and evenly distributed around the quartz tube to form three independent temperature-controlled heating zones –see **Figure 3.6a**. In addition, a 100 mm thick insulating layer of durablanket (Fiberfrax) was wound around the quartz tube and its heating elements. **Figure 3.6b** shows the location of the calibration cell in the furnace with its heating elements. The furnace is further insulated with 50 mm thick building blocks of duraboard (Fiberfrax) forming a box with the following dimensions: 750×400×400 mm (length, width and height) –see **Figure 3.6c**. To control the furnace temperature a device was built with the following components: three current indicators; three power controllers; three solid-state relays; three PID temperature controllers; three fuses; three-phase residual-current devices; and a safety switch –see **Figure 3.6d.** The power controllers functioned as current limiters to the heating elements since the solid-state relay works on an on-off basis. **Figure 3.7** shows a schematic drawing of the furnace with its temperature control unit and the calibration cell placed in the furnace.
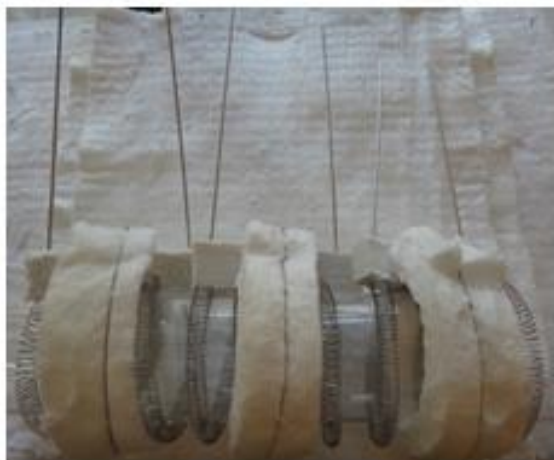
Figure 3.6a. The heating elements wounded around the quartz tube. **b**. Calibration cell in the furnace. **c**. Front view of the furnace. **d**. Furnace temperature control unit.
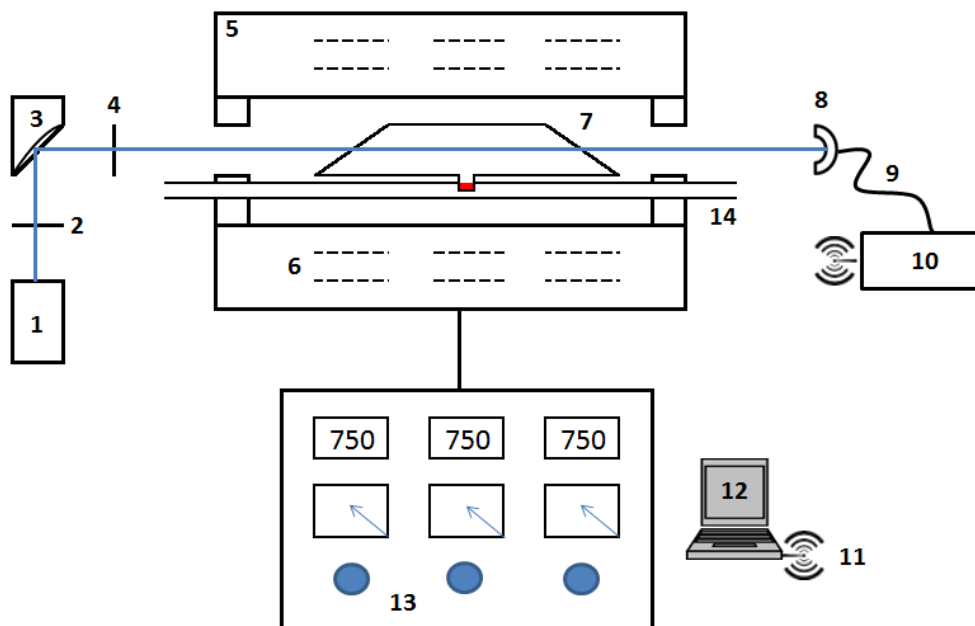
Figure 3.7. Experimental set-up for KCl measurements in the calibration cell. **1**. UV light source (deuterium lamp); **2**. Aperture; **3**. Parabolic mirror; **4**. Aperture; **5**. Furnace; **6**. Heating zone; **7**. Calibration cell; **8**. Parabolic collimator with SMA connector for the optical fibre; **9**. Optical fibre; **10**. Spectrometer; **11**. Bluetooth communication unit **12**. Computer; **13**. Temperature control box for the furnace; and **14**. Pipe for cooling the salt reservoir.

3.6 Modified Perkin-Elmer burner

The burner used for absorption spectroscopy measurements, experimental set-up shown in **Figure 3.8**, and flame studies by means of LI-PFF and Rayleigh scattering thermometry (see **Figure 3.2**) was a modified atom-absorption burner from Perkin-Elmer shown in **Figure 3.9a-d**. This burner has an advanced seeding system for liquid samples, which was used to seed alkali, potassium and sodium of chlorides and hydroxides into CH_4-air flames of different equivalence ratios. The burner consists of an end cap (**Figure 3.9b**), a spray chamber (10, **Figure 3.9c**), and a water-cooled burner head (**Figure 3.9d**) topped by a circular mesh (pore size ~1 mm and a depth of 20 mm) with an inner (23 mm) and an outer compartment for the co-flow (outer part) and the premixed fuel blend (inner part). This allows for stabilization of flat laminar premixed flames (**Figure 3.9d**) on the burner. Five hoses are connected to the end cap of the burner (**Figure 3.9a**): one for auxiliary air (2); a second one for CH_4 (4); a third one for the nebulizer air (5); a fourth one for the drain (6); and a fifth one for the seeded sample

(7). The nebulizer air (5, **Figure 3.9a**) is used for the seeding of alkali solution, which comes via the sample tube. CH_4 and auxiliary air are mixed together with the nebulizer air in the spray chamber of the burner (10, **Figure 3.9c**) to get the correct fuel-air mix.

The alkali solution droplets coming out of the nebulizer hit an impact bead (8, **Figure 3.9b**) and subsequently a flow spoiler (9, **Figure 3.9c**) in the spray chamber that only allows finer aerosol droplets to pass through the chamber to the burner head. The larger droplets are removed through the drain (6, **Figure 3.9b**).

A nitrogen co-flow (1, **Figure 3.9a**) of 10 ln/min was supplied to the burner head to shield the flame. A steel cylinder (**Figure 3.9d**) was mounted 30 mm above the burner for flame stabilization. The total gas flow to the burner was 5.6 (air + fuel) ln/min and the individual flows were controlled by four mass flow controllers: 20, 10, 5 and 1 nl/min (Bronkhorst). Premixed CH_4-air flames of equivalence ratios 0.8 − 1.3 were investigated and the alkali concentration in the seeding solution varied from 0.01 to 3.0 M.
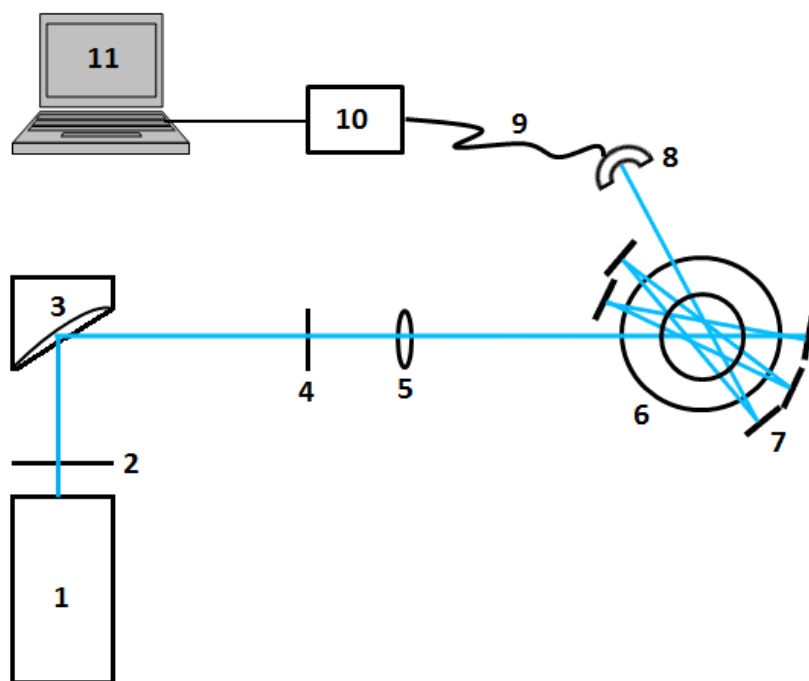
Figure 3.8. Experimental set-up for absorption measurements in the methane-air flame at different equivalence ratios. **1**. UV light source (deuterium lamp); **2**. Aperture; **3**. Parabolic mirror; **4**. Aperture; **5**. Plano-convex lens; **6**. Burner top (modified Perkin-Elmer for atom absorption spectroscopy); **7**. Mirrors; **8**. Parabolic collimator with SMA connector for the optical fibre; **9**. Optical fibre; **10**. Spectrometer; and **11**. Standard computer.
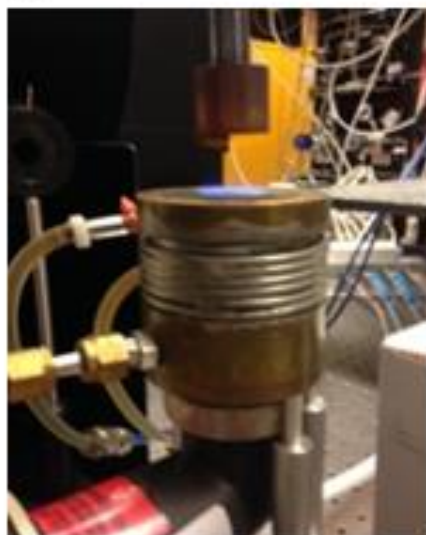
Figure 3.9a. Photo of the Perkin-Elmer burner; **1**. N_2 co-flow; **2**. Auxiliary air; **3**. Cooling water; **4**. Fuel; **5**. Nebulizer air; **6**. Drain; **7**. Sample tube. **b**. Inside of the endcap: **2**. Auxiliary air; **4**. Fuel; **5**. Nebulizer air outlet; **6**. Drain; and **8**. Impact bead. **c**. Endcap removed: **9**. Flow spoiler; **10**. Spray chamber. **d**. The Perkin-Elmer burner with a flat premixed CH_4-air flame.

3.7 Boilers

This section describes the boilers in more detail, together with the operational data used in the experiments and presented in Paper II. That paper reports the use of the IACM instrument as a tool for online fuel quality control, where fuel quality is related to the tendency for corrosion, slagging and fouling. In the research boiler, different types of fuels and fuel mixtures were tested and characterised under well-controlled conditions. The long-term measurements that were carried out during a firing season suggested applications of this instrument for the monitoring of fuel quality.

3.7.1 Research circulating fluidised bed boiler

The CFB research boiler originally designed for 12 MW_{th} and re-built to 8 MW_{th} is the hot-water boiler located at Chalmers University of Technology in Gothenburg, Sweden, described in earlier publications [9, 10]. The operational data of the CFB hot water boiler are a drum pressure of 13.5 bar with a hot water temperature of 195 °C. **Figure 3.10** shows a schematic of the boiler with its key components. During the characterisation of the different fuel mixtures the boiler was run on an average load of 6.3 MW_{th}. The different types of fuel that were mixed together were wood pellets, straw pellets and peat. Three different cases were tested. PVC granules were added to increase the load of chlorine in some of the fuel mixtures.
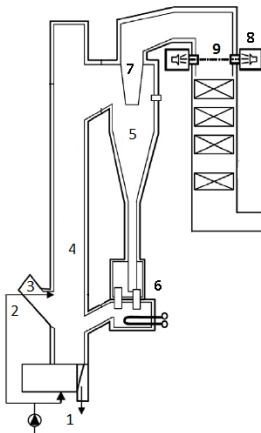

Figure 3.10. Schematic of the CFB boiler with its key components listed below. **1**. Primary air; **2**. Secondary air; **3**. Fuel feeding; **4**. Furnace; **5**. Cyclone; **6**. Particle seal; **7**. Cyclone outlet; **8**. IACM instrument; and **9**. IACM measurement path length.

3.7.2 Full-scale powder fuel boiler

A full-scale tangential pulverised fuel (PF) combined heat and power (CHP) boiler firing pellets and briquettes of wood where the IACM instrument is monitoring the fuel quality during a firing season. **Figure 3.11a** shows a drawing of the boiler indicating the location of the IACM while **Figure 3.11b** shows a 2-D schematic with the location of the IACM between the superheaters 3 and 4. The operational data of the CHP are a steam pressure of 110 bar with a temperature of 520 °C and a mass flow of 78 kg/s. This steam can be turned into 69 MW_e and 138 MW_{th} that could be delivered into the electrical grid and to the district heating grid, respectively. The CHP was originally planned for combustion of oil but changed to coal during the construction phase and then subsequently changed to biomass combustion. From 2006 it has been exclusively run on biomass-only fuel which has led to a CO_2 reduction of 90% and the ash from the CHP plant can now be returned to the forest as fertiliser.
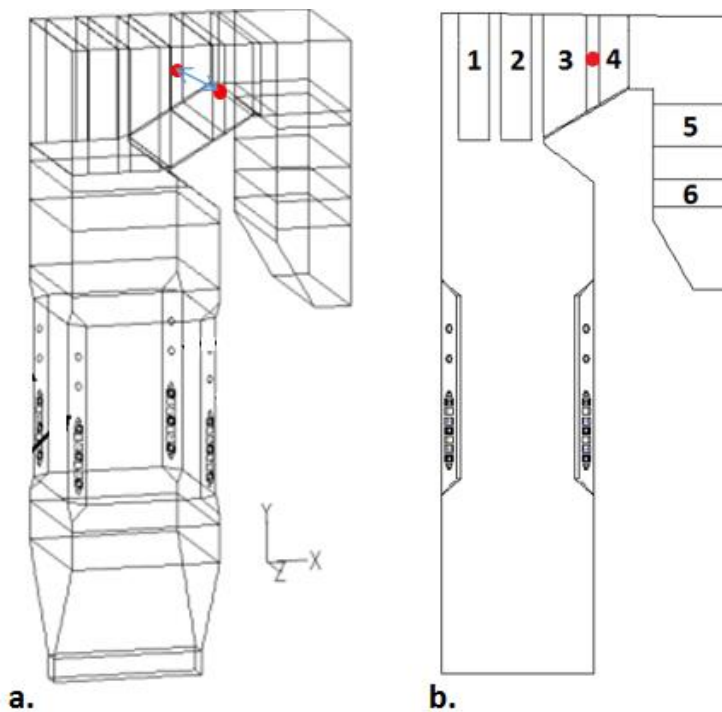

Figure 3.11a. A drawing of the PF boiler with a furnace width in x-direction of 7.6 m and a depth in z-direction of 8.1 m. **b**. The IACM is situated between superheaters 3 and 4. The location is marked with two red dots and the measurement path length is 8 m.

4 Results

The first five subchapters of this section highlight some of the outcomes of experiments carried out in the laboratory. The last subchapters present results obtained with the IACM instrument installed at different large-scale boilers. Examples of the versatility of the IACM instrument in handling different fuel mixtures, types of boilers and types of instrument configurations are presented.

Subchapter **4.1** highlights the spatially-resolved measurements of KCl with the DIAL technique (Paper I). Subchapter **4.2** shows the IACM instrument as a tool for online fuel quality control (Paper II). Subchapter **4.3** presents quantitative imaging of KCl by means of LI-PFF as well as simultaneous imaging of two alkali components, KCl and NaCl (Paper III). Subchapter **4.4** describes the determination of different KCl vapour pressures and shows their absorption spectra for each salt temperature in the newly-developed calibration cell (Paper IV). Subchapter **4.5** discusses the equivalence ratio Φ as an influence on the formation of KCl in premixed combustion (Paper V). Subchapter **4.6** shows IACM measurements in a test unit combusting propane under air- and oxy-fuel conditions. Subchapter **4.7** gives a general overview of different variants of IACM installations where account has been taken of the type of fuel mixtures combusted, types of boilers and their sizes. Most of this chapter is based on previously unpublished measurements. Subchapter **4.7.1** shows the KCl concentration variations over one year (2014) during combustion of biomass in a BFB boiler. Subchapter **4.7.2** analyses IACM data from co-combustion of coal and biomass during injection of ammonium sulphate. Subchapter **4.7.3** describes IACM measurements through one optical access with a mirror probe during combustion of municipal waste in a grate-fired boiler. Subchapter **4.7.4** describes KCl measurements across a corner in a rotating fluidized bed boiler combusting non-hazardous waste. Subchapter **4.7.5** discusses optimization of the ChlorOut concept by means of the IACM instrument in a CFB boiler combusting demolition wood.

4.1 KCl Measurements with the DIAL Technique

Optical measurements carried out in a boiler or a flue gas duct can be limited by the number of optical access ports available. There are occasions when (a) only one port is available, or (b) where two ports are available but are not properly aligned to perform line-of-sight measurements. In either case, opening a new hole for an optical access or re-aligning one of the existing ports could be too costly and a technique for single-ended measurement could be valuable. Paper I reports on a measurement technique, DIAL, using only one optical access port, which was tested in the laboratory to determine its suitability for alkali chloride measurements in the field. This technique utilizes the ratio between intensities of backscattered signal measured at two different wavelengths: λ_{off} and λ_{on}, on and off resonance, respectively, to calculate the concentration as outlined in Subchapter **2.3.4**. In this particular case, measurements on vaporized KCl in a tube furnace were carried out with success. This measuring technique also offers the possibility to provide a spatially-resolved concentration profile compared to an average concentration over the path length when using the line-of-sight technique. **Figure 4.1a** shows the spatially-resolved KCl number density profile measured on vaporized KCl in the tube furnace used during the DIAL measurements. **Figure 4.1b** shows the KCl concentration measured by IACM, ppm recalculated to number density, before and after the DIAL measurements were carried out. The broken part in the KCl concentration curve in **Figure 4.1b** represents the time interval for the DIAL measurement when the mirrors used for the IACM measurements needed to be removed to prevent obstructing the beam path for the DIAL measurements. The average KCl number density during DIAL measurements was determined to ~$8{\cdot}10^{14}$ molecules/cm^3 and for IACM measurements $0.3{\cdot}10^{15}$ molecules/cm^3 and $1.7{\cdot}10^{15}$ molecules/cm^3 after and before the DIAL measurements, respectively. **Figure 4.1b** shows that the average value determined in the DIAL measurements fits well in the broken part of the KCl curve measured by the IACM instrument. The average number density for KCl determined in the DIAL measurements corresponds to a KCl concentration of 130 ppm, which corresponds to the maximum value measured in one of the examples in Subchapter **4.7**. During field measurements KCl concentrations were experienced in the range of 0 – 150 ppm. DIAL allows for concentration measurements at levels encountered during biomass combustion. Further details on the experiment are available in Paper I.
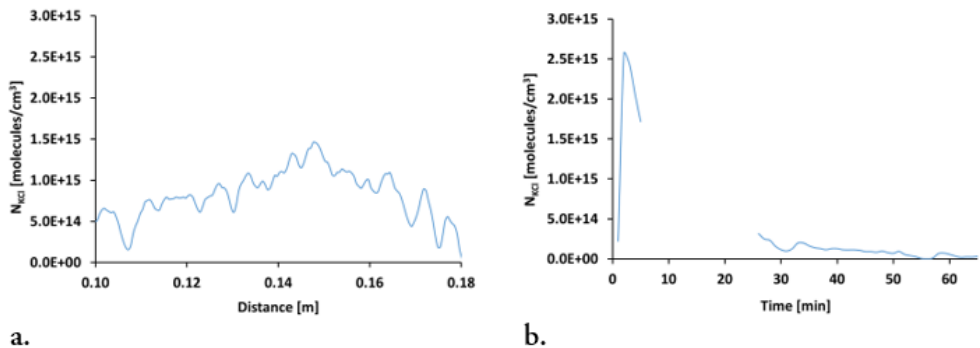
Figure 4.1a. Shows the KCl number density calculated with the simplified DIAL equation Eq. (2-10). **b**. Shows the KCl concentration before and after the DIAL measurements.

4.2 IACM used for Online Fuel Quality Control

The energy industry has gradually shifted from combustion of fossil fuels to combustion of biomass, which has high content of alkali and chlorine. The increased use of biomass has led to shorter times between operation and planned stops concomitant with combustion of biomass fuels. These unplanned stops for maintenance and repair are very costly for the plant owners. Paper II reports on an alkali measuring device, IACM [24], which can be used as a tool for online fuel quality control. This instrument can be also used as a control device for the injection of ammonium sulphate [59] in the flue gas to reduce the gas-phase alkali chlorides and subsequently minimize the above-mentioned problems. **Figure 4.2a** shows changes in the KCl concentration when the chlorine content in the fuel is increased while the alkali content is kept constant. **Figure 4.2b** shows the impact on the KCl concentration during co-combustion when a fuel mixture with a rather high content of alkali and chlorine is mixed with a fuel high in sulphur content and low in alkali and chlorine content. The formation of alkali chlorides during biomass combustion, which releases pathways for K, Cl and S, has been studied by Johansen et al. [7], and seems to be controlled by the amount of Cl and S in the fuel mixture. It has thus been shown that the IACM instrument can be used as an online tool for fuel quality control. It has also been shown that certain conditions need to be considered when mixing the biomass fuel to mitigate problems related to alkali and chlorine.

To compose a less harmful fuel mixture the molar ratio S/Cl needs to be considered since it gives an indication on the corrosiveness of the mix [60]. Depending on the way the sulphur is added –through elemental sulphur via the fuel or in the gas-phase via ammonium sulphate– there are certain key figures to bear in mind. For sulphur to be added via the fuel or contained therein, Salmenoja [61] found that a ratio lower than 2 is regarded as corrosive while a ratio higher than 4 is regarded as non-corrosive. Boiler design and combustion parameters determine the superheater corrosion when the ratio is between 2 and 4. During co-combustion of wood pellets and straw a KCl concentration of approximately 30 ppm was obtained, which was measured with the IACM instrument. Kassman et al. [9] showed that injection of ammonium sulphate $((NH_4)_2SO_4)$ in the gas-phase at a S/Cl molar ratio of 2.1 reduced the KCl concentration to 5 ppm, while a molar ratio of 6.4 for elemental sulphur only decreased the KCl concentration to 10 ppm.
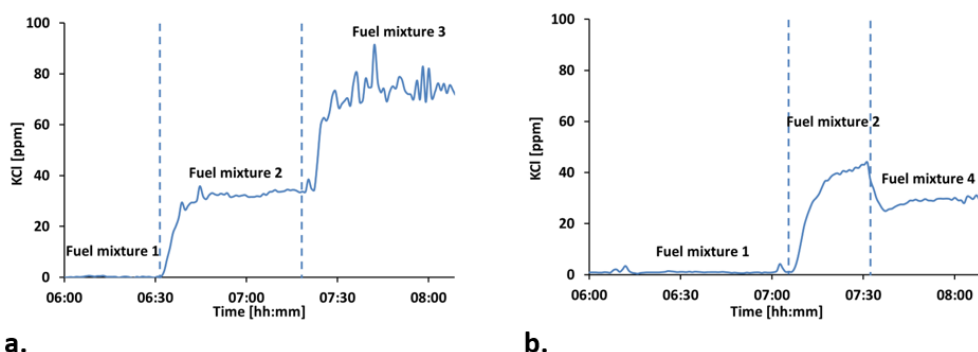

Figure 4.2a. The KCl concentrations for three different fuel mixtures where the chlorine content in each fuel mixture has increased. **b**. KCl concentration dependence on the chlorine and sulphur content in three different fuel mixtures.

4.3 LI-PFF Imaging of Alkali Compounds

A detailed understanding of the formation process and the alkali chemistry can potentially reduce if not resolve the issues associated with alkali compounds in the fuel mixture mentioned earlier. The simultaneous formation process of KCl and NaCl can be studied by means of LI-PFF technique as described in Paper III. This technique has been used on KCl and KOH, which have been seeded into a stabilized premixed laminar

methane-air flames. The images from the initial experiment carried out with this technique can be found in Appendix D.

Figure 4.3a presents the LI-PFF image of a stabilized premixed laminar-air flame at Φ=0.8 seeded with 0.1M KCl solution. It can be seen in the figure that the formation of gas-phase KCl occurs at the edges of the left and right sides, where the temperature is lower. **Figure 4.3b** shows an LI-PFF image where a mixture of 0.1M KCl and 3M ammonium sulphate has been seeded into the flame with the same equivalence ratio as in **Figure 4.3a**. This figure shows that the formation of KCl has been reduced due to the seeding of ammonium sulphate, which is used in the ChlorOut concept to reduce the gas-phase KCl in the flue gas by formation of K_2SO_4 instead. When the amount ammonium sulphate in the KCl and ammonium sulphate solution is increased to 4M the reduction of KCl decreases further, as shown in **Figure 4.3c**.

Figure 4.3d presents an LI-PFF image of a seeded mixture of KCl and NaCl into a turbulent stoichiometric methane-air flame without stabilizer where the image has been captured with an intensified CCD camera. A stereoscope was mounted in front of the camera objective, containing two band pass filters centred at wavelengths 589 and 766 nm to detect the fluorescence signal from excited Na (left) and K (right) atoms. **Figure 4.3e** shows the spectra of NaCl at 589 nm and KCl at 766 nm, which were captured by a spectrometer. Even the LI-PFF image from the turbulent flame shows that the formation of KCl occurs at the left and right sides, where the temperature is lower. This technique, utilizing a stereoscope with band pass filters for detection of simultaneous NaCl and KCl can be used during combustion of waste, which contains compounds of Na, K and Cl. **Figure 4.3e** clearly shows that there are no other interfering components in the seeded mixture of NaCl and KCl.
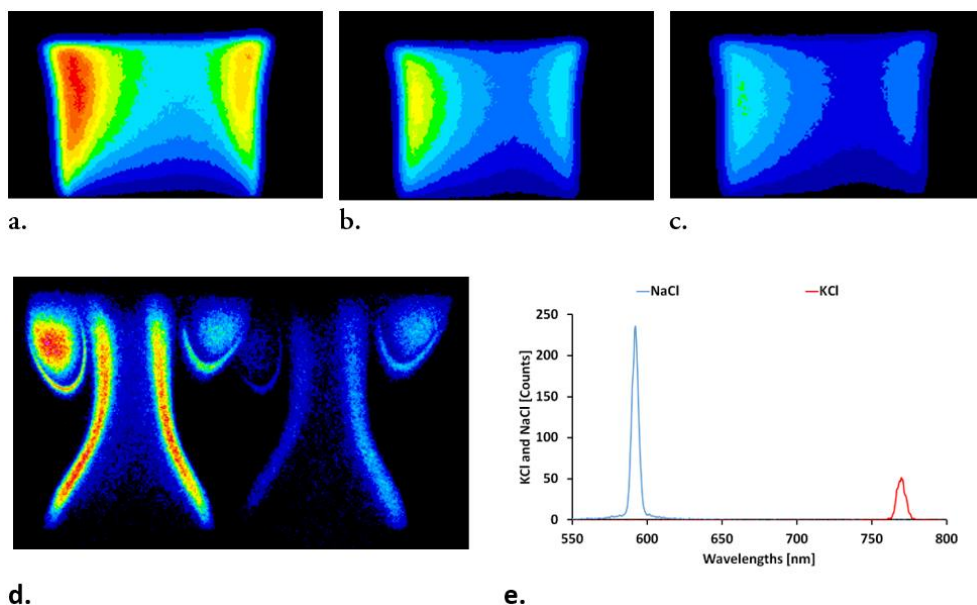
Figure 4.3a. 0.1M KCl seeded into a laminar and stabilised methane-air flame, Φ=0.8 in a modified Perkin-Elmer atom absorption burner. **b.** Same settings as in (a), with additional seeding of 3M ammonium sulphate. **c.** Same settings as in (a), with additional seeding of 4M ammonium sulphate. **d.** NaCl and KCl mixture seeded into a turbulent stoichiometric methane-air flame where the image has been captured with a stereoscope utilizing band pass filters for detection of excited Na atoms (589 nm, left) and excited K atoms (766 nm, right), respectively. **e.** The spectra from Na and K atoms created by Laser-induced Photofragmentation Fluorescence.

4.4 KCl Measurements in a new Calibration Cell

In order to determine the concentration of a species of interest, which in this particular case is gas-phase KCl, a reliable calibration spectrum is needed. In the work described in Paper IV a new calibration cell was developed and characterized in the laboratory. This new calibration cell enables the generation of saturated vapour of KCl in the temperature span 600 – 750 ℃, which could subsequently be superheated in the measuring chamber where the absorption measurements has taken place. The vapour pressure is generated by controlling the temperature of a salt reservoir, which is connected to the measuring chamber. The vapour pressure in the calibration cell has been calculated by means of the Antoine equation, whose coefficients have been determined by experimental data from the literature as presented in Subchapter **2.4.1**. This construction allows to investigate if the absorption cross-section has any temperature dependence. **Figure 4.4a** shows vapour pressures calculated with the Antoine equation at the following temperatures: 600, 650, 700, 730 and 750 ℃. Each

vapour pressure generates a KCl absorption spectrum (see **Figure 4.4b**). **Figure 4.4b** shows the reference spectrum and measured spectra for five different vapour pressures, which have been measured at the following temperatures: 650, 700, 750, 780 and 800 °C. It should be noted that to avoid condensation in the measuring chamber each absorption spectrum is measured at a temperature 50 °C higher than that at the salt reservoir. It can be observed in **Figure 4.4b** that absorption measurements should not be carried out at salt reservoir temperatures lower than 600 °C, where the measured KCl value reaches the detection limit for the actual set-up. The measuring spectra provided in the new calibration cell are used to calculate a more reliable absorption cross-section that enables a more accurate calibration and quantitative KCl measurements. The KCl absorption cross-sections for wavelengths λ = 197.6 nm and λ = 246.2 nm were calculated to be $3.4 \cdot 10^{-17}$ and $2.9 \cdot 10^{-17}$ cm^2/molecule, respectively.
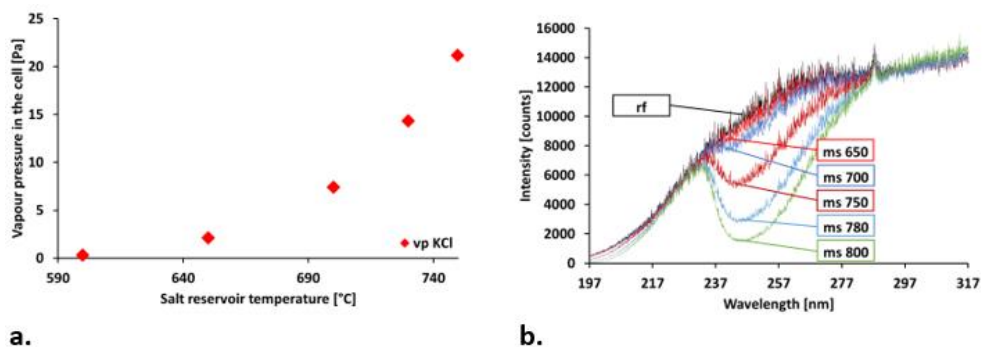

Figure 4.4a Calculated KCl vapour pressure at the five investigated temperatures (red diamonds). **b** The corresponding absorption spectra for these temperatures.

Figures of merit for precision and sensitivity of the IACM instrument were determined in the newly-developed calibration cell for temperatures 600 – 750 °C. The precision, i.e. the absolute standard deviation in evaluated vapour pressure ranges between 0.20 – 0.94 Pa. The coefficient of variation (CV), i.e. the ratio between the standard deviation and average value, varies between 12 – 5% when the vapour pressure for the lowest temperature is excluded due to the uncertainty in salt reservoir temperature. However, it was observed that the standard deviation could be further reduced with an improved temperature controller (previously manually controlled). The calibration sensitivity was determined to 0.089 Pa^{-1} and an analytical detection sensitivity corresponding to one standard deviation ranges between 0.03 – 0.07 Pa. Practical detection limits of three standard deviations then become 0.1 – 0.2 Pa. Figures of merits have been calculated according to the book, *Principles of Instrumental Analysis, 6th Edition* [62]. Details about the accuracy of the IACM are outlined in more detail in Paper IV.

4.5 Experimental Investigations of Potassium Chemistry in Premixed Flames

The increased combustion of a broad variety of biomass fuels can be problematic due to their relatively high contents of alkali, chlorine and low amount of sulphur. To abate these kind of issues calls for a deeper understanding of formation of KCl, KOH and K, to mention a few. The formation of these components has been discussed in Paper V, which deals with different flame equivalence ratios and chlorine loads with different spectroscopic techniques. The KCl and KOH formation was measured by UV absorption and LI-PFF while K atoms were measured by using tuneable diode-laser spectroscopy. Results from these measurements unveiled a decreased level of KCl and KOH in fuel-rich flames, which was the opposite trend observed for free K atoms. **Figure 4.5a** shows the KCl concentration using the IACM instrument for different equivalence ratios while **Figure 4.5b** shows the same result using LI-PFF technique where the LI-PFF signal has been recalculated to ppm.

As can be appreciated in **Figure 4.5a** and **b**, measurements with UV absorption and LI-PFF render similar results. **Figure 4.5c** exhibits the Rayleigh temperature measurements together with KCl LI-PFF signal evaluated from images measured across the flame –see **Figure 4.3** for Φ=0.9 and **Figure 4.5d** for Φ=1.3. The temperature is slightly higher in the fuel-rich case, while the K LI-PFF signal in the flame centre is higher in the fuel-lean case. Temperature is rather stable in central part of the flame and decreases towards the edges since the KCl formation is enhanced at lower temperatures [63]. In addition, KCl condensation and nucleation occur at low temperatures. This is supported by the strong signal seen at the edges in the Rayleigh scattering images as shown in **Figure 2.1**.

Lower KCl concentrations in fuel-rich flames as measured by absorption and LI-PFF can be explained as reactions with hydrogen atoms, which have a tendency to form higher concentrations of free K atoms [64]. The reduced KCl concentrations and increased formation of free K atoms result in overall lower LI-PFF signal. The K atoms also absorb the fluorescence light emitted from the photofragmented KCl molecules and further reduces the LI-PFF signal in the experiment. This can be seen comparing **Figure 4.5c** and **Figure 4.5d** where the profile measured in the fuel-rich flame is more suppressed and flat in the centre. Paper V describes more in detail the measurements on

potassium components for different equivalence ratios and effects on the absorption and LI-PFF techniques.

a.

b.

c.

d.

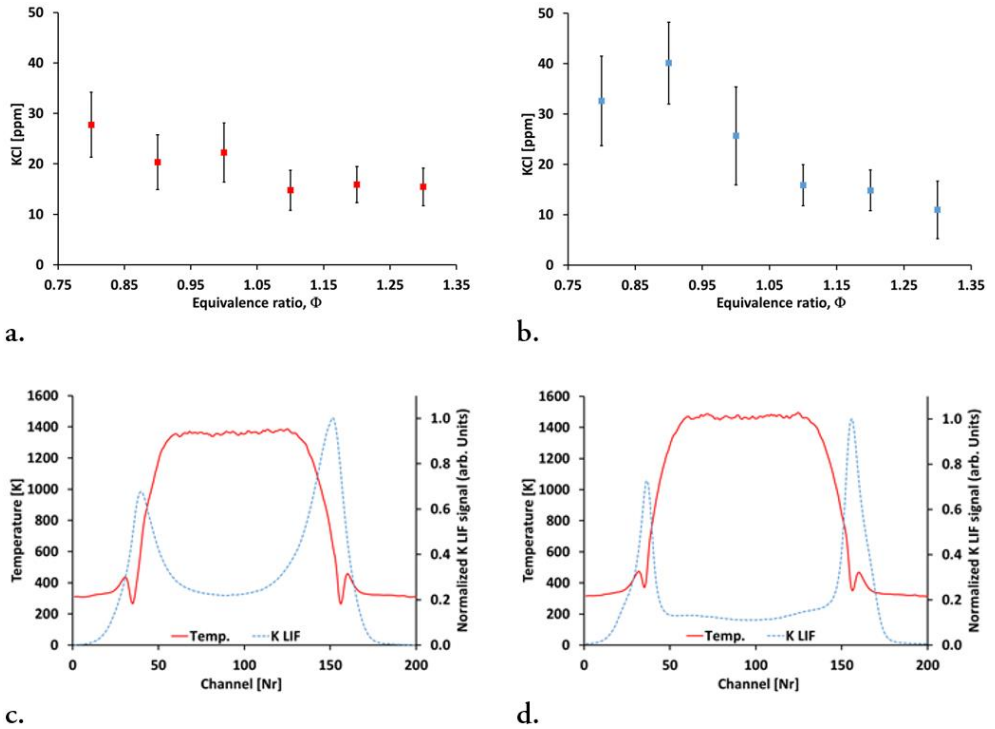**Figure 4.5a.** KCl concentrations from absorption measurements at different equivalence ratios measured with the IACM. **b**. KCl concentration from LI-PFF measurements recalculated to ppm. **c**. Rayleigh temperature measurement and K LIF signal in a 1 M KCl seeded methane-air flame at $\Phi = 0.9$. **d**. Rayleigh temperature measurement and K LIF signal in a 1 M KCl seeded methane-air flame at $\Phi = 1.3$.

4.6 Combustion of propane in air- and oxy-fuel mode in a test unit

Figure 4.6a shows results from KCl measurements in a 100 kW test unit, operated in air- and oxy-fuel mode at a load of 80 kW. Air mode: a constant propane flow of 1.73 g/s and air (O_2=21% and N_2=79%) to maintain an air-fuel equivalence ratio of λ=1.15. Oxy-fuel mode: a constant propane flow of 1.73 g/s and Recycled Flue Gas (RFG) and O_2 (CO_2=75% and O_2=25%) kept at an air-fuel equivalence ratio of λ=1.15. The cross-stack version of the modified IACM instrument was used, with a measuring path length of 0.8 m at a temperature of 748 °C for the oxy-fuel mode case and 855 °C for the air mode case –see **Figure 4.6b**. A KCl-water solution was blended and was seeded into the flame to render a KCl concentration of 100 ppm in the flue gas during air combustion. In the oxy-fuel mode the same amount of injected KCl-water solution should give a KCl concentration of 110 ppm caused by the higher content of O_2 in the combustion air, which is 25% instead of 21% during air mode. The average KCl concentration in oxy-fuel mode was 90 ppm and 96 ppm in air mode. The discrepancy in concentration between the oxy-fuel- and the air mode is believed to be caused by differences in the effective measuring of the path length. The reason could be due to changes in purge gas from N_2 (in air mode) to argon (in oxy-fuel mode) in the wall channels in the insulating material changing the effective absorption path length (for details, see **Fig. 1** in [65]). The results show that the IACM instrument can be used for alkali chloride measurements in an oxy-fuel combustion mode. Special measures such as dilution of the flue gas and measurements on dry flue gas would have been necessary to consider using an instrument that is based on the IR-technique (FTIR). These data were obtained during an experiment to study the K-Cl-S chemistry in air- and oxy-fuel mode. The main conclusions from the experiment were: the increased SO_2 concentration in oxy-fuel mode compared to the air mode is the main reason for the increased sulphation of KCl. The elevated CO_2 concentration seems to have a chemical influence shown in the modelling and the residence time in the combustor. This also affects the sulphation; however, this effect is small [65].
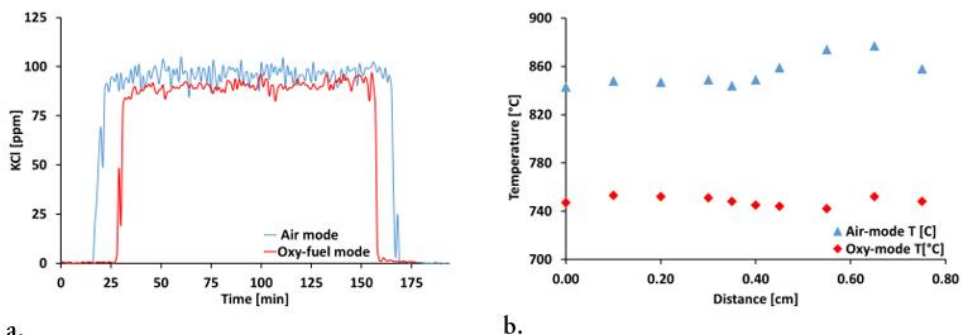
Figure 4.6a. IACM measurement in a test unit for combustion of propane in air- and oxy-fuel mode. The cross-stack version of IACM with the new optical set-up with a deuterium lamp as a light source with a measuring path length of 0.8 m at a flue gas temperature of 748 °C (oxy-fuel mode) and 860 °C (air mode). **b**. The temperature profile across the measuring path length for both cases.

4.7 Field Measurements with the IACM Instrument

This section describes a variety of IACM installations in different types and sizes of boilers, such as Bubbling Fluidized Bed (BFB), CFB and grate-fired boilers The idea behind this section is to provide a broader audience such as power plant operators and boiler owners with easy to digest examples of the IACM instrument in corrosion abatement, fuel-quality control and process diagnostics. A diversity of different biomass fuels has been fired in these boilers, namely wood chips, agricultural waste, non-hazardous waste, municipal waste, waste wood chips, coal and energy crops. Wood chips, constituting the main fuel, have been mixed with other types of biomass fuels and in addition to this, co-combustion of coal and biomass fuel has occurred. Before the installation of an IACM instrument, there are a few aspects that need to be taken into consideration. First, a suitable position should be identified –preferably close to a superheater in a temperature region of 650 – 1000 °C and with an optical access of one or two ports. This is in line with the discussion in Subchapter **2.3.3** about low temperature and high content of alkali and chlorine in the fuel mix. Second, it should be borne in mind that the amount of alkali chlorides formed during the combustion of the fuel impose a limit on the measuring path length as the absorption becomes too strong –see Eq. **(2-3)**. Depending on the wall-to-wall distance for the so-called cross-stack implementation of the instrument, the measuring path length may need to be reduced, and this can be achieved by using temperature-resistant steel pipes mounted

together with the IACM instrument to reduce the path length. Another alternative would be to use a water-cooled mirror probe, which is a modified version of the IACM instrument that only needs one optical access. The collimated light in the mirror probe sent into the flue gas duct is reflected by a water-cooled mirror mounted at the end of the probe and collected in the spectrometer. This solution is not sustainable for long-term measurements, since it requires one person to operate the instrument and the lifetime of the mirror in this environment is limited. There is also an increased deposit build-up on the pipes that feed cooling water to the mirror at the opposite end of the probe, which is located in the flue-gas duct. This increased deposit build-up gradually blocks the light on its way to the mirror and needs to be removed, frequently depending on the environment where the probe is being used. A third alternative would be to mount the IACM instrument in a corner so as to reduce the optical path length. Appendix C shows photos of the different IACM configurations. Attention should also be paid to the environment where the instrument is located, particularly concerning the ambient temperature or the location of the instrument (i.e. mounted indoors or outdoors). Five different IACM installations will be presented to illustrate the versatility of the instrument and the way the constraints described above may be overcome.

4.7.1 Combustion of biomass in a BFB boiler

Data from long-term measurements between January 2014 and December 2014 presented in **Figure 4.7** were obtained from a BFB boiler. The BFB boiler had the following steam data: a steam pressure of 102 bar(a), a steam temperature of 540 °C and a steam flow of 195 t/h. The maximum electrical output from the plant generator was 50 MW_e at a fuel input of 147.5 MW_{th}. The fuel consumption was around 800,000 t/year of wood, a combination of sawmill chips, round wood, energy crops and other biomass. In this boiler the cross-stack version of the IACM was utilized with a measuring path length of 9.32 m in a temperature region of about 860 °C. This boiler used the ChlorOut concept, i.e. injection of a sulphate, to avoid high-temperature corrosion and deposit growth on the superheaters. The amount of injected ammonium sulphate in this case had been set to a fixed flow of about 15 l/h. The result from deposit probe measurements showed that the amount of injected ammonium sulphate was sufficient to remove the chlorine in the deposits. **Figure 4.7** presents a rather stable concentration of KCl and SO_2 over the year. The average concentration over the year for KCl has been 10.5 ppm with a standard deviation of 2.2 ppm and for SO_2 it has been 11.0 ppm with a standard deviation of 2.9 ppm, which indicates a homogenous fuel over the year.
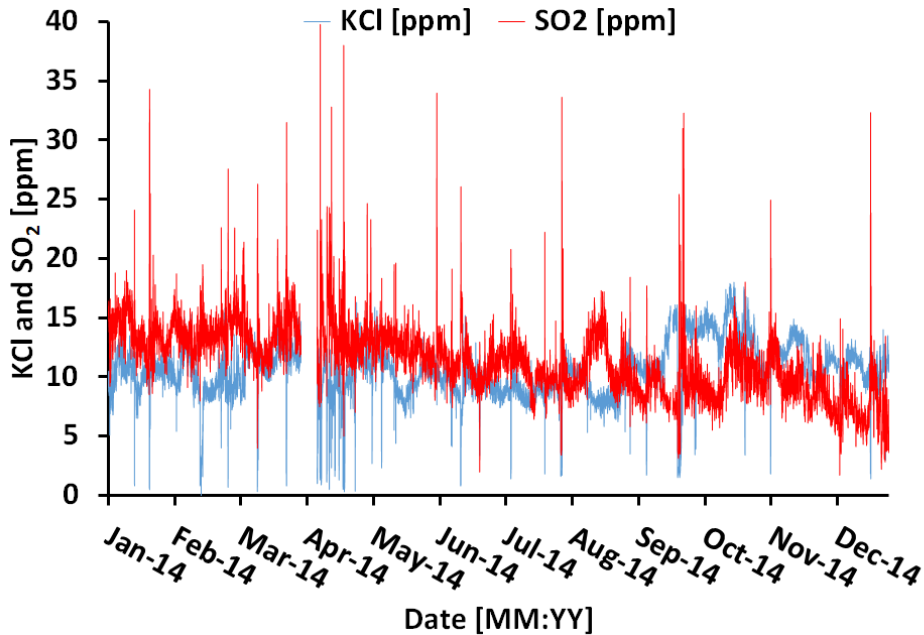
Figure 4.7. Long-term IACM measurements in a BFB boiler from 2014. The cross-stack version of the IACM at a path length of 9.32 m at a flue gas temperature of 860 °C.

4.7.2 Co-Combustion of coal and biomass in a CFB boiler

Figure 4.8 presents data from a CFB boiler with the following steam data: a steam pressure of 124 bar, a steam temperature of 540 °C and a steam flow of 370 t/h. The maximum electrical output of the generator is 105 MW_e at a fuel input of 265 – 270 MW_{th}. This CFB boiler was designed for the co-combustion of palm kernel shells together with coal and wood pellets to meet environmental regulatory requirements. This boiler used the ChlorOut concept, i.e. injection of a sulphate, to avoid high-temperature corrosion and deposit growth on the superheaters. In this boiler the cross-stack version of the IACM instrument was utilized at a measuring path length of 10.5 m and a temperature of 860 °C. The green curve in the figure shows the integration time, which decreased from around 160 to 120 ms due to a shift in the fuel mixture from coal and palm kernels and shell to coal and demolition wood. A fuel mixture containing palm kernels and shells generated more aerosols, which scattered the light away from the detector and induced a longer integration time. The increased use of demolition wood furthered the KCl concentration in the flue gas. Moreover, part of the evaluated alkali concentration could be due to the sodium in the coal since the IACM measures both alkali compounds. The KCl concentrations show two peaks at 14:00 and

18:00 caused by stops in the ammonium sulphate injection. The disturbance in the SO_2 concentration during the same time was caused by the reduced amount of sulphur coming from the ammonium sulphate injection.
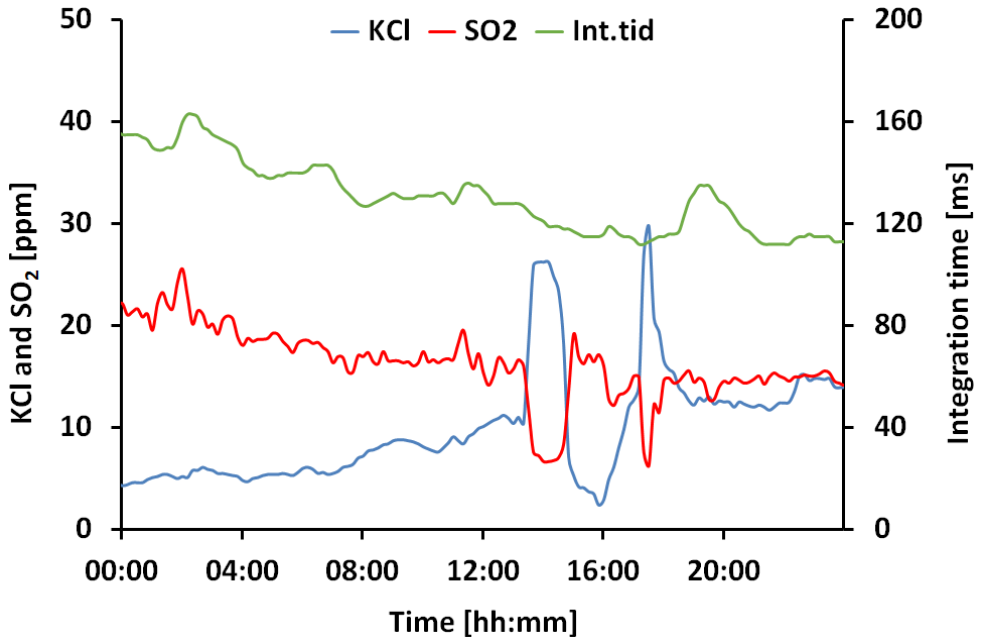

Figure 4.8. IACM measurements in a CFB boiler during co-combustion of coal, palm kernels and shells and demolition wood during simultaneous injection of ammonium sulphate. The cross-stack version of IACM at a path length of 10.5 m at a flue gas temperature of 860 °C.

4.7.3 Combustion of municipal waste in a grate-fired boiler

Figure 4.9 presents results from a grate-fired boiler with the following data: combustion around 15 t/h of municipal waste, generating 40 t/h of steam for the electricity production. The steam produced was superheated to 415 °C. The municipal waste was burnt at temperatures in excess of 1000 °C. In this installation the mirror probe version of the IACM was used due to the fact that there was only one optical port available. The probe was installed at a position with a temperature of 850 °C and the path length was 1 m. This proves it is possible to measure the KCl concentration when only one optical access is available during combustion of municipal waste in a grate-fired boiler. However, the measurements were performed quite close to the wall, where the KCl concentrations probably were higher due to lower temperature compared with locations

further into the flue gas duct. This boiler was operated without the ChlorOut concept so the measured sulphur originated from fuel. The municipal waste fuel had high contents of alkali and chlorine, which rendered high concentrations of alkali chlorides without use of the ChlorOut concept.
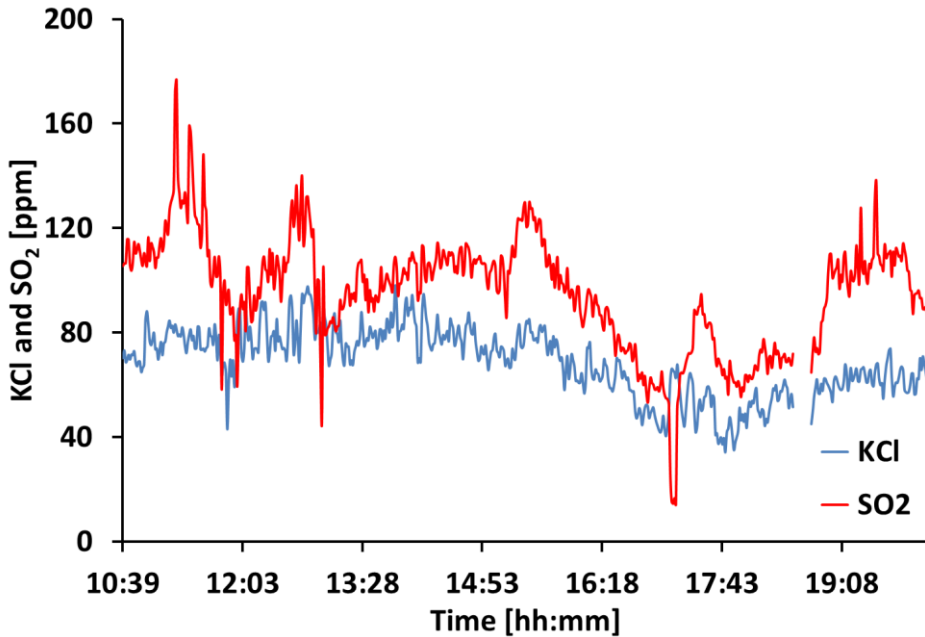

Figure 4.9. IACM measurements in a grate-fired boiler during municipal waste combustion. The mirror probe version of the IACM at a path length of 1.0 m at a flue gas temperature of 850 °C.

4.7.4 Waste incineration in a rotating fluidized boiler

The data presented in **Figure 4.10** were measured in a fluidized bed incinerator based on rotating fluidized bed incineration technology, which had the following stem data: a steam pressure of 41 bar(a), a stem temperature of 400 °C and a steam flow of 61.5 t/h. The maximum thermal capacity was 48 MW_{th} at a fuel consumption of 77,600 t/year, which consisted of a mix of non-hazardous waste and sludge. In this installation the cross-stack version of the IACM was used over a corner with a measuring path length of 2.1 m at a temperature of 920 °C. The Figure shows that the concentrations of KCl and SO_2 were rather high and varied considerably over time. These fast and instantaneous fluctuations in KCl and SO_2 concentrations and also variations over time

75

are characteristic of an inhomogeneous waste fuel where the content of alkali, chlorides, sulphur and calorific value varies considerably. During the time span shown in **Figure 4.10** mixed waste was combusted. The ChlorOut concept used to reduce the alkali chlorides in the flue gas was in this particular case not installed.
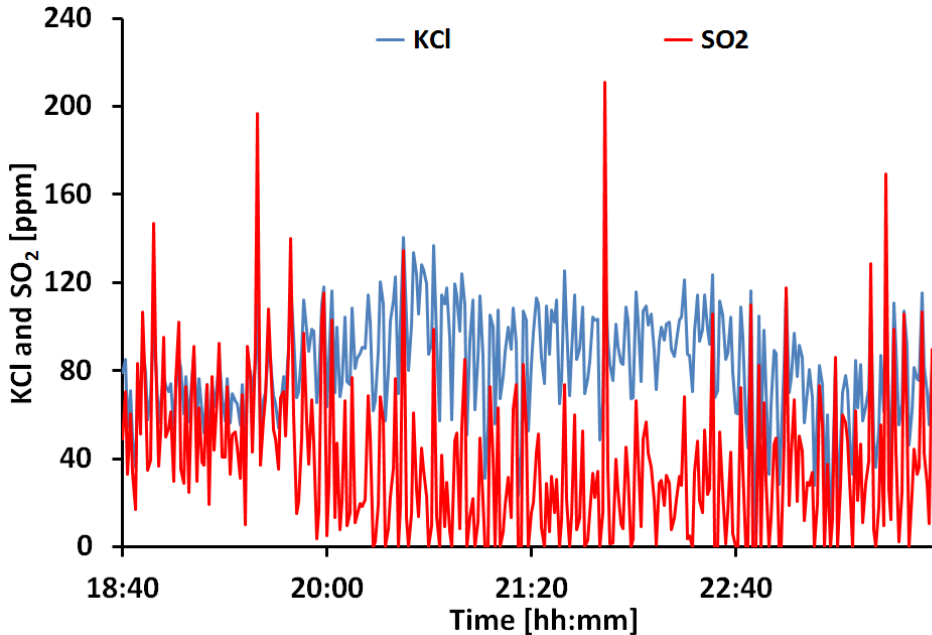

Figure 4.10. IACM measurement in a rotating BFB boiler combusting non-hazardous waste and sludge. The cross-stack version of IACM over a corner with a path length of 2.1 m at a flue gas temperature of 920 °C.

4.7.5 Combustion of demolition wood in a CFB boiler

Figure 4.11 shows data from an injection test campaign where ammonium sulphate was injected in a CFB boiler at a position normally used for Selective Non-Catalytic Reduction (SNCR) of NO_x. SNCR 1 is the injection position before the cyclone and SNCR 2 is the injection position after the cyclone. The reason behind this test campaign was to investigate if the ChlorOut concept could be a possible solution to corrosion problems on the superheater. The CFB boiler had the following steam data: a stem pressure of 95.1 bar(a), a steam temperature of 510 °C and a steam flow of 113.4 t/h. The thermal output is 88 MW_{th} and the fuel mixture consisted of wood chips of biomass and waste wood. The IACM instrument was located in front of the first superheater

where the temperature was about 860 °C. The high alkali and chlorine content in the fuel mixture resulted in an installation of the cross-stack version of IACM over a corner to reduce the measuring path length to 3 m. The results from the different experiments carried out were used to optimize the reduction of KCl. It can be seen in the figure that the SNCR 2 is the best location for injection and the amount of ammonium sulphate should be around 160 to 250 l/h. A more thorough optimization to determine the optimal amount for injection can be attained by means of deposit probe measurements.
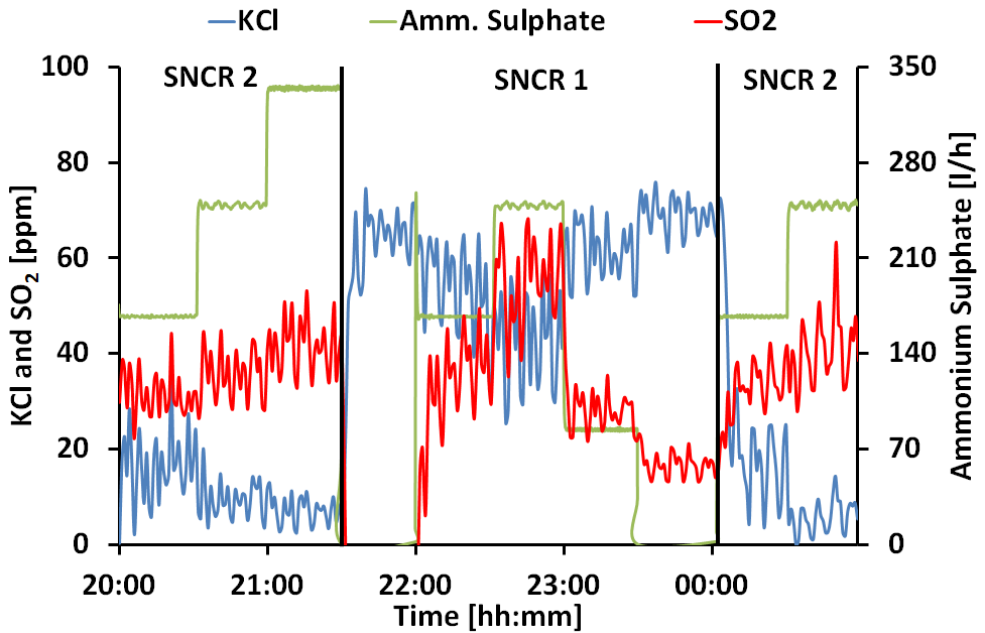

Figure 4.11. IACM measurements in a CFB boiler during combustion of wood chips and waste wood and simultaneous optimization test of ammonium sulphate injection. The cross-stack version of IACM at a path length of 3.0 m at a flue gas temperature of 860 °C.

5 Summary

The research conducted at the Division of Combustion Physics during the life-cycle of this thesis can be divided into three parts: fundamental, applied industrial and innovative part. There have also been occasions spent outside the department concerning field campaigns on behalf of Vattenfall AB where measurements were carried out. Results from these measurements are also to some extent included in this thesis.

The fundamental part of the research focuses on the development of a new calibration cell for KCl. The main purpose of the research is to be able to carry out KCl calibration under well-controlled conditions to enable the possibility to calculate the accuracy and precision of the IACM instrument. This calibration cell has also facilitated thorough spectral investigations of the absorption cross-section. Considerable time has been spent on this part of the research, including cell design, furnace development and control of the vapour pressure of the KCl.

To further increase the fundamental knowledge on formation of alkali species during combustion, an experimental investigation of potassium chemistry was carried out in premixed flames of different equivalence ratios. Measurements were carried out with multiple optical diagnostic techniques such as broadband UV absorption spectroscopy, LI-PFF and diode-laser absorption spectroscopy. The quantification of the potassium species was in good agreement with simulations run with a simplified model. The results can be used for validation of chemical kinetic models of alkali chemistry in combustion.

The applied part of the research focuses on testing a new optical set-up with a new light source and the possibility to use the IACM instrument to measure the KCl concentration in a boiler operated in oxy-fuel mode. The following changes were made to IACMs optics: a lens was replaced by a parabolic mirror and the spherical collecting mirror was replaced with a parabolic mirror with a fibre connector. These changes are intended to remove the spherical- and chromatic aberrations. The original xenon lamp was replaced with a deuterium lamp to increase intensity of the shorter wavelengths. The IACM instrument with the amended optics and light source was tested in a 100 kW test unit at Chalmers University of Technology in both air- and oxy-fuel mode with good results.

The innovative part of the work includes investigations of the DIAL technique for KCl measurements and development of the LI-PFF technique for quantitative imaging and simultaneous measurements of two species in flames. The DIAL technique, which was successfully tested on KCl measurements in the laboratory, proved it can be used when only one optical access is available in a boiler. The LI-PFF technique utilizing a stereoscope mounted on the camera together with two optical filters made it possible for simultaneous imaging and detection of KCl and NaCl formation in laboratory flames.

On different occasions, field measurements and IACM installations were carried out in power plant boilers combusting a broad variety of biomass fuels and waste, e.g. demolition wood, virgin woodchips, woodchips of eucalyptus, palm kernels and shells waste, municipal waste and non-hazardous waste, to name a few. On those occasions, different type of IACM set-ups were used, including IACM cross-stack, mirror probe, IACM with reduced path length and IACM installed over a corner, to mention a few. These measurements can be considered part of the applied work and indicate the kind of environment where good measurement techniques and further knowledge of the alkali chloride chemistry is needed.

6 Conclusion

The main focus of the work carried out during these five years has revolved around a tripartite axis of a fundamental, an applied industrial and an innovative nature. The centre of interest has been the detection, calibration and visualisation of alkali chlorides in the laboratory as well as in the field of different power plant boilers.

The main takeaways from the fundamental part are:

- The development of a calibration cell for potassium chloride allows to set a predetermined potassium chloride concentration and study its absorption cross-section at different temperatures –this is described in more detail in **Paper IV**;

- Flame studies in alkali-seeded premixed methane-air flames of different equivalence ratios by means of LI-PFF, UV absorption, Rayleigh scattering and tuneable diode-laser spectroscopy measurements –details are available in **Paper V**.

The main conclusions from the applied industrial part are:

- It has been demonstrated that the IACM instrument with amended optics and light source works in a 100 kW test unit for air- and oxy-fuel mode, as mentioned in **Paper A**;

- This research proves that the IACM instrument is a valuable instrument for online fuel quality control –for further details see **Paper II**;

- The developed calibration cell can be used to calibrate an IACM instrument for a fuel mixture and flue gas temperature that is specific for a power plant – more details are available in **Paper IV**.

The main conclusions from the innovative part are:

- It has been demonstrated that the DIAL technique can be utilized for alkali-chloride measurements when only one optical access is available –for example in a boiler at a power plant –more details can be found in **Paper I**;

- The applicability of the LI-PFF technique permits to visualise the location of the formations of alkali chlorides in the flame and post flame regions –more details can be found in **Paper III.**

7 Outlook

Five years may appear like a rather long time where a project could come to a closure with relative ease. Starting up a project from an idea where everything seems to be crystal clear is quite easy. During the project journey, however, there is usually a point of realization that unforeseen challenges do crop up along the path and that suddenly time becomes of the essence or, rather, appears insufficient. Since research programmes such as this one come along with inevitable time constraints, there are still a few aspects that have fallen by the wayside, some of which will be mentioned below.

There are still some parameters that can be further optimized when it comes to the calibration cell and the furnace. One aspect that could be considered for change in respect of the calibration cell relates to the re-design of the salt reservoir to make it less bulky and so that it contains less potassium chloride to get an even more well-defined salt temperature and subsequently a more accurate vapour pressure, where the concentration is determined from. In addition to this it would be advisable to change the position of the thermocouples that measure the cell temperature to ensure that they are not affected by radiation from the tube, where the cooling media is transported to the salt reservoir. A further aspect worth looking into is the re-design of the manner in which the temperature is measured on the salt reservoir so that the thermocouple does not displace and measure an incorrect salt reservoir temperature. The self-designed furnace renders a small inhomogeneity in the cell temperature. Hopefully this issue could be solved or at least be minimized in collaboration with a furnace company. Further investigation should be pursued targeting the incorporation of the new optics with the parabolic mirrors and the deuterium lamp into the IACM instrument. The obtained knowledge about the absorption region of KOH and NaOH introduces some curiosity to broaden the spectral range of the spectrometer to be able to determine the contribution of those two alkali compounds. The DIAL technique that was used in the laboratory for spatially-resolved measurements of KCl concentrations seems to be hard to implement at this stage based on my experience in the field. However, to avoid use of complex short-pulse lasers an initial approach would be to test this concept by means of the recently introduced Scheimpflug technique for LIDAR. Finally, flame studies by

means of LI-PFF measurement designed for specific measurements of chlorides and hydroxides to further investigate the formation of alkali chlorides in the flame at different air to fuel ratio are also of interest.

Acknowledgements

During my time as a PhD student at the Department of Combustion Physics at Lund University I have met a lot of interesting people who have played a role in the research and thesis to be defended in December. Since five years is a long time, it can be difficult to remember everyone that has kindly helped or contributed to this work. I will therefore start by expressing my deepest gratitude to those whose names I may have forgotten to mention in this section. You know who you are.

I want to thank Marcus Aldén (Head of Division), for opening the doors of the Department of Combustion Physics and providing me with two supervisors competent in their fields: Zhongshan Li, my main supervisor, and Christian Brackmann, as co-supervisor. I would like to thank Zhongshan and Christian for their time and patience and for helping me to carry out this project successfully.

I also want to thank my colleagues at Vattenfall AB: Magnus Berg, Lennart Gårdman, Håkan Kassman, Elin Edvardsson, Jonas Alin, Ylva Odemark, Mattias Mattsson, Åsa Astervik, Shahriar Badiei, and Patrik Lidberg for their role in this project.

I thank my financial sponsors ChlorOut AB, Vattenfall AB, Lund University and CECOST for their support during these five years.

This type of projects also calls for assistance from an administrative and technical perspective, so I thank Minna Ramkull, Cecilia Bille, Igor Buzuk, Rutger Lorensson, and Håkan Ivansson for all the help during the years I have spent at the department.

I have also been a frequent visitor to Lund University's library, in particular the Physics Department, to borrow books and get copies of articles so I would like to profess my appreciation to Marianne Madsen and her colleagues.

I have also received help from people external to the university. Thanks are in order to Ingvar Artiles from Akademiska Hus as well as Leif Lundberg and colleagues from Scientific Lab Glass in Lund AB.

I also want to thank all my colleagues at Combustion Physics. Special thanks go to Pär Samuelsson for sharing the office space with me for his advice on Matlab and other

Appendix A

a. Calibration cell version 1

b. Calibration cell version 2

c. Calibration cell version 3
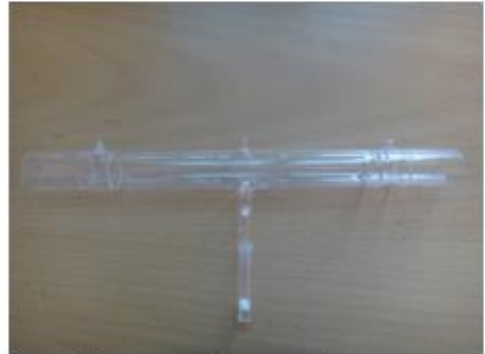
d. Calibration cell version 4

e. Calibration cell version 5

f. Calibration cell version 6

Appendix A. Development steps of the calibration cell.

Appendix B

a. Furnace version 1

b. Furnace version 2
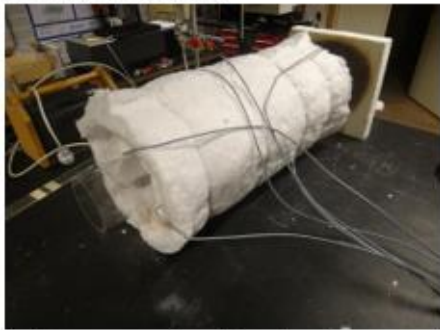
c. Furnace version 1 insulated

d. Furnace version 2 insulated

e. Furnace version 1 in operation

f. Furnace version 2 in operation

Appendix B. Two versions of the furnace. Version 2 was the final design.

Appendix C

a. IACM receiver, cross-stack

b. IACM transmitter, cross-stack

c. Shortening of path length, outside

d. Shortening of path length, inside

e. IACM receiver, cross-stack over a corner

f. IACM transmitter, cross-stack over a corner

g. IACM mirror probe used when only one access port is available

Appendix C. Possible IACM installations: cross-stack, reduced path length, corner mounting and with the mirror probe using one optical access port.

Appendix D
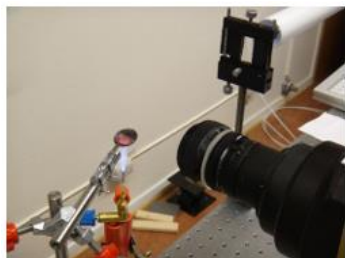
a. Generation of Gas-phase KCl by heating crystals of KCl in a spoon.
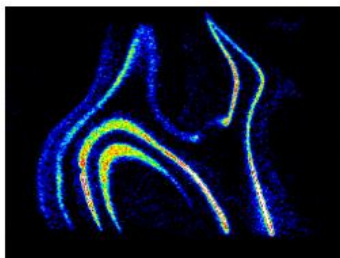
b. The firs image of photofragmented KCl vapour.
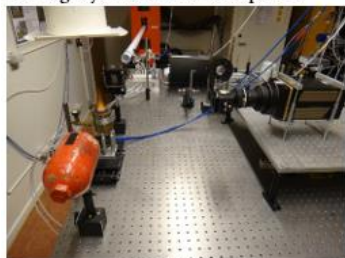
c. Generation of gas-phase KCl and NaCl in the product zone in a methane-air flame seeded with liquid mix of KCl and NaCl solution.
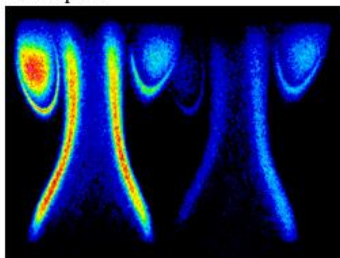
d. Image of gas-phase KCl and NaCl in the product zone from a methane-air flame seeded with a liquid mix of KCl and NaCl solution using a stereoscope.
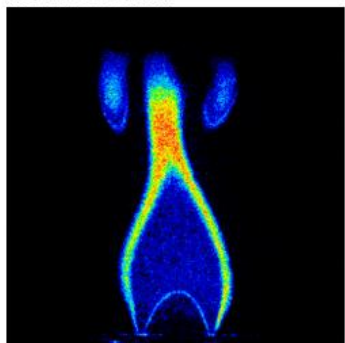
e. KCl image with double height of the laser sheet (same as in d).
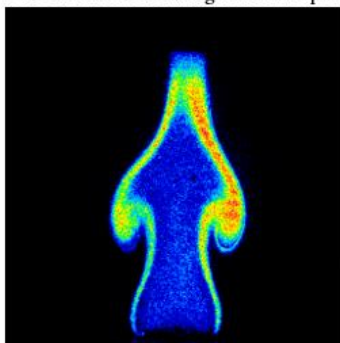
f. KCl image with double height of the laser sheet (same as in d).

Appendix D. The first photofragmentation images on KCl vapour: a smelt in a spoon and images from a stereoscope with two notch filters, including one for potassium (766 nm) and one for sodium (589 nm) obtained from a methane-air flame seeded with a mixture of KCl and NaCl.

References

1.   Balat, H., *Prospects of biofuels for a sustainable energy future: A critical assessment.* Energy Education Science and Technology Part a-Energy Science and Research, 2010. **24**(2): p. 85-111.

2.   Demirbas, A., *Potential applications of renewable energy sources, biomass combustion problems in boiler power systems and combustion related environmental issues/*Progress in Energy and Combustion Science, 2005. **31**(2): p. 171-192.

3.   Vassilev, S.V., D. Baxter, L.K. Andersen, and C.G. Vassileva, *An overview of the chemical composition of biomass.* Fuel, 2010. **89**(5): p. 913-933.

4.   Khan, A.A., W. de Jong, P.J. Jansens, and H. Spliethoff, *Biomass combustion in fluidized bed boilers: Potential problems and remedies.* Fuel Processing Technology, 2009. **90**(1): p. 21-50.

5.   Nielsen, H.P., F.J. Frandsen, K. Dam-Johansen, and L.L. Baxter, *The implications of chlorine-associated corrosion on the operation of biomass-fired boilers.* Progress in Energy and Combustion Science, 2000. **26**(3): p. 283-298.

6.   Öhman, M., A. Nordin, B.J. Skrifvars, R. Backman, and M. Hupa, *Bed Agglomeration Characteristics during Fluidized Bed Combustion of Biomass Fuels.* Energy & Fuels, 2000. **14**(1): p. 169-178.

7.   Johansen, J.M., J.G. Jakobsen, F.J. Frandsen, and P. Glarborg, *Release of K, Cl, and S during Pyrolysis and Combustion of High-Chlorine Biomass.* Energy & Fuels, 2011. **25**(11): p. 4961-4971.

8.   Forsberg, C., M. Broström, R. Backman, E. Edvardsson, S. Badiei, M. Berg, and H. Kassman, *Principle, calibration, and application of the in situ alkali chloride monitor.* Review of Scientific Instruments, 2009. **80**(2).

9.   Kassman, H., L. Bäfver, and L.E. Åmand, *The importance of SO_2 and SO_3 for sulphation of gaseous KCl - An experimental investigation in a biomass fired CFB boiler.* Combustion and Flame, 2010. **157**(9): p. 1649-1657.

10.   Kassman, H., J. Pettersson, B.M. Steenari, and L.E. Åmand, *Two strategies to reduce gaseous KCl and chlorine in deposits during biomass combustion - injection of ammonium sulphate and co-combustion with peat.* Fuel Processing Technology, 2013. **105**: p. 170-180.

11.   Sorvajärvi, T., J. Maunula, J. Silvennoinen, and J. Toivonen, *Optical detection of KCl vapor in 4 MW CFB boiler during straw combustion and ferric sulfate*

injection. in European Combustion Meeting, Lund, Sweden, June 25 - 28, 2013, 2013.

12. Leffler, T., C. Brackmann, M. Berg, Z.S. Li, and M. Aldén, *On-line Alkali Measurement for Fuel Quality Control in Biomass-operated Boilers.* Industrial Combustion, 2016.

13. Lee, C.D., W.M. Hird, P.A. Schofield, and I.R. Fantom. *Novel probe for alkali vapour sampling on the grimethorpe PFBC.* in *Proceedings of the 11th International Conference on Fluidized Bed Combustion.* 1991. New York, NY, United States, Montreal, Que, Can: Publ by ASME.

14. Mojtahedi, W., E. Kurkela, and M. Nieminen, *Release of Sodium and Potassium in the Pfb Gasification of Peat.* Journal of the Institute of Energy, 1990. **63**(456): p. 95-100.

15. Hald, P., *Alkali Metals at Combustion and Gasification, Equilibrium Calculations and Gas Phase Measurings*, in *Department of Chemical Engineering.* 1994, Technical University of Denmark.

16. Monkhouse, P., *On-line spectroscopic and spectrometric methods for the determination of metal species in industrial processes.* Progress in Energy and Combustion Science, 2011. **37**(2): p. 125-171.

17. Gottwald, U. and P. Monkhouse, *Single-port optical access for spectroscopic measurements in industrial flue gas ducts.* Applied Physics B-Lasers and Optics, 1999. **69**(2): p. 151-154.

18. Gottwald, U., P. Monkhouse, N. Wulgaris, and B. Bonn, *Simultaneous detection of nickel and potassium in the flue gas of a fluidised bed coal combustor by excimer laser-induced fragmentation fluorescence.* Fuel Processing Technology, 2003. **80**(2): p. 143-153.

19. Glazer, M.P., N.A. Khan, W. de Jong, H. Spliethoff, H. Schurmann, and P. Monkhouse, *Alkali metals in circulating fluidized bed combustion of biomass and coal: Measurements and chemical equilibrium analysis.* Energy & Fuels, 2005. **19**(5): p. 1889-1897.

20. Erbel, C., M. Mayerhofer, P. Monkhouse, M. Gaderer, and H. Spliethoff, *Continuous in situ measurements of alkali species in the gasification of biomass.* Proceedings of the Combustion Institute, 2013. **34**: p. 2331-2338.

21. He, Y., J. Zhu, B. Li, Z. Wang, Z. Li, M. Aldén, and K. Cen, *In-situ measurement of sodium and potassium release during oxy-fuel combustion of lignite using laser-induced breakdown spectroscopy: Effects of O_2 and CO_2 concentration.* Energy and Fuels, 2013. **27**(2): p. 1123-1130.

22. Sorvajärvi, T., N. DeMartini, J. Rossi, and J. Toivonen, *In situ measurement technique for simultaneous detection of K, KCl, and KOH vapors released during*

combustion of solid biomass fuel in a single particle reactor. Appl Spectrosc, 2014. **68**(2): p. 179-84.

23.   Davidsson, K.O., K. Engvall, M. Hagström, J.G. Korsgren, B. Lönn, and J.B.C. Pettersson, *A surface ionization instrument for on-line measurements of alkali metal components in combustion: Instrument description and applications.* Energy & Fuels, 2002. **16**(6): p. 1369-1377.

24.   Andersson, C.S., *European Patent EP 1221036 (2006).* VATTENFALL AB PUBL (SE).

25.   Leffler, T., C. Brackmann, A. Ehn, B. Kaldvee, M. Aldén, M. Berg, and J. Bood, *Range-resolved detection of potassium chloride using picosecond differential absorption light detection and ranging.* Applied Optics, 2015. **54**(5): p. 1058-1064.

26.   Banwell, C.N. and E.M. McCash, *Fundamentals of molecular spectroscopy.* 1994, London; New York: McGraw-Hill.

27.   Eckbreth, A.C., *Laser diagnostics for combustion temperature and species.* 1988, Australia [etc.]: Gordon and Breach.

28.   Zhao, F.Q. and H. Hiroyasu, *The Applications of Laser Rayleigh-Scattering to Combustion Diagnostics.* Progress in Energy and Combustion Science, 1993. **19**(6): p. 447-485.

29.   Miles, R.B., W.R. Lempert, and J.N. Forkey, *Laser Rayleigh scattering.* Measurement Science and Technology, 2001. **12**(5): p. R33-R51.

30.   Kohse-Höinghaus, K. and J.B. Jeffries, *Applied combustion diagnostics.* 2002, New York: Taylor & Francis.

31.   Rodgers, M.O., K. Asai, and D.D. Davis, *Photofragmentation Laser-Induced Fluorescence - a New Method for Detecting Atmospheric Trace Gases.* Applied Optics, 1980. **19**(21): p. 3597-3605.

32.   Simeonsson, J.B. and R.C. Sausa, *A critical review of laser photofragmentation fragment detection techniques for gas phase chemical analysis.* Applied Spectroscopy Reviews, 1996. **31**(1-2): p. 1-72.

33.   Sorvajärvi, T., J. Saarela, and J. Toivonen, *Optical detection of potassium chloride vapor using collinear photofragmentation and atomic absorption spectroscopy.* Optics Letters, 2012. **37**(19): p. 4011-4013.

34.   Johansson, O., J. Bood, M. Aldén, and U. Lindblad, *Detection of hydrogen peroxide using photofragmentation laser-induced fluorescence.* Applied Spectroscopy, 2008. **62**(1): p. 66-72.

35.   Oldenborg, R.C. and S.L. Baughcum, *Photofragment Fluorescence as an Analytical Technique - Application to Gas-Phase Alkali Chlorides.* Analytical Chemistry, 1986. **58**(7): p. 1430-1436.

36.   Hartinger, T.K., S. Nord, and B.P. Monkhouse, *Quenching of fluorescence from Na(32P) and K(42P) atoms following photodissociation of NaCl and KCl at 193 nm.* Applied Physics B, 1997. **64**(3): p. 363-367.

37.   Hartinger, K.T., P.B. Monkhouse, and J. Wolfrum, *Determination of Alkali Traces in Coal Combustion by Excimer-Laser Induced Fragmentation Fluorescence.* Berichte Der Bunsen-Gesellschaft-Physical Chemistry Chemical Physics, 1993. **97**(12): p. 1731-1734.

38.   Chadwick, B.L., G. Domazetis, and R.J.S. Morrison, *Multiwavelength Monitoring of Photofragment Fluorescence after 193-Nm Photolysis of Nacl and Naoh - Application to Measuring the Sodium Species Released from Coal at High-Temperatures.* Analytical Chemistry, 1995. **67**(4): p. 710-716.

39.   Strong, F.C., *Theoretical Basis of the Bouguer-Beer Law of Radiation Absorption.* Analytical Chemistry, 1952. **24**(2): p. 338-342.

40.   Davidovi.P and D.C. Brodhead, *Ultraviolet Absorption Cross Sections for Alkali Halide Vapors.* Journal of Chemical Physics, 1967. **46**(8): p. 2968-&.

41.   Terenin, A., *Anregung von Atomen und Molekülen zur Lichtemission durch Einstrahlung. II.* Zeitschrift für Physik, 1926. **37**(1-2): p. 98-125.

42.   Hanson, R.K., R.M. Spearrin, and C.S. Goldenstein, *Spectroscopy and optical diagnostics for gases.* 2016.

43.   Davidovits, P. and D.L. McFadden, *Alkali halide vapors : structure, spectra, and reaction dynamics.* 1979, New York: Academic Press.

44.   Platt, U.P., D, *Measurements of Atmospheric Trace Gases by Long Path Differential UV/Visible Absorption Spectroscopy*, in *Optical and Laser Remote Sensing*, D.K. Killinger and A. Mooradian, Editors. 1983, Springer-Verla Berlin Heidelberg New York. p. 97-105.

45.   Mellqvist, J., H. Axelsson, and A. Rosén, *DOAS for flue gas monitoring .3. In-situ monitoring of sulfur dioxide, nitrogen monoxide and ammonia.* Journal of Quantitative Spectroscopy & Radiative Transfer, 1996. **56**(2): p. 225-240.

46.   Mellqvist, J. and A. Rosén, *DOAS for flue gas monitoring .1. Temperature effects in the UV/visible absorption spectra of NO, NO₂, SO₂ and NH₃.* Journal of Quantitative Spectroscopy & Radiative Transfer, 1996. **56**(2): p. 187-208.

47.   Mellqvist, J. and A. Rosén, *DOAS for flue gas monitoring .2. Deviations from the Beer-Lambert law for the UV/visible absorption spectra of NO, NO₂, SO₂ and NH₃.* Journal of Quantitative Spectroscopy & Radiative Transfer, 1996. **56**(2): p. 209-224.

48.   Platt, U. and J. Stutz, *Differential optical absorption spectroscopy : principles and applications.* 2008, Berlin: Springer.

49.   Weitkamp, C., *Lidar : range-resolved optical remote sensing of the atmosphere.* 2005.

50. Kaldvee, B., J. Bood, and M. Aldén, *Picosecond-lidar thermometry in a measurement volume surrounded by highly scattering media.* Measurement Science and Technology, 2011. **22**(12).

51. Kaldvee, B., C. Brackmann, M. Aldén, and J. Bood, *Highly range-resolved ammonia detection using near-field picosecond differential absorption lidar.* Optics Express, 2012. **20**(18): p. 20688-20697.

52. Deitz, V., *The vapor pressure of potassium chloride and caesium iodide crystals.* Journal of Chemical Physics, 1936. 4(9): p. 575-580.

53. Vanderkemp, W.J.M., L.C. Jacobs, H.A.J. Oonk, and A. Schuijff, *The Vapor Composition and Pressure over Solid Potassium-Chloride - New Mass-Spectrometric Results and Effusion Masses.* Journal of Chemical Thermodynamics, 1991. **23**(6): p. 593-604.

54. Mayer, J.E. and I.H. Wintner, *Measurements of low vapor pressures of alkali halides.* Journal of Chemical Physics, 1938. **6**(6): p. 301-306.

55. Roine, A., *Outukumpu HSC chemistry for windows version 7.1.* 2011, Outokumpu Research: Pori, Finland

56. Thomson, G.W., *The Antoine Equation for Vapor-pressure Data.* Chemical Reviews, 1946. **38**(1): p. 1-39.

57. Alvarez, H., *Energiteknik. D. 1 D. 1.* 2003, Lund: Studentlitteratur.

58. Kasunic, K.J., *Optical systems engineering.* 2011, New York, NY [u.a.]: McGraw-Hill.

59. Andersson, C.S., *European Patent EP 1354167 (2006).* VATTENFALL AB PUBL (SE).

60. Van Loo, S. and J. Koppejan, *The handbook of biomass combustion and co-firing.* 2008.

61. Salmenoja, K., *Field and laboratory studies on chlorine-induced superheater corrosion in boilers fired with biofuels.* 2000, Åbo Akademi: Åbo.

62. Skoog, D.A., F.J. Holler, and S.R. Crouch, *Principles of instrumental analysis.* 2007.

63. Li, B., Z.W. Sun, Z.S. Li, M. Aldén, J.G. Jakobsen, S. Hansen, and P. Glarborg, *Post-flame gas-phase sulfation of potassium chloride.* Combustion and Flame, 2013. **160**(5): p. 959-969.

64. Schofield, K., *The chemical nature of combustion deposition and corrosion: The case of alkali chlorides.* Combustion and Flame, 2012. **159**(5): p. 1987-1996.

65. Ekvall, T., K. Andersson, T. Leffler, and M. Berg, *K–Cl–S chemistry in air and oxy-combustion atmospheres.* Proceedings of the Combustion Institute (2016).

Paper I

Range-resolved detection of potassium chloride using picosecond differential absorption light detection and ranging

Tomas Leffler,[1,2,*] Christian Brackmann,[1] Andreas Ehn,[1] Billy Kaldvee,[1] Marcus Aldén,[1] Magnus Berg,[2] and Joakim Bood[1]

[1]Division of Combustion Physics, Lund University, Box 118, 221 00 Lund, Sweden

[2]Vattenfall Research and Development AB, 814 26 Älvkarleby, Sweden

*Corresponding author: tomas.leffler@forbrf.lth.se

A laser diagnostic concept for measurement of potassium chloride (KCl) and potentially other alkali compounds in large-scale boilers and furnaces of limited optical access is presented. Single-ended, range-resolved, quantitative detection of KCl is achieved by differential absorption light detection and ranging (DIAL) based on picosecond laser pulses. Picosecond DIAL results have been compared experimentally with line-of-sight measurements using a commercial instrument, the *in situ* alkali chloride monitor (IACM), utilizing differential optical absorption spectroscopy. For centimeter-scale range resolution and a collection distance of 2.5 m, picosecond DIAL allowed for measurement of KCl concentrations around 130 ppm at 1200 K, in good agreement with values obtained by IACM. The DIAL data indicate a KCl detection limit of around 30 ppm for the present experimental conditions. In addition, a double-pulse DIAL setup has been developed and demonstrated for measurements under dynamic conditions with strong Mie scattering. The picosecond DIAL results are discussed and related to possible implementations of the method for measurements in industrial environments.   © 2015 Optical Society of America

OCIS codes: (280.1910) DIAL, differential absorption lidar; (280.3640) Lidar; (300.1030) Absorption.

http://dx.doi.org/10.1364/AO.54.001058

1. Introduction

Increasing fuel prices, environmental issues, and overall efforts to achieve sustainable energy supply require power-plant operators to increasingly consider utilization of fuels from biomass or municipal waste [1,2]. However, these types of fuels result in production of alkali chlorides such as potassium- and sodium-chloride (KCl and NaCl) in power-plant boilers. While KCl is mainly generated from biomass fuels such as demolition wood and agricultural residues, NaCl primarily originates from municipal waste [3]. These alkali chlorides are key components for slagging and fouling in power-plant boilers and affect heat-exchange surfaces [3]. Slagging occurs in the hotter parts, e.g., at the furnace walls due to flame radiation. Fouling occurs in the colder parts, e.g., in the convection area, due to decrease in the temperature of the flue gas and suspended fly ash. Moreover, chlorine exposure increases the risk of corrosion on the furnace walls, super heaters, and economizers. Minimizing problems related to slagging, fouling, and high-temperature corrosion will increase operational time, improve steam data, and reduce maintenance costs.

There are a few methods to mitigate the problems related to alkali chlorides: switching to a fuel with less content of alkali and chlorine, co-combustion with a fuel that contains sulphur and minerals, or using the commercially available ChlorOut concept

[4,5]. The ChlorOut concept is based on the injection of a sulphate-containing additive for the conversion of gas-phase alkali chlorides to potassium sulphate (K_2SO_4), which is less harmful [6]. While the first two methods do not necessarily need a measuring device for the alkali chlorides, it is a great advantage in the third method, ChlorOut, for determination of the correct amount of sulphate-containing additives to reduce the concentration of the alkali chlorides. The concentration of gas-phase alkali chlorides (KCl + NaCl) can be measured with the *in situ* alkali chloride monitor (IACM), based on differential optical absorption spectroscopy (DOAS) in the wavelength range 200–300 nm [7,8].

Other optical methods for alkali chloride detection have also been developed, for example, a method for KCl detection based on KCl photofragmentation using UV laser pulses followed by infrared absorption [9,10]. Alternatively, alkali chlorides may be detected using photofragmentation fluorescence [11–13]. An extensive review of these and other methods for detection of metal species in industrial processes has been presented by Monkhouse [13]. The absorption methods mentioned above provide line-of-sight data, lacking spatial information on the alkali-chloride distributions. Laser-based diagnostic methods such as photofragmentation fluorescence allow for imaging with high spatial resolution provided that the optical access is sufficient [13]. However, optical access may be limited in boiler configurations. Nevertheless, spatially resolved measurements could clearly be of value when localizing regions with high alkali-chloride concentrations for improved assessment and handling of surface deposits and corrosion.

The light detection and ranging (LIDAR) concept provides a method for range-resolved detection of backscattered laser light, which is beneficial under conditions with only one optical access to the measurement region. Extension to differential absorption LIDAR (DIAL), utilizing two different wavelengths with different absorption cross sections for the species of interest, allows for species-specific measurements. LIDAR and DIAL, which are mature techniques for long-range (km) atmospheric measurements [14] with range resolution on the order of 10–100 m, have both been demonstrated for short-range (1–10 m) applications in combustion environments [15–17] with range resolution down to sub-cm level. This work demonstrates and evaluates short-range DIAL, based on picosecond laser pulses, as a measurement technique for range-resolved KCl detection. The result is compared quantitatively with the concentration from the IACM instrument, which constitutes the reference. In addition, a double-pulse LIDAR setup is demonstrated to perform DIAL of KCl under dynamic measurement conditions with strongly varying scattering.

2. Experimental Setup

The experimental setup is schematically outlined in Fig. 1. The fundamental radiation, 1064 nm, of a mode-locked picosecond Nd:YAG laser (Ekspla, PL
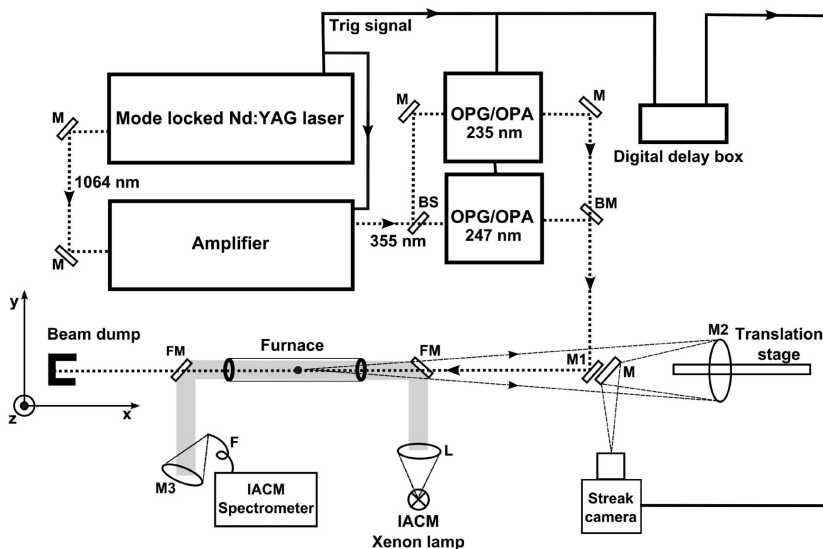
Fig. 1. Experimental setup for combined DIAL and IACM measurements on vaporized KCl. M designate planar mirrors, BS a beam splitter, and BM a beam combining mirror. The laser beams are guided into the furnace by mirror M1 and backscattered laser light is collected with concave spherical mirror M2. For IACM, L is a plano–convex lens for collimation of the Xenon lamp light (gray), FM indicates flip-in mirrors, and M3 is a concave spherical collection mirror.

2143C) is used to pump an external amplifier (Ekspla, APL 70-1100), which supplies two Optical Parametric Generator/Amplifier (OPG/OPA) systems (Ekspla PG401-P80-SH) with third harmonic radiation (355 nm). The OPG/OPA systems are tunable in the range 210–2300 nm with a line width specified to <4 cm^{-1}. Wavelengths of 247 and 235 nm were used for excitation on and off KCl resonance, respectively. Typical pulse energies used during the experiments were 0.3 to 1 mJ in the ultraviolet (UV) region. The laser pulses of 80 ps duration are generated at a repetition rate of 10 Hz, and the typical beam diameter is 12 mm.

Backscattered light was collected by a Newtonian-style telescope, having a concave 10 cm diameter primary mirror, M2, with a focal length of 45 cm and UV-enhanced aluminum coating. The primary mirror is placed on a 30 cm translation stage, allowing adjustable position of the focal plane. The collected light is directed toward the detector using a planar mirror M, having similar coating as M2.

A. Combined DIAL and IACM

Detection of KCl was investigated using two experimental configurations for DIAL. In experiments combined with IACM, backscattering along the y axis (see the Cartesian reference system in Fig. 1) was imaged onto the horizontal slit of a streak camera (Optronis, OptoScope, 19.5 × 14.4 mm CCD chip with 1392 × 1024 pixels). The streak camera enables time-resolved measurements where each point in time corresponds to a certain position of the laser pulse along the x axis. Thus, in the resulting streak-camera image the horizontal axis corresponds to time, i.e., position along the x axis, and the vertical axis represents position along the slit, i.e., location along the y axis. The ultimate time resolution is dictated by the laser pulse duration, i.e., 80 ps, corresponding to a range resolution of 0.5 cm. However, the time resolution, and accordingly the range resolution, is also dependent on the temporal response of the detector, governed by the streak rate, which can be set from 10 ps/mm to 1 ns/mm. As shown in Fig. 1, DIAL can be implemented using laser pulses from separate OPG sources, which in principle allow for simultaneous DIAL measurements using single-image acquisition, provided that the signals are sufficiently separated in the image. Nevertheless, to obtain maximum freedom of choice of detection parameters, DIAL measurements on and off KCl resonance were in this case made separately. If no KCl or any other interfering absorbing species is present, the ratio between the LIDAR signals recorded at the two wavelengths should ideally be constant throughout the measurement volume. Compensation for small imperfections in the coaxial alignment of the two laser beams could be obtained from reference measurements at the two wavelengths, carried out before KCl was placed in the measurement volume.

The IACM setup consists of a transmitter, a receiver, and a computer. Light from the transmitter high-pressure xenon lamp (Hamamatsu, L2273) is collimated using a 50 mm diameter plano–convex UV-grade fused silica lens, L, having a focal length of 150 mm. A pair of UV coated aluminum flip-in mirrors, FM, was used to direct the collimated light through the measurement volume toward the receiver. The light is collected and focused with a 2″ diameter spherical enhanced-aluminum mirror, M3, having a focal length of 2″, into an optical fiber (Azpect Photonics, FC-UV600-0.5-SR), F, connected to a deep-UV spectrometer. The spectrometer (Azpect Photonics, AVABENCH-75-2048) has an entrance slit of 50 μm width and a grating with 2400 grooves/mm.

For vaporization of KCl grains, a tube furnace was designed with the following components: ceramic tube (inner diameter 30 mm, length 300 mm), coiled with heating wire (Kanthal) and insulated (Fibrax) all the way out toward the ends to achieve temperature distribution that is as uniform as possible inside and reduce condensation of KCl. The tube was positioned at a distance of 2.5 m from the LIDAR telescope collection mirror M2.

The combined DIAL/IACM measurement procedure consisted of the following steps: 235 nm LIDAR reference measurement, insertion of a mirror at position BM for reflection of 247 nm, followed by a LIDAR reference measurement at this wavelength. Then the IACM mirrors (FM) were raised in position, a KCl grain was placed close to the furnace center, and IACM data were acquired during the initial vaporization. Thereafter, the IACM mirrors were lowered to their original position and the 247 nm on-resonance LIDAR measurement was carried out. The mirror at position BM for the 247 nm beam was then removed and the 235 nm off-resonance LIDAR measurement was carried out. To obtain similar total signal strengths, 250 LIDAR curves were accumulated for the 235 nm measurement, while 500 LIDAR curves were accumulated for the 247 nm measurement.

B. Double-pulse Differential Absorption Light Detection and Ranging

In the double-pulse DIAL experiments, KCl excitation on and off resonance was made with combined beams from the OPG units, which in principle allows for simultaneous measurements and data acquisition on a single-shot basis. The experimental arrangement for DIAL was similar to that shown in Fig. 1; however the mirror used at position BM was replaced by a dichroic mirror, reflecting the 247 nm beam while transmitting the 235 nm beam.

In addition, for improved sensitivity the backscattered signal was detected with a micro-channel-plate photomultiplier tube (MCP-PMT, Hamamatsu R5916U-50) characterized by rise and fall times of 170 and 730 ps, respectively. The PMT signal was acquired with a 3 GHz bandwidth digital oscilloscope (Lecroy Wavemaster 8300). Temporally, the laser pulses were separated by ~5 ns, with the

on-resonance pulses preceding the off-resonance pulses. The delay was chosen to enable scattering from both beams to be captured in the same oscilloscope sweep while avoiding interference from light scattered off the beam dump. Data from 100 laser pulse pairs were acquired in six measurements.

The response function of the PMT limits the optical resolution of the present setup to ~9 cm, however a longer (40.3 cm) tube furnace (Entech 89260 1.4 kW) used in these experiments ensured that a number of measurement points in the center is unaffected by the temperature drop at the edges of the tube. The tube furnace has a 5.8 cm diameter main tube, open in both ends, and a shorter perpendicular tube connected at the middle. An evaporation vessel of metal, with a volume of ~13 cm³, was partially filled with solid KCl and positioned in the shorter tube, perpendicular to the beam path, not to interfere with the optical path through the furnace. The short tube was plugged with glass wool to reduce the flow of vaporized KCl through the main tube. An air flow going from the short tube, where KCl was vaporized, through the main tube of the furnace was formed by having local exhaust ventilation at the openings of the main tube. The KCl temperature was measured to 1085 K, using a type-S thermocouple (Microtherma 2 thermometer), which is slightly above the melting temperature of KCl (1046 K)

3. Methods

A. Differential Absorption Light Detection and Ranging

Range-resolved concentration profiles are calculated using the simplified DIAL equation, Eq. (1), which is a part of the full DIAL equation [14]:

$$N(R) = \frac{1}{2\Delta\sigma}\frac{d}{dR}\ln\frac{P(R,\lambda_{\text{off}})}{P(R,\lambda_{\text{on}})}. \quad (1)$$

$N(R)$ is the number density of the absorbing molecule (KCl) at spatial coordinate R, $\Delta\sigma$ is the difference in KCl absorption cross section between the two wavelengths λ_{on} (247 nm), and λ_{off} (235 nm), shown in Fig. 2, and $P(R,\lambda_i)$ are the LIDAR signals detected on and off resonance.

From absorption cross-section data presented by Davidovits and Brodhead [18], the differential absorption cross section was determined to 1.2×10^{-17} cm². For the simplified DIAL equation to be valid, i.e., Eq. (1), extinction by gases other than KCl is assumed to be the same for both wavelengths. For the prevailing experimental conditions the only difference in extinction is due to the difference in the scattering cross section, δ_{sca}, at the two wavelengths. The contribution from this error source is <0.1 ppm. A further prerequisite for the simplified DIAL equation to be valid is that the ratio of the backscattering coefficients for the two wavelengths, δ_{sca}, is assumed to be range independent. Molecular scattering exhibits species-specific wavelength dependence, hence δ_{sca} becomes range dependent when large variations
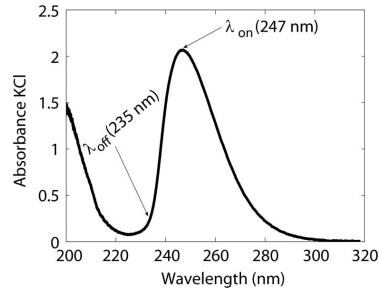

Fig. 2. Absorption spectrum of KCl with the DIAL excitation wavelengths λ_{off} (235 nm) and λ_{on} (247 nm) indicated.

in bulk-gas composition occur. To calculate the magnitude of this error, wavelength-dependent scattering cross sections for the bulk gases must be available. This error is often negligible and on sub-ppm level, but careful treatment of the measurement results should be practiced in regions with large bulk-gas variations. Moreover, to account for differences in the overlap of the laser-beam paths corresponding to λ_{off} and λ_{on}, the signal ratio $P(R,\lambda_{\text{off}})/P(R,\lambda_{\text{on}})$ in Eq. (1) can be compensated with a reference measurement ratio, $C(R)$, acquired with no KCl present.

B. In Situ Alkali Chloride Monitor

The IACM measurement technique is based on DOAS for which the Beer–Lambert law provides a linear relationship between absorbance and the concentration of the absorbing species. Given that optical path length and absorption cross section are known, species concentration can be determined. The operation principle and calibration routine of the IACM is described in detail by Forsberg et al. [7] and the total alkali chloride (KCl + NaCl) detection limit is 1 ppm for a measurement path of 5 m [7].

4. Results

A. Measurements on Single Grain KCl Vaporization

In order to make an adequate comparison, three complete time-reference series were recorded using IACM during the vaporization of single KCl grains of mass 0.03 g. These measurements gave a good indication of the full temporal-concentration profile. Figure 3 shows the average of three such vaporizing experiments that were performed before the combined DIAL/IACM experiment. Strong development of gas-phase KCl occurs during vaporization in the first few minutes followed by a slower decay due to gradual ventilation of the furnace.

Figure 4(a) shows an accumulated streak-camera LIDAR image employing the λ_{on} wavelength 247 nm. The image pixel intensities represent backscattered light, and horizontal image coordinates represent positions along the laser-beam path. The vertical image coordinate represents position on the streak-camera slit. An arrangement with the collection
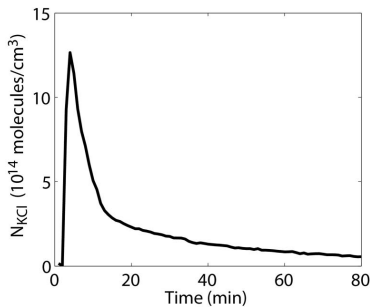
Fig. 3. KCl concentration versus time measured by IACM during single grain vaporization. The profile is an average of three experiments.

mirror placed in an off-axis position to improve signal collection [19], results in backscattered light from different axis positions to be imaged on different positions on the slit. This results in the diagonal image structure observed in Fig. 4(a). The intense vertical structure indicated by an asterisk is scattering from a reference object used to correct for time jitter between the laser pulse and laser-trigger signal when averaging multiple LIDAR images. Strong signals indicated by arrows are also obtained close to the openings of the tube furnace due to Mie scattering from cooled and condensed KCl as it mixes with the ambient laboratory atmosphere. The gas flow in these regions results in time-varying KCl concentrations, which cannot be evaluated from sequentially acquired DIAL data. However, inside the furnace conditions are more stable and the white box indicates an unaffected region inside the furnace for which the signal was integrated in vertical direction to yield one-dimensional LIDAR intensity curves. The ratio between two such LIDAR curves recorded using λ_{off} and λ_{on}, respectively, is shown in Fig. 4(b) while the final result is presented in Fig. 4(c). The concentration curve shows the highest KCl concentrations around the distance 0.15 m, corresponding to the middle of the furnace and lower KCl levels toward the edges. The mean number density of the evaluated region is ~8×10^{14} cm^{-3}, which corresponds to ~130 ppm at a temperature of 1200 K, measured by a thermocouple attached to the middle of the furnace. The results from the IACM measurements carried out before and after the DIAL measurements are shown in Fig. 5, indicating that in the time interval of the DIAL measurements, the average KCl concentration in the tube furnace could be expected to be in the range 0.3–1.7 × 10^{15} cm^{-3}. While the slow decrease in the KCl concentration observed toward the furnace edges, as shown in Fig. 4(c), represent dilution with ambient air, the short-range variations represent the measurement and evaluation accuracy for this configuration. These variations suggest a detection limit of 2×10^{14} cm^{-3} corresponding to 30 ppm at 1200 K. For comparison, alkali chloride
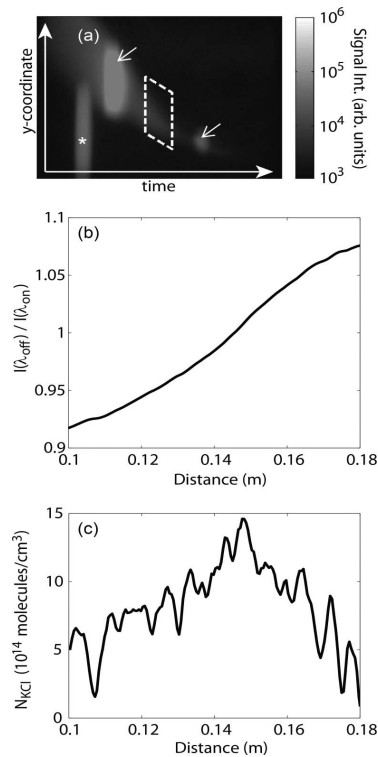
Fig. 4. Panel (a) shows a streak-camera image recorded with the laser tuned to $\lambda_{on} = 247$ nm, white box indicates the region integrated to yield one-dimensional LIDAR curves. Panel (b) shows the ratio between two such LIDAR curves measured on and off KCl resonance at 247 and 235 nm, respectively. The evaluated KCl number density is shown in panel (c).

concentrations down to 1 ppm have been measured with IACM at similar temperature for an absorption path length of 5 meters [7]. Scaling this limit to

Fig. 5. KCl concentration profile monitored by IACM before and after the ps-DIAL measurements carried out during the time interval where the curve is broken.

centimeter scale comparable with the ps-DIAL range resolution suggests that concentration levels at least down to 100 ppm should be detectable, i.e., in reasonable agreement with the detection limit estimated from the DIAL data.
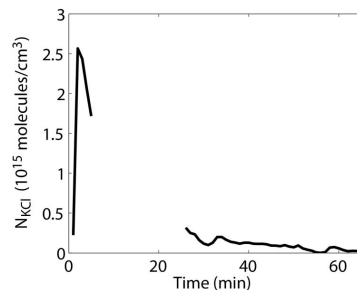
B. Double-pulse LIDAR Setup for DIAL Measurements in Harsh Conditions

Non-stationary conditions require simultaneous measurements at the two DIAL wavelengths, which can be achieved using the double-pulse LIDAR setup. Local condensation of KCl was observed as condensation streaks along the vapor flow inside the tube furnace and resulted in dynamic fluctuations in the backscattering signals.

Condensation has a two-fold effect as it reduces gas-phase KCl concentration but also enhances the amount of condensed KCl, which has a much higher back-scattering cross section than KCl in gas phase.

Six separate double-pulse measurements were conducted within a 40 minute time frame and the data are shown in Figs. 6(a) and 6(b) where each signal pair is displayed in different color. The differences in LIDAR signals between the six pairs

are evident. Equation (1) was employed to determine the KCl concentration, and evaluated profiles are shown in Fig. 6(c). The lower spatial resolution obtained for detection using the PMT results in some spatial averaging over the evaluated range. However, the sequentially measured profiles show good agreement, confirming that double-pulse DIAL provides consistent KCl concentrations despite the large signal fluctuations. This is further demonstrated in Fig. 6(d), showing KCl concentrations evaluated from the six different measurements at distance 0.57 m.

The evaluated number densities for the six measurements, shown in Fig. 6(d), are in the range $6-8 \times 10^{14}$ cm^{-3}. The higher values around 7.5×10^{14} cm^{-3} correspond to the KCl vapor pressure calculated for 930 K and a relative concentration of 95 ppm at this temperature. The comparison with vapor pressure suggests that the gas temperature could thus be as much as 150 K lower than that measured in the KCl reservoir. A lower gas temperature seems realistic due to mixing with colder ambient air during ventilation of the furnace.

To further point out the necessity of the double-pulse concept under these experimental conditions,
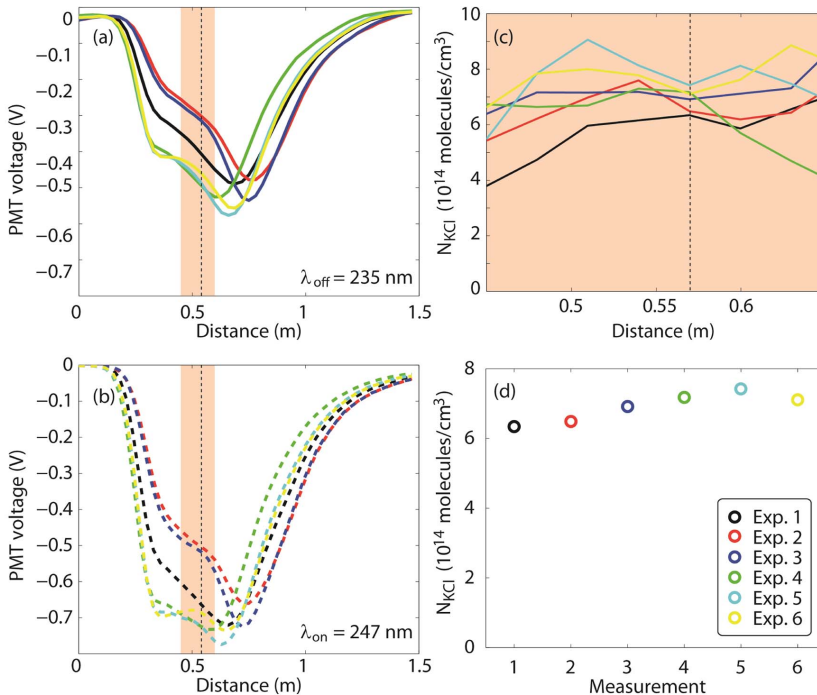
Fig. 6. Double-pulse ps-DIAL data, each signal consists of 100 single shots and each pair is displayed in different color coding. Raw-data of the back-scattered signal from (a) 235 nm and (b) 247 nm. (c) Range-resolved concentration data of KCl inside the tube furnace. The range is indicated with a colored area in (a) and (b). (d) Number densities evaluated for the six signal pairs at distance 0.57 m, indicated by a dashed line in (a), (b), and (c).

sequential measurements at the two wavelengths have been mimicked by mixing signal pairs. The curves from the six different measurements were paired in cyclic order with a mismatch offset, starting with pairing $P_1(R, \lambda_{\text{off}})$ with $P_2(R, \lambda_{\text{on}})$, ... and $P_6(R, \lambda_{\text{off}})$ with $P_1(R, \lambda_{\text{on}})$, which has an offset of 1. In addition, four more evaluations were performed with offsets from 2 to 5. The values obtained from the correct double-pulse signal pairing evaluation, presented in Fig. 6(d), have a standard deviation of 5×10^{13} cm^{-3}, whereas the datasets of mixed signal pairs had standard deviations of 6.4×10^{14} cm^{-3}, i.e., more than one order of magnitude larger and similar to the evaluated KCl number densities. This analysis clearly confirms that a double-pulse setup is needed in order to perform correct ps-DIAL measurements under non-stationary conditions.

5. Conclusions

When evaporating single KCl grains, combined DIAL and IACM measurements show good agreement, which indicates that the quantitative result achieved is accurate. The shape of the concentration profile shown in Fig. 4(c) also seems realistic since it is reasonable to believe that the concentration should be higher in the center of the tube furnace where the grain of KCl is evaporated. The demonstrated double-pulse concept has potential for measurements under time-varying measurement conditions. Implementation of picosecond DIAL for applied measurements needs to consider the choice of laser source as well as detection system. Even though picosecond laser units have shown a continued technical development, tunable OPG units in their current stage are probably not sufficiently robust for use in the vicinity of combustion installations such as large boilers and furnaces. A more realistic approach could be to use the fourth and fifth harmonic of a single Nd:YAG laser at 266 and 213 nm, respectively. These wavelengths could provide reasonable on and off resonance measurements (see the KCl absorption spectrum in Fig. 2) however resulting in a differential absorption cross section reduced by a factor of two and correspondingly reduced detection sensitivity. In addition, the use of a single laser would permit implementation of the double-pulse concept if necessary. Alternatively, Raman shifting (in hydrogen) of the Nd:YAG fourth harmonic [20] could provide a beam around 300 nm to be used for off-resonance measurements. The choice of detector for picosecond DIAL is determined by the length of the measurement region, desired range resolution, and the amount of backscattered signal. Potentially, IACM combined with a picosecond DIAL setup designed for applied measurements could provide quantitative as well as range-resolved data on alkali-chloride concentrations. Altogether the picosecond DIAL technique permits single-ended range-resolved detection of KCl and shows good potential for further development and application in power-plant boilers and other industrial processes.

References

1. H. Balat, "Prospects of biofuels for a sustainable energy future: a critical assessment," Energy Educ. Sci. Tech. A **24**, 85–111 (2010).
2. A. Demirbas, "Potential applications of renewable energy sources, biomass combustion problems in boiler power systems and combustion related environmental issues," Prog. Energy Combust. **31**, 171–192 (2005).
3. S. van Loo and J. Koppejan, *The Handbook of Biomass Combustion and Co-Firing* (Earthscan, 2008).
4. C. Andersson, "A method for operating a heat-producing plant for burning chlorine-containing fuels," European Patent EP 1354167 B1 (17 May 2006).
5. P. Henderson, P. Szakalos, R. Pettersson, C. Andersson, and J. Högberg, "Reducing superheater corrosion in wood-fired boilers," Mater. Corros. **57**, 128–134 (2006).
6. M. Broström, H. Kassman, A. Helgesson, M. Berg, C. Andersson, R. Backman, and A. Nordin, "Sulfation of corrosive alkali chlorides by ammonium sulfate in a biomass fired CFB boiler," Fuel Process Technol. **88**, 1171–1177 (2007).
7. C. Forsberg, M. Broström, R. Backman, S. Badiei, M. Berg, and H. Kassman, "Principle, calibration, and application of the *in situ* alkali chloride monitor," Rev. Sci. Instrum. **80**, 023104 (2009).
8. C. Andersson, "A method and device for measuring, by photospectrometry, the concentration of harmful gases in the fumes through a heat-producing plant," European Patent EP 1221036 B1 (05 April 2006).
9. T. Sorvajärvi, J. Saarela, and J. Toivonen, "Optical detection of potassium chloride vapor using collinear photofragmentation and atomic absorption spectroscopy," Opt. Lett. **37**, 4011–4013 (2012).
10. T. Sorvajärvi and J. Toivonen, "Principles and calibration of collinear photofragmentation and atomic absorption spectroscopy," Appl. Phys. B **115**, 533–539 (2014).
11. U. Gottwald and P. Monkhouse, "Single-port optical access for spectroscopic measurements in industrial flue gas ducts," Appl. Phys. B **69**, 151–154 (1999).
12. C. Erbel, M. Mayerhofer, P. Monkhouse, M. Gaderer, and H. Spliethoff, "Continuous *in situ* measurements of alkali species in the gasification of biomass," Proc. Combust. Inst. **34**, 2331–2338 (2013).
13. P. Monkhouse, "On-line spectroscopic and spectrometric methods for the determination of metal species in industrial processes," Prog. Energy Combust. Sci. **37**, 125–171 (2011).
14. C. Weitkamp, *LIDAR: Range-Resolved Optical Remote Sensing of the Atmosphere*, (Springer, 2005).
15. B. Kaldvee, A. Ehn, J. Bood, and M. Aldén, "Development of a picosecond LIDAR system for large-scale combustion diagnostics," Appl. Opt. **48**, B65–B72 (2009).
16. B. Kaldvee, J. Bood, and M. Aldén, "Picosecond-LIDAR thermometry in a measurement volume surrounded by highly scattering media," Meas. Sci. Technol. **22**, 125302 (2011).
17. B. Kaldvee, C. Brackmann, M. Aldén, and J. Bood, "Highly range-resolved ammonia detection using near-field picosecond differential absorption LIDAR," Opt. Express **20**, 20688–20697 (2012).
18. P. Davidovits and D. C. Brodhead, "Ultraviolet absorption cross sections for alkali halide vapors," J. Chem. Phys. **46**, 2968–2973 (1967).
19. B. Kaldvee, "Development and application of single-ended picosecond laser diagnostics," Doctoral thesis (Lund University, 2012), pp. 45–46.
20. C. W. Wilkerson, E. Sekreta, and J. P. Reilly, "Raman shifting of picosecond light-pulses in hydrogen gas," Appl. Opt. **30**, 3855–3861 (1991).

Paper II

ON-LINE ALKALI MEASUREMENT FOR FUEL QUALITY CONTROL IN BIOMASS-OPERATED BOILERS

T. Leffler[1,2]*, C. Brackmann[2], M. Berg[1], Z. S. Li[2], M. Aldén[2]

[1]R&D, Strategic Development, Vattenfall AB, 814 26 Älvkarleby, Sweden

[2]Division of Combustion Physics, Lund University, Box 118, S-221 00 Lund, Sweden

*Corresponding author: Tomas Leffler, tomas.leffler@forbrf.lth.se

ABSTRACT

Today's power plants are shifting their combustion toward a more complex fuel mix on the grounds of environmental impact, cost, availability and regulations. Certain new types of fuel can be classified into the following groups: herbaceous material (straw and grass), agricultural by-products (pits, shells and hulls), wood, and waste fuels. These fuels contain various amounts of alkali metals, mainly potassium and sodium, as well as chlorine and sulphur, which are easily vaporised in the combustion process and are involved in processes that cause severe slagging, fouling and high-temperature corrosion problems in the furnace and further downstream in the boiler. In this study, combustion of three different biomass fuel mixes was investigated in a circulating fluidized bed boiler. An on-line alkali-chloride monitoring instrument was used to gather valuable information for evaluating the fuel quality in terms of harmful alkali chlorides, measuring the sum of alkali chlorides (potassium chloride and sodium chloride) based on ultraviolet absorption. In addition, two batches of wood biomass fuel were compared during combustion in a full-scale powder fuel boiler. In all cases the impact of changes in fuel composition on alkali-chloride formation levels were monitored quantitatively with a time resolution in the order of seconds, allowing for analysis and countermeasures. The study concluded that the employment of an on-line alkali monitoring device to prevent alkali-chloride problems is a cost-efficient, sustainable solution that extends the operational time of the boiler and reduces its maintenance costs.

Keywords: alkali metals, prevention of slagging, fouling and high-temperature corrosion, reduced maintenance cost

INTRODUCTION

Traditional combustion of oil, gas and coal for electricity generation and district heating has evolved toward the use of more complex fuel mixes of biomass. Such fuel mixes often have a base of wood chips and bark, which are then mixed with a moderate percentage of herbaceous material (straw and grass), agricultural by-products (e.g. almond pits, shells and hulls), forest residue, or peat. This change in fuel mix has come from environmental issues, availability, cost considerations, and regulations.

This type of biomass fuel mix is rich in alkali metals such as potassium (K) and sodium (Na), and also has a high content of chlorine (Cl). The alkali metals and the Cl react with each other during combustion, creating the more harmful gas-phase potassium chloride (KCl) and sodium chloride (NaCl) compounds. The chemistry of potassium and chlorine release from biomass fuels during combustion has for example been surveyed by Johansen et al. [1]. Vaporised alkali chlorides have the potential to cause severe slagging, fouling and high-temperature corrosion problems in the boiler further downstream when condensed on heat-exchanging surfaces. A key component concerning the severity of high-temperature corrosion is the amount of sulphur in the fuel mix, which has the ability to reduce alkali [2]. In addition, the risk for corrosion is determined by the boiler design and temperature in its different regions. Many boilers that are using this type of fuel mix were originally designed for coal-firing and have been converted to biomass-firing and are thus not ideally suited for this type of fuel.

Slagging and fouling decrease the operational time between planned maintenance stops of the plant and high-temperature corrosion increases the maintenance cost. A sustainable solution for these issues is needed to enable running these plants in a more cost-efficient manner.

A significant amount of research has been conducted in this field, aiming at understanding the formation and fate of alkali metals and chlorides from the different types of fuel to the flue gas, which later on condense on the heat-exchanging surfaces in the boiler. This requires sophisticated methods and instruments to detect alkali chlorides. In the beginning

of the 1990s alkali metal vapour was collected by means of sampling systems. British Coal and the Technical Research Centre of Finland both developed their own sampling systems to collect vapour of alkali metals in the flue gas. Hald [3] took the development of the sampling technique a bit further and included the total amount of chlorine in her construction, which, however, required certain conditions on the sampled flue gas flow to be fulfilled.

Later research has driven the development toward on-line measurements of metal species in the flue gas –in particular K and Na. The review by Monkhouse [4] gives the current status up to 2011 of different techniques for on-line detection of alkali metals in the flue gas. Glazer *et al* [5] utilize the Excimer Laser Induced Fluorescence (ELIF) technique for the detection of gas-phase alkali metals (K and Na) in the flue gas from Circulating Fluidized Bed (CFB) combustion of biomass with a high content of alkali and coal. Erbel *et al* [6] used the ELIF technique in gasification of biomass to detect K and Na. Sorvajärvi *et al* [7] have taken the fluorescence technique of detecting alkali metal (in this case potassium) vapour in the flue gas even further by combining it with diode laser absorption spectroscopy, allowing the tracking of the different chemical compounds of potassium, such as atomic K, potassium hydroxide (KOH) and KCl. In addition to optical methods, surface ionisation (SI) is another on-line measurement technique that offers detection of alkali metals in gas-phase and condensed on particles. This technique has been evaluated in power plants in Idbäcken and Nässjö in Sweden [8].

Today's environmental issues, emission legislations, different types of biomass fuels and their availability require power plants to run on more complex fuel mixes where the fuel quality, and in particular the contents of Cl, sulphur (S) and alkali metals such as K and Na, fluctuate considerably depending on which types of fuels are being used. To be able to minimise deposit growth on heat transfer surfaces and high-temperature corrosion that causes unnecessary disruption in the production of district heating and electricity for the power grid, a robust and reliable on-line flue gas measuring instrument that monitors the gas-phase alkali chlorides in the flue gas is needed. The concentration read from the instrument indicates how severe the actual fuel mix is for the boiler.

This article presents studies of the feasibility of using an instrument based on absorption spectroscopy in the ultraviolet regime, the In-situ Alkali Chloride Monitor (IACM) [9] as a tool for on-line control of fuel quality. It measures alkali-chloride levels that can be related to the corrosiveness of biomass fuel mixes (wood chips, bark, herbaceous material, agricultural by-products, forest residue, PVC and peat) in power plants. An additional feature of the IACM instrument is the possibility of measuring the sulphur dioxide concentration (SO_2) in the flue gas. Two cases will be presented. The first case shows in a well-controlled way that different fuel mixes (wood and straw pellets, wood and straw pellets + PVC and wood and straw pellets + peat) can render different concentrations of alkali chlorides in the flue gas monitored by the IACM. The second case shows the ability to detect differences in quality of fuel batches from different suppliers.

METHOD

Research circulating fluidised bed boiler

The 12 MW$_{th}$ Circulating Fluidised Bed (CFB) boiler used in this experiment is the well-known research boiler at Chalmers University of Technology in Gothenburg, Sweden, which has been described in several earlier publications [2, 10]. This CFB boiler has a nominal load of 8 MW$_{th}$ and was run on an average load of 6.3 MW$_{th}$ with a standard deviation of 0.3 MW$_{th}$ during the experiments. The main components of the boiler are shown in Figure 1a. The combustion air supplied to the boiler is divided into primary air (1) and secondary air (2). The fuel enters the boiler via the fuel feeder (3) located at the bottom part of the boiler and is combusted in the furnace (4), which has a cross section of 2.25 m^2 and a height of 13.6 m. The mix of sand and flue gas is separated in the cyclone (5) and the sand is transported back into the furnace via the particle seal (6). The concentration of gas-phase alkali chlorides, i.e. the sum of KCl and NaCl, are measured with the In-situ Alkali Chloride Monitor (IACM) (8) once the flue gas has left the cyclone via the cyclone outlet (7) and before it reaches the first heat exchanging surface. The measurement path length is 2.55 m (9).

Full-scale powder fuel boiler

The boiler used for long-term measurements is a pulverised fuel (PF) combined heat and power (CHP) boiler firing pellets and briquettes of wood. A schematic obtained from a CFD-model of the boiler is shown in Figure 1b. It was originally planned to run on oil, but was converted to coal during the construction phase and subsequently changed to biomass. The boiler has been fired exclusively with biomass from 2006 onwards and the conversion from firing fossil fuel to biomass-only fuel has led to a reduction of over 90% in emissions of CO_2. The ash from the pellet firing can be returned to the forest as fertiliser. The CHP can deliver 69 MW_e to the electrical grid and 138 MW_{th} to the district heating. The CHP's steam is delivered to the turbine at a pressure of 110 bar, a temperature of 520 °C and a mass flow of 78 kg/s.
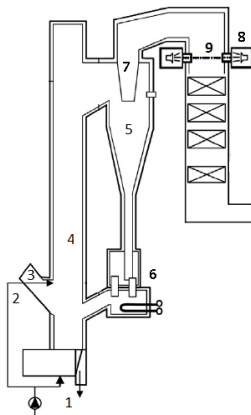
Figure 1a. Principle sketch of the Circulating Fluidized Bed (CFB) boiler with its key components listed below. 1. Primary air 2. Secondary air 3. Fuel feeding 4. Furnace 5. Cyclone 6. Particle seal 7. Cyclone outlet 8. IACM and 9. Measurement path length.
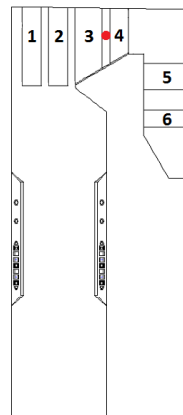
Figure 1b. Principle sketch of the PF boiler where the IACM is situated between superheater lll (3) and superheater lb (4). The location is marked with a red dot and the measurement path length is 8 m.

The IACM instrument

The IACM instrument consists of a receiver (Figure 2a), a transmitter (Figure 2b) and a computer. The UV light sent from the transmitter's high pressure xenon lamp (Hamamatsu, L2273) is collimated using a 50 mm diameter plano-convex UV grade fused silica lens with a focal length of 150 mm. The collimated light passes through the measurement volume, indicated by the number 9 in Figure 1a, toward the receiver. In the receiver the transmitted UV light is collected by a 50 mm diameter spherical UV-enhanced aluminium-coated mirror that has a focal length of 100 mm. Light from the spherical mirror is then focused onto an optical fibre (Azpect Photonics, FC-UV600-0.5-SR) that is connected in the opposite end to a deep-UV spectrometer (Azpect Photonics, AVABENCH-75-2048). The spectrometer has an entrance slit of 50 µm width and a 2400 L/mm grating. The signal from the spectrometer is evaluated and stored on a PC. A typical time resolution for the instrument is about 5 seconds with each read out being an average of 200 spectra, each in turn with an integration time of 25 ms. Photos of the installed IACM instrument boiler can be seen in Figure 2c (receiver) and Figure 2d (transmitter) for the research CFB boiler and in Figure 2e (transmitter) and Figure 2f (receiver) for long-term measurements in the PF boiler.
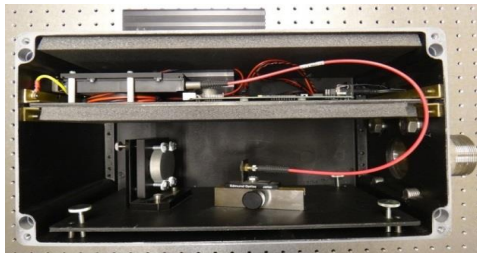
a. The IACM receiver showing collection mirror, optical fibre and spectrometer.

b. The IACM transmitter with xenon lamp and collimating lens.

c. The receiver mounted on the research CFB boiler.

d. The transmitter mounted on the research CFB boiler.

e. The transmitter mounted on the full-scale CHP boiler during long-term measurements.

f. The receiver mounted on the full-scale CHP boiler during long-term measurements.

Figure 2. Experimental set-up of the IACM system.

The IACM measurement technique is based on molecular absorption spectroscopy with broadband UV light in the wavelength region of 200 – 320 nm. The evaluation procedure is based on Differential Optical Absorption Spectroscopy (DOAS) [11] where the Beer-Lambert law provides a linear relationship between absorbance and the concentration of the absorbing species – see Equation 1.

$$I_t = I_0 \times e^{-cl\sigma} \tag{1}$$

$$Absorbance = \ln\frac{I_0}{I_t} = cl\sigma$$

$$I_t = transmitted\ light\ intensity$$

$$I_0 = incident\ light\ intensity$$

$$c = number\ density\ (molecules/cm^3)$$

$$I = optical\ path\ length\ (cm)$$
$$\sigma = absorption\ cross-section\ (cm^2/molecule)$$

Due to similarities in their UV absorption spectra, the IACM instrument is unable to distinguish between gas-phase KCl and NaCl, so the total alkali concentration measured is the sum of both, and the detection limit is 1 ppm for an optical path length of 5 m. The IACM instrument can be used in grate-fired boilers, bubbling fluidised bed boilers (BFB), circulating fluidised bed boilers (CFB) and powder fuel boilers (PF). The preferred position for installation is in front of the first super heater or in regions where the temperature is about 650 – 1300 °C. The positions for measurements in the CFB research boiler and the full-scale PF CHP boiler are indicated in Figure 1a and 1b.

The IACM instrument also has the ability to simultaneously measure the SO_2 and alkali chloride concentrations on-line in the flue gas. SO_2 has strong absorption bands in the wavelength ranges 200 – 230 and 290 - 310 nm [11], i.e. in the spectral regime already covered by the instrument. An instrument that measures these two parameters on-line is a powerful tool that effectively monitors the corrosiveness conditions during combustion of a particular fuel mixture.

Fuels used in the research circulating fluidised bed boiler

The research experiments using the circulating fluidized bed boiler are presented in the work published in [2]. Mixes of three different types of fuel (wood pellets, straw pellets, and peat) were used and a detailed fuel analysis is provided in Table 1. These fuel types have been selected to represent expected future fuel mixes for co-combustion of biomass and agricultural residues, and also give a broad fuel spectrum with significantly different ash chemistry. The experiment evaluated how the different fuel mixes, with different contents of K, Na, Cl and S, affect the composition of the flue gas and specifically relate to gas-phase alkali chlorides. To increase the load of chlorine in the fuel, PVC-granulates (Norvinyl, HYDRO) were fed to the fuel mix for some measurements. The three investigated fuel mixes, Case 1, Case 2, and Case 3, with their respective compositions, are described in detail in Table 2. Case 1 represents a fuel flow of 1035 kg(dry)/h wood pellets and 364kg(dry)/h straw pellets. Case 2 constitutes 1046 kg(dry)/h wood pellets,

310 kg(dry)/h straw pellets and an additional amount of 1.2 kg/h PVC to double the chlorine load compared to Case 1. Lastly, Case 3 represents co-combustion of 312 kg(dry)/h wood pellets, 340 kg(dry)/h straw pellets and 596 kg(dry)/h peat. The average amount of straw pellets in the fuel on an energy-basis during the experiment was 23.6% with a standard deviation of 2.0%. The calculations are based on the lower heating value (LHV), H, daf (Table 1) of each individual fuel.

	Wood pellets	Straw pellets	Peat
Proximate analysis			
Water (wt%, raw)	8.5	9.5	42
Ash (wt%, dry)	0.6	5.3	4.1
Combustibles (wt%, dry)	99.4	94.7	95.9
Volatiles (wt%, daf)	82	81	70
Ultimate analysis (wt%, daf)			
C	50.5	49.3	56.9
H	6	6.1	6.05
O	43.4	43.8	34
S	0.01	0.08	0.3
N	0.06	0.46	2.71
Cl	0.02	0.27	0.04
Ash analysis (g/kg dry ash)			
K	138	157	3.6
Na	7.5	6.3	1.3
Al	6.7	4	77
Si	116	230	150
Fe	8.8	3.4	159
Ca	152	72.4	92.7
Mg	29.8	12.2	13.1
P	13	12	11.9
Ti	0.4	0.3	1.5
Ba	2.2	0.7	1.6
Lower heating value (MJ/kg)			
H, daf	19.1	18.4	21.9
H, raw	17.1	15.5	11.2

daf = dry and ash free, raw = as received

Fuel-flow [kg(dry)/h]	Case 1	Case 2	Case 3
Wood pellets	1035	1046	312
Straw pellets	364	310	340
Peat			596
PVC		1.2	
Molar flows [mol/h]			
Alkali, (Na + K)	98	86	80
Chlorine, (Cl)	32.6	66.5	33.4
Sulphur, (S)	12.4	11.1	63.3
Molar ratios			
S/Cl	0.38	0.17	1.90
(Na + K)/2*S	3.95	3.87	0.63
(Na + K)/Cl	3.01	1.29	2.40

Table 1. Fuel element analysis [2].   Table 2. The compositions of the different fuel mixes [2].

Step response measurements

The alkali chloride measurements with the IACM instrument took place in position 8 indicated in Figure 1a. The optical path length at the measurement location was 2.55 m, the average temperature during the experiments was 795.4 °C, with a standard deviation of 8.0 °C, and the averaged excess air ratio was 1.24, with a standard deviation of 0.03. Three step-response experiments were carried out on three different fuel mixes.

Long-term measurements

The long-term alkali chloride measurements with the IACM instrument took place in the full-scale CHP boiler during the firing season between 20 November 2013 and 4 March 2014. The optical path length at the measurement point was 8 m and the flue gas temperature was 750 °C (Figure 1b).

RESULTS AND DISCUSSION

The results from the well-controlled experiments incorporating fuel step responses with different fuel mixes performed in the CFB research boiler are shown in Figures 3, 4 and 5, the fuel mix changes marked with vertical dashed lines. The results from long-term monitoring of the alkali chlorides in a commercial full-scale CHP pulverised fuel boiler are shown in Figure 6.

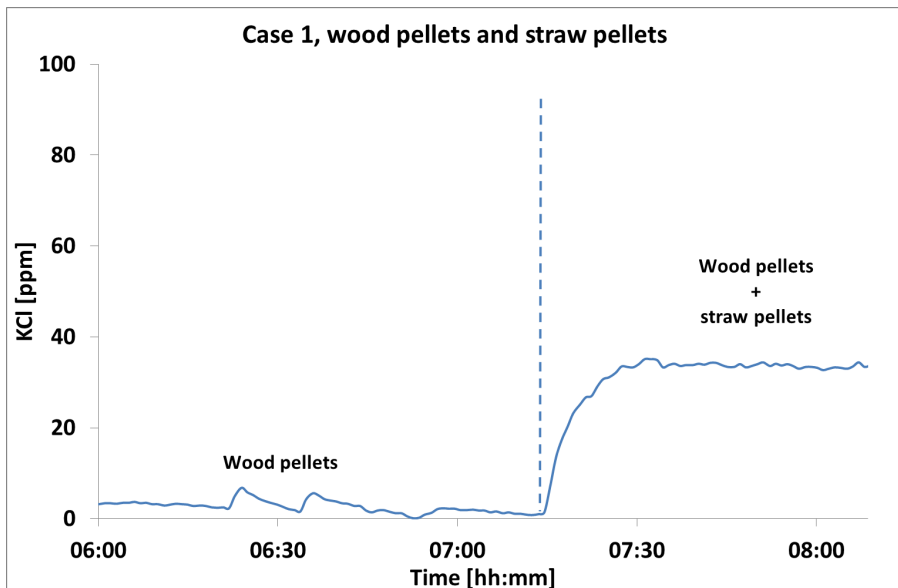**Fuel mix changes in the research circulating fluidised bed boiler**

Figure 3. Alkali-chloride concentration measured in the step-response experiment - Case 1, with a fuel mix of wood pellets and straw pellets (1035 + 364 kg(dry)/h). Note the rapid increase in KCl concentration after addition of straw pellets at 07:15 h.

Case 1

Figure 3 shows the step response for the gas-phase alkali concentration for Case 1, with a fuel mix of wood and straw pellets (1035 + 364 kg(dry)/h). Even though the wood pellets have a high potassium content, the amount of chlorine is low, resulting in a low average baseline KCl concentration of 3.7 ppm before the introduction of straw pellets to the fuel. At about 07:15 h, straw pellets, containing slightly higher levels of potassium compared to the wood but considerably more chlorine, are introduced in the fuel and the KCl concentration monitored by IACM increases instantaneously and reaches an average of 33.5 ppm in about 20 minutes.
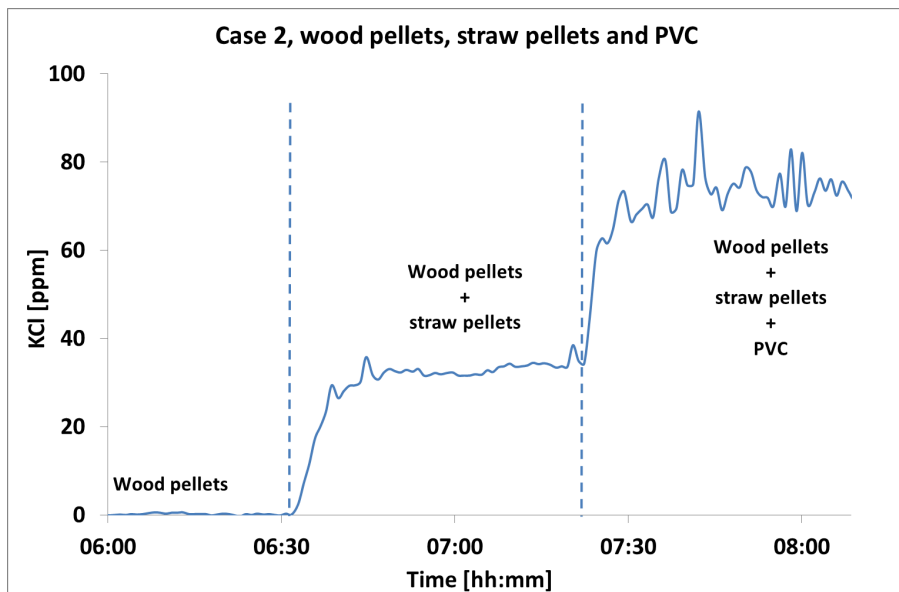

Figure 4. Alkali-chloride concentration measured in the step-response experiment - Case 2, with wood pellets, straw pellets and PVC (1046 + 3102 + 1.2 kg(dry)/h). Note the increase in KCl concentration after addition of straw pellets (06:30 h) and PVC granulates (07:23).

Case 2

Figure 4 presents the step responses for Case 2, with a fuel mix of wood pellets, straw pellets and PVC (1046 + 3102 + 1.2 kg(dry)/h). In this case, the baseline for KCl before the introduction of straw pellets and PVC is below the detection limit of 2 ppm under these conditions. At about 06:30 h, straw pellets are introduced in the fuel and similar to Case 1 the concentration of KCl reaches an average concentration of 32.5 ppm after approximately 20 minutes. At 07:23 h, the chlorine load in the fuel is increased to an amount double of that for Case 1, via the addition of PVC granulates. Approximately 25 minutes later an average KCl concentration of 71.7 ppm has been reached.

There are a few key fuel molar ratios that can be used to determine the environment to which the heat transfer surfaces will be exposed. Three are described below. The S/Cl, $(Na + K)/2S$ and $(Na + K)/Cl$ molar ratios describe which non-silicate alkali metal compound in the deposits are favoured at low or high temperature in a reducing or oxidising environment [3] and [12, 13]. Case 1 and Case 2 have fuel molar ratios of $(Na + K)/2S > 1$ and $(Na + K)/Cl > 1$, a temperature of 800 °C and an excess air ratio of 1.21. In these two cases, condensed non-silicate alkali metals exist in sulphates, carbonates and chlorides at temperatures below 800 °C but only in sulphates and carbonates at temperatures above 800°C [3]. The alkali-sulphur ratio $(Na + K)/2S$ is 3.95 and 3.87 for Cases 1 and 2, respectively, and the corresponding values of the sulphur-chlorine ratio S/Cl are 0.38 and 0.17. In both cases there is excess of alkali and chlorine and insufficient amounts of sulphur are available to completely reduce the alkali chlorides by formation of K_2SO_4. The alkali-chlorine ratio $(Na + K)/Cl$ is 3.01 and 1.29 for Cases 1 and 2, respectively, which indicates that the chlorine level is the limiting factor for alkali-chloride formation. This is also confirmed by the results of Case 2 (Figure 4) since the measured alkali chloride concentration increases by a factor close to two when doubling the chlorine load of the fuel mixture. In addition, this confirms that the IACM readout is linearly dependent on the alkali chloride concentration under the investigated experimental conditions.
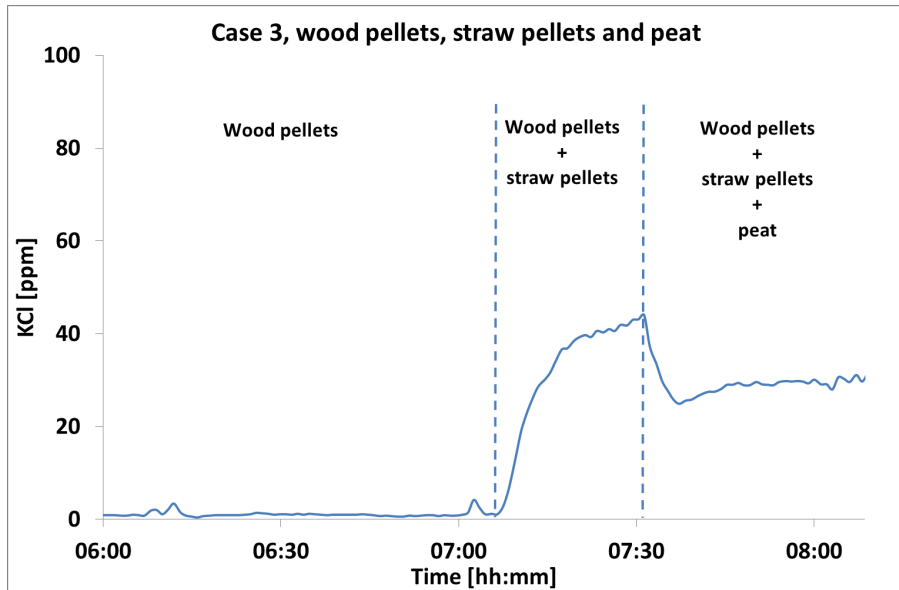
Figure 5. Alkali-chloride concentration measured in the step-response experiment - Case 3, with wood pellets, straw pellets and peat (312 + 340 + 596 kg(dry)/h). Note the changes in KCl concentration when introducing potassium- and chlorine-rich straw pellets at 07:15 h and sulphur-containing peat at 07:30 h, the latter resulting in KCl reduction.

Case 3

Figure 5 shows the step responses for Case 3, with a fuel mix of wood pellets, straw pellets and peat (312 + 340 + 596 kg(dry)/h). The baseline concentration of KCl before the introduction of straw pellets and peat is also in this case below the detection limit. At 07:07 h, straw pellets are introduced into the fuel and 25 minutes later the concentration has increased to 44 ppm but has not fully stabilised when the peat is introduced to the fuel at 17.32 h. After 30 minutes the concentration of KCl has stabilized at 32.2 ppm on average.

When practicing co-combustion, the fuel mix should be carefully chosen in respect of the alkali metals (K and Na), Cl and S in the fuel mix, as illustrated in Figure 5. Here the addition of sulphur-containing peat allows formation of K_2SO_4,

$2KCl + SO_2 + H_2O + 1/2\ O_2 \rightarrow K_2SO_4 + 2HCl$, consuming Cl and thus reducing the formation of alkali chlorides and the KCl level.

Case 3 has fuel molar ratios of $(Na + K)/2S < 1$ and of $(Na + K)/Cl > 1$, a temperature of 800 °C and an excess air ratio of 1.21. Condensed non-silicate alkali metals under these conditions exist in the form of sulphates at all temperatures [3]. The alkali-sulphur ratio of 0.63 is lower than the values for Case 1 (3.95) and Case 2 (3.87), while the alkali-chlorine ratio of 1.90 is higher than the values for Case 1 (0.38) and Case 2 (0.17). This indicates that the fuel mix in Case 3 is less harmful than the fuel mixes in Case 1 and Case 2, and that there should be no chlorides in the deposits.

The fuel molar ratio S/Cl can be used to compose a less harmful fuel mix for co-combustion, since it measures to which extent the fuel mix is corrosive [12]. Salmenoja [13] has developed a few rules of thumb to determine the corrosion tendency. If the S/Cl molar ratio in the fuel is lower than 2, it is regarded as corrosive and if it is higher than 4, it is regarded as non-corrosive. For intermediate values between 2 and 4, the corrosion in the super heaters is determined by boiler design and combustion parameters. These rules of thumb indicate that the fuel mixes used in Case 1 and Case 2 are strongly corrosive while the fuel mix in Case 3 is still corrosive but to a greater extent ruled by boiler design and combustion parameters.

Kassman [14] shows that the corrosive measure of the S/Cl molar ratio is also dependent on the form of the sulphur introduced into the boiler, which can be elemental sulphur or sulphates (SO_3), e.g. injected in the form of ammonium sulphate. The gas-phase alkali chlorides can be removed from the flue gas by the injection of ammonium sulphate at a S/Cl ratio that is lower than the ratio needed with elemental sulphur.

Figures 3 – 5 have shown that the In-situ Alkali Chloride Monitor (IACM) is able to rapidly detect changes in the fuel mix resulting in formation of harmful alkali chlorides. The response of the instrument allows for instantaneous on-line monitoring as clearly shown by the data presented. If a fuel mix contains a large amount of K, Na or both, it is

important to keep the Cl level low to prevent alkali chloride formation as shown in Figure 4, where addition of Cl by means of PVC allowed more of the K available in the biomass fuel to be utilised for KCl formation.

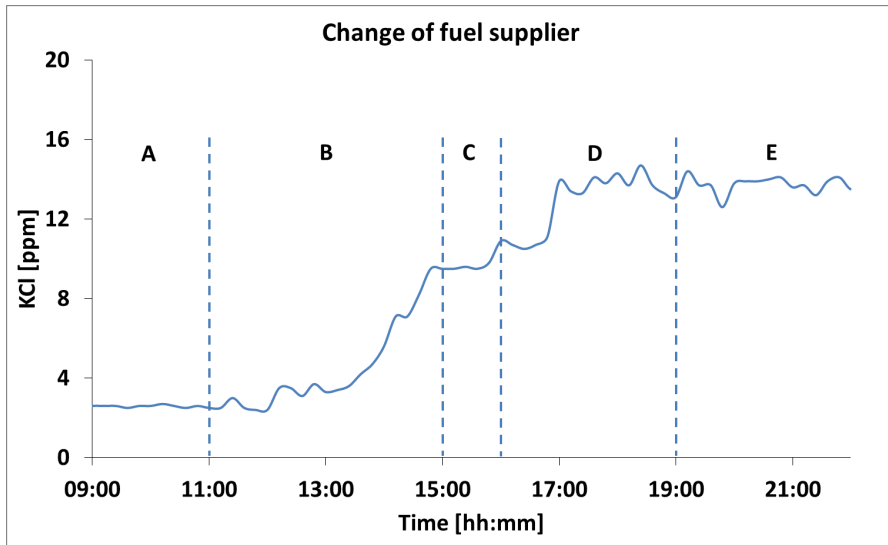**Long-term measurements in the full scale CHP boiler**

Figure 6. Alkali-chloride concentration measured during long-term monitoring of wood pellet combustion. A change in alkali-chloride concentration could be observed at around 12:00 h when changing to pellets from a different supplier. The sections indicated by dashed lines and labelled A-E represent different operational modes of the boiler.

Figure 6 shows results from long-term monitoring of alkali chlorides in a full-scale boiler during combustion of wood pellets. Sections A – E in Figure 6 describe different boiler load configurations during the case studied. The boiler load is expressed as a percentage of the boiler's total steam flow (78 kg/s). In section A, the boiler load started to decrease and the average value during this time span was 63.5%, while the average air excess ratio was 1.23. During section B, the boiler load was constant at an average of 59.2%, with an average air excess ratio of 1.24. Section C starts with a boiler load reduction, which ends at around 16:00 h. During that time span the boiler load had an average value of 55.6%

and an air excess ratio of 1.27. In section D, the boiler load was constant and had an average value of 50.0% and an air excess ratio of 1.29. In the final section, E, the boiler load decreased and reached its lowest average value of 44.5% while the air excess ratio reached its highest value of 1.32. During the 12 hours during which the case study was carried out the average standard deviation for the load was 1.6 % and for the air excess ratio it was 0.02. The flue gas temperature in the measurement region was determined to be about 750 °C on average and it is estimated that it can fluctuate 50 °C around the average value.

A gradual response due to a change in fuel quality is observed when introducing pellets from another fuel supplier. The baseline of KCl in section A, prior to the change in fuel, was 3.1 ppm on average. At around 12:00 h an increasing trend for the KCl concentration due to changes in the fuel composition starts, and it stabilises at an average concentration of 12.3 ppm at approximately 18:00 h, in section D. This demonstrates the feasibility of the IACM instrument for fuel-quality monitoring, clearly having sufficient sensitivity to distinguish differences in alkali-chloride formation between different batches of the same type of fuel.

CONCLUSION

To be able to correctly determine the corrosiveness of a fuel mix in co-combustion in a cost-effective and sustainable way and to institute a good means of avoiding potential deposit and corrosion problems, an on-line alkali chloride monitor would clearly be a valuable analysis tool. This has been proven by using an In-situ Alkali-Chloride Monitoring (IACM) device during three controlled fuel-step responses in a CFB research boiler as well as in long-term measurements in a full scale CHP boiler. The IACM instrument was able to accurately measure concentrations of gas-phase alkali chlorides on-line under relevant combustion conditions and showed instantaneous responses to changes in the fuel mixture composition. The detection sensitivity of the instrument is at ppm-level and was sufficient to detect a difference in alkali-chloride concentration of around 8 ppm between two batches of wood pellets provided by different fuel suppliers. The IACM instrument is therefore a valuable tool for on-line fuel quality control since it

detects changes in alkali-chloride formation from different fuels and provides opportunities to design proper fuel mixes for co-combustion while minimising corrosion problems.

REFERENCES

1. Johansen, J.M., et al., *Release of K, Cl, and S during Pyrolysis and Combustion of High-Chlorine Biomass.* Energy & Fuels, 2011. 25(11): p. 4961-4971.

2. Kassman, H., et al., *Two strategies to reduce gaseous KCl and chlorine in deposits during biomass combustion - injection of ammonium sulphate and co-combustion with peat.* Fuel Processing Technology, 2013. 105: p. 170-180.

3. Hald, P., *Alkali Metals at Combustion and Gasification, Equilibrium Calculations and Gas Phase Measurings*, in *Department of Chemical Engineering*. 1994, Technical University of Denmark.

4. Monkhouse, P., *On-line spectroscopic and spectrometric methods for the determination of metal species in industrial processes.* Progress in Energy and Combustion Science, 2011. 37(2): p. 125-171.

5. Glazer, M.P., et al., *Alkali metals in circulating fluidized bed combustion of biomass and coal: Measurements and chemical equilibrium analysis.* Energy & Fuels, 2005. 19(5): p. 1889-1897.

6. Erbel, C., et al., *Continuous in situ measurements of alkali species in the gasification of biomass.* Proceedings of the Combustion Institute, 2013. 34: p. 2331-2338.

7. Sorvajarvi, T., et al., *In Situ Measurement Technique for Simultaneous Detection of K, KCl, and KOH Vapors Released During Combustion of Solid Biomass Fuel in a Single Particle Reactor.* Applied Spectroscopy, 2014. 68(2): p. 179-184.

8. Davidsson, K.O., et al., *A surface ionization instrument for on-line measurements of alkali metal components in combustion: Instrument description and applications.* Energy & Fuels, 2002. 16(6): p. 1369-1377.

9. Forsberg, C., et al., *Principle, calibration, and application of the in situ alkali chloride monitor.* Review of Scientific Instruments, 2009. 80(2).

10. Kassman, H., L. Bafver, and L.E. Amand, *The importance of SO2 and SO3 for sulphation of gaseous KCl - An experimental investigation in a biomass fired CFB boiler.* Combustion and Flame, 2010. 157(9): p. 1649-1657.

11. Platt, U.P., D, *Measurements of Atmospheric Trace Gases by Long Path Differential UV/Visible Absorption Spectroscopy*, in *Optical and Laser Remote Sensing*, D.K. Killinger and A. Mooradian, Editors. 1983, Springer-Verla Berlin Heidelberg New York. p. 97-105.

12. van Loo, S. and J. Koppejan, *The handbook of biomass combustion and co-firing*. 2008, UK and USA in 2008: Earthscan.

13. Salmenoja, K., *Field and Laboratory Studies on Chlorine-induced Superheater, Corrosion in Boilers Fired with Biofuels*. 2000, Åbo Akademi, Åbo.

14. Kassman, H., *Strategies to Reduce Gaseous KCl and Chlorine in Deposits during Combustion of Biomass in Fluidised Bed Boilers*, in *Department of Energy and Environment Division of Energy Technology*. 2012, Chalmers University of Technology, Gothenburg, Sweden.

Paper III

Laser-Induced Photofragmentation Fluorescence Imaging of Alkali Compounds in Flames

Tomas Leffler[1,2], Christian Brackmann[1*], Marcus Aldén[1], Zhongshan Li[1]

[1]*Division of Combustion Physics, Lund University, Box 118, SE-221 00, Lund, Sweden*

[2]*Vattenfall Research and Development AB, SE-814 26 Älvkarleby, Sweden*

[*]*corresponding author: christian.brackmann@forbrf.lth.se*

ABSTRACT

Laser-induced photofragmentation fluorescence has been investigated for imaging of alkali compounds in premixed laminar methane-air flames. An ArF Excimer laser, providing pulses of wavelength 193 nm, was used to photodissociate KCl, KOH, and NaCl molecules in the post-flame region and fluorescence from the excited atomic alkali fragment was detected. Fluorescence emission spectra showed distinct lines of the alkali atoms allowing for efficient background filtering. Temperature data from Rayleigh scattering measurements together with simulations of potassium chemistry presented in literature allowed for conclusions on the relative contributions of potassium species KOH and KCl to the detected signal. Experimental approaches for separate measurements of these components are discussed. Signal power dependence and calculated fractions of dissociated molecules indicate the saturation of the photolysis process, independent on absorption cross section, under the experimental conditions. Quantitative KCl concentrations up to 20 ppm were evaluated from the fluorescence data and showed good agreement with results from ultraviolet absorption measurements. Detection limits for KCl photofragmentation fluorescence imaging of 0.5 and 1.0 ppm were determined for averaged and single-shot data, respectively. Moreover, simultaneous imaging of KCl and NaCl was demonstrated using a stereoscope with filters. The results indicate that the photofragmentation method can be employed for detailed studies of alkali chemistry in laboratory flames for validation of chemical kinetic mechanisms crucial for efficient biomass fuel utilization.

INTRODUCTION

Environmental issues and overall efforts to achieve a sustainable energy supply require power plant operators to increasingly consider utilization of a broader variety of biomass sources in the fuel mixture, such as herbaceous material (straw and grass), agricultural by-products (pits, shells and hulls) and municipal waste.[1, 2] However, many of these fuels result in the formation of alkali chlorides such as KCl and NaCl during combustion in power plant boilers. Alkali chlorides are key components for slagging and fouling and they also affect heat-exchange surfaces.[3] In addition, chlorine exposure increases the risk of corrosion on furnace walls, super heaters, and economizers.[4]

Problems related to alkali chlorides can be avoided using fuels with low content of alkali and chlorine, or suppressed by adding sulphur to the process – either by co-combustion with a sulphur-containing fuel or by injection of sulphur-containing additives.[5] Nevertheless, optimum reduction of alkali chlorides requires detailed understanding of the formation process and validation of mechanisms for alkali chemistry, which can be achieved by studies in laboratory flames under well-controlled conditions, see for example Li *et al.*[6] Potassium is the main alkali metal in many biomass fuels[7, 8] and a major component in many of the problems outlined above, thus knowledge on potassium chemistry is highly relevant for proper combustion of biomass fuels.

Laser-based techniques provide non-intrusive probing, in many cases species-specific, with high temporal and spatial resolution for detailed studies of combustion processes. A comprehensive review by Monkhouse[9] summarizes the status up to 2011 of different techniques for online detection of alkali metals in flue gas. Alkali chlorides, such as KCl and NaCl, can be detected by means of photofragmentation fluorescence for which Oldenborg *et al.*[10] used high-power laser pulses in the ultraviolet regime for photodissociation of alkali compounds followed by detection of fluorescence from the excited atomic alkali fragment. Furthermore, Chadwick et al.[11] investigated photofragmentation fluorescence detection of NaCl and NaOH (sodium hydroxide) using an Excimer laser of wavelength 193 nm for photodissociation and subsequent measurement of Na fluorescence signals at 589 and 819 nm for detection of NaCl and NaOH, respectively. Further investigations of the photofragmentation fluorescence technique have included NaOH detection by multi-photon fragmentation using the 355 nm third-harmonic output from a Nd:YAG laser[12] and studies of collisional quenching of the alkali metal atom fragments.[13]

The photofragmentation fluorescence technique has been applied for detection of alkali compounds in flue gas of Circulating Fluidized Bed (CFB) boilers. Investigations have been made for combustion of coal only[14-16] as well as for co-combustion with biomass with a high content of alkali.[17] Moreover, Erbel *et al.* used the technique in a study of biomass gasification.[18] Sorvajärvi et al. have further developed the technique, combining photofragmentation with absorption measurements of the atomic K fragments for enhanced sensitivity and quantitative concentration measurements.[19, 20] Furthermore, Sorvajärvi et al. have demonstrated this combination for simultaneous measurements of nascent atomic K, KCl, and KOH (potassium hydroxide) employing wavelengths 266 and 320 nm for photofragmentation of KCl and KOH, respectively.[21]

While previous studies include measurements in a single point or averaged along a line, also in practical combustion devices, spatially resolved imaging measurements are also of interest. Employed for detailed studies in laboratory flames such measurements could provide valuable insights for model development and validation. To investigate this approach photofragmentation fluorescence imaging is characterized in this study for detection of KCl and KOH in the post-flame region of premixed laminar methane-air flames seeded with alkali compounds. Investigations include assessment of interferences, comparison of signal levels, quantification, and estimation of detection limits. Moreover, simultaneous imaging of alkali species is demonstrated for NaCl and KCl in flame.

METHODS

Photofragmentation fluorescence measurements. The experimental set-up for photofragmentation fluorescence, schematically shown in Fig. 1a, contains an ArF Excimer laser (Compex 102, Lambda Physik), which provided pulses at wavelength 193 nm with 25 ns pulse duration and output pulse energy of 50 mJ.
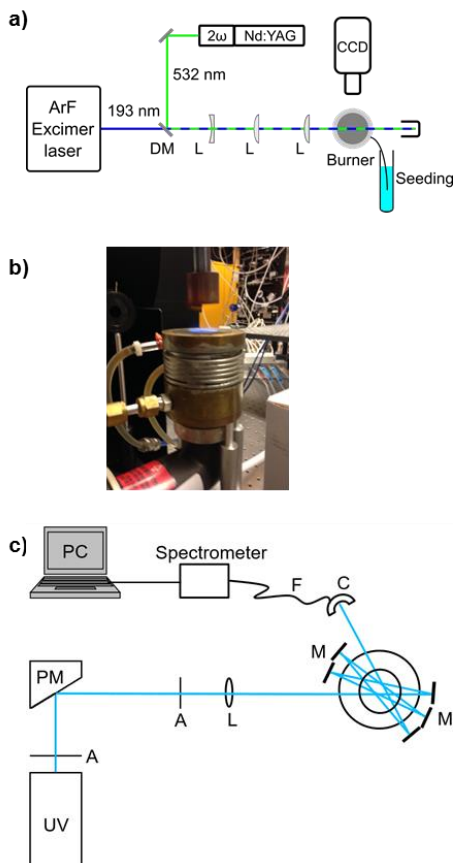
Fig. 1. a) Experimental set-up for laser-induced photofragmentation fluorescence and Rayleigh scattering using an ArF Excimer laser and a Nd:YAG laser, emitting wavelengths 193 nm and 532 nm, respectively. DM=Dichroic mirror, L=lenses. Measurements were made in premixed methane-air flames seeded with liquid alkali solution as illustrated to the right in the schematic. b) Photo of Perkin-Elmer burner with flat premixed methane-air flame. c) Set-up for UV absorption measurements. UV=light source, A=Aperture, PM=Parabolic mirror, L=Plano-convex lens, M=Mirrors, C=collimator, F=optical fibre.

For photofragmentation fluorescence measurements the 193 nm laser beam was focused into vertical sheets using different combinations of lenses. Measurements of photofragmentation fluorescence emission spectra of KCl, KOH, and NaCl were made with the beam focused into a 50 mm sheet using a cylindrical lens of focal length f=300 mm. The fluorescence was collected into a spectrometer (Acton SP-150, grating 300 grooves/mm, Princeton Instruments) using an UV condenser, f=60 mm, and a long-pass filter (WG280, Schott) to suppress scattered laser light. The signals were detected with an intensified CCD camera (PI-MAX I, Princeton Instruments) connected to the spectrometer. For imaging the detector was instead equipped with an f=50 mm objective (Nikkor f/1.4).

In measurements for quantitative analysis of the photofragmentation fluorescence signal, the 193 nm laser beam was focused using cylindrical lenses of focal lengths f=1000 mm and f=500 mm, which combined with an arrangement of razorblades resulted in a 20 mm vertical sheet. Measurements of potassium species were made using a bandpass filter centred at 766 nm (50 mm dia., OD 4, FWHM 10 nm, Edmund Optics) for detection of K-atom fluorescence and suppression of scattered laser radiation. Simultaneous measurements of KCl and NaCl were made using a stereoscope (Lavision) mounted in front of the objective. Band-pass filters centred at wavelengths 766 and 589 nm (50 mm dia., OD 4, FWHM 10 nm, Edmund Optics) were inserted in the stereoscope for detection of K- and Na-atom fluorescence signals, respectively.

A burner originally made for atomic absorption spectroscopy (Perkin-Elmer), shown in the photo of Fig. 1b, was used for measurements in alkali-seeded methane-air flames. The burner consists of a spray chamber and a water-cooled head with a central compartment for the premixed fuel-air blend and an outer channel for a co-flow shielding the flame. The diameter of the inner compartment is 23 mm and the head is topped by a circular mesh plate (pore size ~1 mm and length 20 mm). The burner allows for stabilization of flat laminar premixed flames (cf. Fig. 1b). Alkali-seeding is achieved using a nebulizer fed with part of the supplied air, which extracts liquid KCl-solution via a sample tube. The KCl-solution from the nebulizer is pre-treated in order to have only finer aerosol droplets to pass through the chamber to the burner head whereas larger droplets are removed via a drain tube. Methane and auxiliary air are mixed together with the nebulizer air in the burner's spray chamber to get the total correct fuel-air equivalence ratio (Φ) of the mixture.

A nitrogen co-flow of 10 l/min was supplied to the burner head to shield the flame. A steel cylinder (cf. Fig. 1b) was mounted 30 mm above the burner for flame stabilization required for quantitative signal analysis and to be able to make sequential photofragmentation and Rayleigh

scattering measurements under steady-state conditions. The total gas flow of air and fuel to the burner was 5.6 l/min and individual flows of nitrogen, air to the nebulizer, primary air, and fuel were controlled by four mass flow controllers with maximum flows of 20, 10, 5 and 1 l/min (Bronkhorst), respectively. Premixed stoichiometric methane-air flames were investigated and the KCl concentration in the seeding solution was varied from 0.01 to 3.0 M.

Rayleigh scattering measurements. The 532 nm second harmonic of a Nd:YAG laser (Brilliant B, Quantel) with a pulse duration of 7 ns and a pulse energy of 120 mJ was used for Rayleigh scattering measurements. The 532 nm beam was aligned into the beam path using a dichroic mirror, cf. Fig. 1a, and further shaped into a laser sheet of 10 mm height using cylindrical lenses of focal lengths f=-40 mm, f=200 mm, and f=500 mm. A half-wave plate positioned in the beam path was adjusted to achieve vertical polarization for optimal Rayleigh scattering.

Absorption measurements. KCl absorption measurements were made in the flames using the experimental set-up shown in Fig. 1c. UV light from a high-intensity (150 W) UV light source (L1314, Hamamatsu) was radiated through an aperture and collimated using a 90° off-axis parabolic mirror coated with UV-enhanced aluminium and a reflective focal length of f=150 mm (diameter 50 mm, Thorlabs). The collimated UV light beam subsequently passed through another aperture and a plano-convex focusing quartz lens of focal length f=150 mm. After the lens the UV beam passed over the burner top and was reflected five times using UV-enhanced aluminium mirrors (diameter 25.4 mm, Thorlabs) before it was collected in an UV-enhanced collimator (250 - 450 nm, diameter 12 mm beam, SMA, Thorlabs). This construction resulted in a total absorption path length of 138 mm. The collected UV light was then transferred through an optical fibre (FC-UV600-0.5-SR, Azpect Photonics) and subsequently dispersed in a spectrometer (grating 2400 grooves/mm, slit width 50 μm, AVABENCH-75-2048, Azpect Photonics). KCl concentrations were evaluated from the collected spectra by a least-squares fit to a calibration spectrum measured at 860 °C following the procedure presented by Forsberg et al.[22]

Fluorescence data evaluation. Alkali species concentrations have been evaluated from the photofragmentation fluorescence signal, F, which can be expressed in emitted photons by Eq. (1)

$$F = \frac{\Omega}{4\pi} l \varepsilon_F A \frac{A_{fi}}{A_{fi} + Q} TN \qquad (1)$$

where Ω the detection solid angle, l the probe volume length, ε_F the detection efficiency for the fluorescence signal, and A the probe volume cross section area. The ratio $\dfrac{A_{fi}}{A_{fi}+Q}$ represents the fluorescence quantum yield where A_{fi} is the Einstein coefficient for spontaneous emission, Q the collisional quenching rate, and T represents a factor accounting for fluorescence losses due to absorption, so-called trapping. The quantity N is the concentration of alkali atoms generated in the excited K-atom 4^2P states by photofragmentation. The fluorescence is obtained from the 4^2P transitions at 766 and 769 nm and the frequencies are $v=3.91\cdot10^{14}$ s^{-1} and $v=3.89\cdot10^{14}$ s^{-1}, respectively. Assuming that K-atom photofragments are distributed between both the 4^2P states, the average of the coefficient for spontaneous emission for the two transitions can be employed in the evaluation, using values presented by Nandy et al. [23] give $A_{fi}=3.8\cdot10^7$ s^{-1}. Collisional quenching data has been presented by Jenkins[24] and using concentrations of CO, CO_2, O_2, N_2, H_2, and H_2O determined from equilibrium calculations resulted in a total quenching rate of $Q=4.1\cdot10^8$ s^{-1} for a stoichiometric flame. The beam cross section area A, is determined by dimensions of the focused laser sheet.

Tuneable diode laser absorption measurements of the potassium D1 line at 769.9 nm were made using a single-mode external cavity laser (DL 100, Toptica Photonics) with output power of 40 mW. The laser was scanned over a frequency range of 25 GHz covering the potassium line and the transmitted laser beam passing through the flame 21 mm above the burner surface was detected by a photodiode (DTE 210, Thorlabs). Analysis of scanned spectra of the K-atom line allowed for determination of potassium atom concentration. The K-atom line shape in the flame was given by a Voigt profile with a Gaussian width of 0.11 cm^{-1} and a Lorenzian width of 0.05 cm^{-1}. An average integrated absorption cross section for the two 4^2P transitions was determined to be $8.36\cdot10^{-6}$ cm^{2}s^{-1} which distributed over the measured line profile resulted in a peak absorption cross section of $1.6\cdot10^{-11}$ cm^2. Combined with the measured K-atom concentrations and assuming a path length of 1 cm for passage to the detector in the central region of the flame, the absorption was calculated for the different parts of the K-atom line employing the Beer-Lambert law. Trapping of the photofragmentation fluorescence signal was then calculated by integration over the attenuated line profile.

The quantities related to signal collection and detection efficiency can be retrieved by means of Rayleigh scattering measurements for which the signal, S, expressed in number of photons is given by Eq. (2)

$$S = \frac{E_{Rayleigh}}{h\nu_{Rayeligh}} \frac{\partial\sigma}{\partial\Omega} \Omega l\varepsilon_R N_{tot} \qquad (2)$$

In Eq. (2) $E_{Rayleigh}$ is the laser pulse energy for Rayleigh scattering measurements, h Planck's constant, $\nu_{Rayleigh}$ the Rayleigh photon frequency, $\frac{\partial\sigma}{\partial\Omega}$ the differential Rayleigh scattering cross section, ε_R the detection efficiency for the Rayleigh scattering signal, and N_{tot} the total gas number density in the probe volume. The cross section for air at ambient pressure and temperature for wavelength 532 nm is $6.25 \cdot 10^{-32}$ m^2/sr.[25] Using the Rayleigh scattering signal for calibration provides the detection solid angle, Ω, and the probe volume length, l, in the concentration evaluation using Eq. (1). The detector quantum efficiencies are specified to 10% and 3.3% at 532 and 766 nm, respectively. These values together with the transmission, 85%, of the interference filter used for fluorescence detection have been employed for determination of ε_R and ε_F.

In addition, Rayleigh scattering can be utilized for flame temperature measurements by comparison of signals measured in flame and at ambient conditions, taking differences in cross sections into account. For the investigated stoichiometric flame, using Rayleigh scattering cross section data compiled by Zetterberg[26] and major species concentrations determined from chemical equilibrium calculations, the Rayleigh scattering cross section of the product gas in the post-flame region was found to be a factor of 1.1 higher than that of ambient air. Including this factor in the ratio between Rayleigh signals measured in flame and ambient air allowed for temperature measurements in the flame.

The relation between the concentrations of K atoms, N, and parent species, N_{KCl}, is given by Eq. (3)[27]

$$N = N_{KCl}\Phi(1 - e^{\frac{-\sigma E}{h\nu_{laser}A}}) \qquad (3)$$

The factor Φ is the yield of photofragments generated from the parent species and is equal to 1 for the investigated case since dissociation of one KCl molecule results in creation of one K atom. Furthermore, σ is the absorption cross section, E the laser pulse energy, and ν_{laser} the laser frequency. Equation (1) can be solved for the concentration of alkali atoms N and the product of Ω and l can be retrieved using Eq. (2). Solving Eq. (3) for N_{KCl} using the obtained value of N in turn allows for evaluation of alkali compound concentrations from the photofragmentation fluorescence data.

RESULTS AND DISCUSSION

Prior to imaging experiments, fluorescence emission spectra were measured to identify potential interferences. Figure 2a shows photofragmentation fluorescence emission spectra measured in stoichiometric flames seeded with KCl (black) and NaCl (grey).
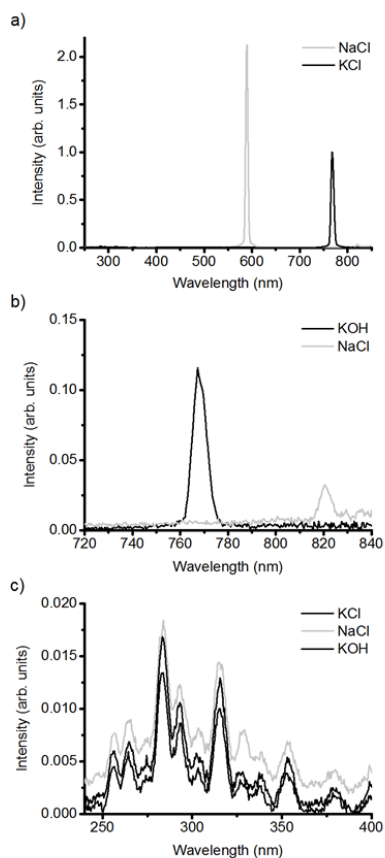

Fig. 2. a) Fluorescence emission spectra measured in stoichiometric flame seeded with KCl and NaCl. Spectral lines of atomic K (black) and Na (grey) are observed at 766 and 589 nm, respectively. b) Spectrum measured for KOH-seeding (black) shows a K-atom signal ~8 times lower than for KCl-seeding as shown in a. The spectrum for NaCl-seeding (grey) shows a line at 820 nm attributed to Na generated by photodissociation of NaOH c) Close-up of the spectra for KCl/KOH/NaCl-seeding in the ultraviolet region showing lines attributed to OH radicals of dissociated H_2O.

Distinct spectral lines from atomic Na and K can be observed at wavelengths 589 and 766 nm, respectively. K-atom fluorescence at 766 nm is also obtained for KOH-seeding as shown in a higher resolution in the spectrum of Fig. 2b, although the line is approximately eight times weaker compared with the case of KCl-seeding. In Fig. 2b the spectrum measured for NaCl seeding also shows a line from Na at 820 nm, also observed previously by Chadwick et al.[11] and mainly attributed to photofragmentation of NaOH formed during combustion. All spectra show fluorescence peaks at wavelengths 250 – 350 nm, shown in Fig. 2c, mainly attributed to OH radicals generated from photodissociation of H_2O. This could potentially interfere in imaging experiments, but can be removed with suitable filters transmitting the strong contributions of atomic Na and K.

Fluorescence images, averaged over 300 laser pulses, showing photofragmentation fluorescence signals in the product zone of stoichiometric Φ=1.0 methane-air flames are shown in Fig. 3.
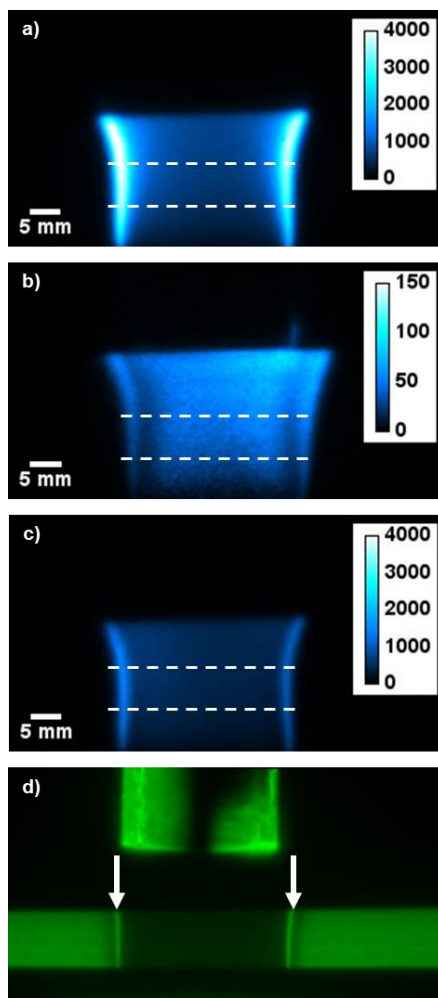

Fig. 3. *Averaged (300 frames) photofragmentation fluorescence images measured in premixed methane-air flames of equivalence ratio Φ=1.0 seeded with potassium compounds **a**) 0.5 M KCl **b**) 0.01 M KCl, and **c**) 0.5 M KOH **d**) Rayleigh scattering image measured in KCl-seeded (1.0 M) methane-air flame of Φ=1.0. Narrow regions of high signal at the flame edges, indicated by arrows, suggest KCl condensation. Temperature evaluation from Rayleigh scattering data was made for the regions between the horizontal lines in images a-c.*

The images were acquired for seeding with KCl solutions of concentrations 0.5 (a) and 0.01 M (b) and with KOH solution of 0.5 M concentration (c). The images show that signal levels close to the flame front region, located towards the lower image boundary, are low but increase further up in the post-flame region where the major potassium compounds to consider are KCl and KOH. With KCl-seeding, K and Cl elements entering the flame are able to form KCl in the post-flame region. However, via reactions involving water, K atoms are also able to form KOH. Thus, with KCl-seeding flame chemistry allows for formation of both KCl and KOH in the post-flame region, while KOH-seeding merely results in KOH formation. Figure 3d shows a Rayleigh scattering image measured in a stoichiometric flame seeded with 1.0 M KCl solution. The Rayleigh scattering signal of the propagating laser sheet can be seen across the image together with scattered light from the flame stabilizer located above the burner. The lower signal in the hot post-flame region is clearly observed and images of this type have allowed for temperature measurements of the investigated flames. Narrow vertical regions of stronger Rayleigh signal, indicated with arrows, can be observed at the flame edges and is interpreted as scattering from condensed KCl.

Further insights into image interpretation and evaluation can be obtained from profiles of fluorescence signals across the post-flame region. Profiles averaged over a region indicated by the dashed horizontal lines in Fig. 3, covering 13-20 mm above the burner, are plotted in Fig. 4 together with temperature profiles determined by Rayleigh scattering.
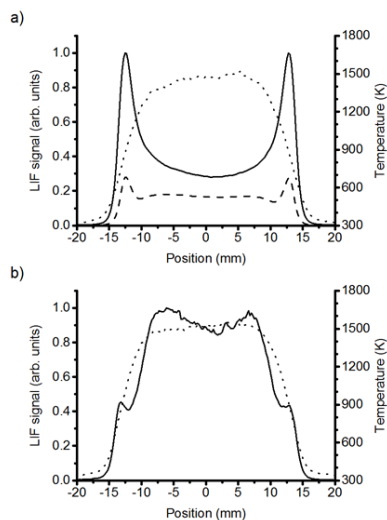
Fig. 4. *Temperature (dotted) and alkali compound profiles measured across the post-flame region in stoichiometric methane-air flames **a)** seeding of 0.5 M KCl (solid) and 0.5 M KOH (dashed) **b)** 0.01 M KCl-seeding (solid). High alkali seeding (a) gives profiles attenuated at the flame center (position 0 mm) due to absorption of the emitted fluorescence. The alkali fluorescence profiles have been compensated for gas number density to obtain profiles representing relative concentrations.*

The fluorescence signal is proportional to gas number density and the profiles have been compensated by multiplication with the temperature profiles in order to obtain profiles representing relative concentrations. Profiles for the two KCl-seeding concentrations show apparent differences. The 0.5 M KCl-seeding results in maximum signal at the flame edges, cf. Fig. 3a and 4a, where two distinct peaks can be observed. In contrast the image and profile measured for 0.01 M KCl-seeding, cf. Fig. 3b and 4b, show strong signal across the flame though with some signal decrease at the flame center, as shown in Fig 4b. The major reason for the observed trends is absorption of the fluorescence signal by K atoms formed in the flame chemistry, i.e. fluorescence trapping, during its passage through the flame. This must thus be considered in quantitative evaluation of the flame data, in particular at high seeding levels. Potassium atom levels determined from diode laser absorption spectroscopy (data not shown) were 1 and 0.02 ppm for 0.5 M and 0.01 M KCl-seeding, respectively. For comparison, broadband UV absorption measurements and evaluation of fluorescence data, discussed in the following, show potassium compound concentrations to be around 10 ppm for the 0.5 M flame and around 0.1 ppm for the 0.01 M flame. For the 0.5 M seeding trapping results in a transmission of the photofragmentation signal to the detector calculated to be 4%. Furthermore,

the trapping effect could be confirmed by comparing the signal versus KCl-seeding for the central region of the post-flame region, exhibiting strong trapping, and the edge region where the impact of trapping is lower.

As flame chemistry produces both KOH and KCl, and both of these result in K-atom photofragmentation fluorescence, as shown in Figs. 2 and 3, it is relevant to discuss the contributions of these compounds to the observed signal. Figure 4a also shows a profile measured with 0.5 M KOH-seeding of the stoichiometric flame, corresponding to the image in Fig. 3c. Similar to the KCl profile the KOH profile shows lower signal at the center of the flame where the temperature has reached a stable level around 1470 K. The profiles of KOH and KCl shows signals at the edges that are stronger than the signal at the flame center by a factor of two and three, respectively. The ratio of the signals generated for KCl- and KOH-seeding is around 2 in the central part of the post-flame region.

The energies required for dissociation and generation of a K-atom fragment in the excited 4^2P state is 5.31 eV and 5.91 eV for KOH and KCl, respectively. While the energy provided by 193 nm photons is insufficient for excitation of K atoms from KCl into higher excited states, dissociation of KOH, requiring less energy than KCl, allows for generation of K-atom fragments in the 5^2S and 3^2D states.[23] Compared with the case of KCl this would introduce additional emission coefficients A_{fi} and collisional quenching rates Q in the fluorescence quantum yield, cf. Eq. 1. Thus, as only the 4^2P emission is detected the photofragmentation fluorescence quantum yield for KOH can be expected to be lower than for KCl.

In addition to the comparison between KCl and KOH presented in Fig. 4a corresponding measurements were made in lean and rich flames of equivalence ratios $\Phi=0.8$ and $\Phi=1.3$. Photofragmentation fluorescence signals for KCl-seeded flames were on average a factor of 2.1 stronger with variations of 15%. From the broadband UV absorption measurements, the 0.5 M KCl-seeding is estimated to generate about 10 ppm KCl in the post-flame region. For this amount of KCl, chemical equilibrium calculations at the measured temperature predicts 6-7 ppm of KOH, i.e. about 40% of the total concentration of KCl and KOH. Diode laser absorption measurements indicated 1 ppm of potassium atoms in the post-flame region for both flames and chemiluminescence measured by the CCD camera also indicated similar K-atom levels for both cases. For the 0.5 M KOH-seeding, without chlorine introduced into the flame, it can thus be expected that ~16 ppm of KOH is formed. Considering this, the photofragmentation fluorescence quantum yield of KOH can be estimated to be around 40% of the yield of KCl. This suggests KCl to be the major signal contribution in the image measured in the KCl-seeded

flame for which the temperature is around 1500 K. In the KOH-seeded flame the lack of chlorine results in more K atoms available for formation of KOH, which becomes the major post-flame potassium compound.

The formation and distribution of KOH and KCl are temperature-dependent which also could affect the shapes of the profiles in Fig. 4. Formation of KCl is reportedly promoted at lower temperature while the formation of KOH is promoted at higher temperature.[6] The larger difference in signal between the edge and the central part of the flame observed for KCl compared with KOH-seeding could also partially be due to enhanced KCl formation and suppressed KOH-formation in the low-temperature region at the flame edges. In addition, data measured in KCl-seeded flames indicate condensation in the regions of lower temperature at the flame edges. This is demonstrated in the Rayleigh scattering image shown in Fig. 3d, measured in a stoichiometric flame seeded with 1.0 M KCl-solution and showing thin regions of high signal, indicated by arrows, at the flame edges. The enhanced elastic scattering indicates formation of aerosols due to KCl condensation. Calculated vapor pressures using the HSC chemistry software[30] are higher for KOH than for KCl, which then becomes more susceptible to condensation.

Chadwick et al.[11] have shown that it is possible to discriminate between NaCl and NaOH in photofragmentation fluorescence measurements. For both species the photofragmentation process produces Na atoms in the excited 3^2P state, resulting in emission at 589 nm. However, the dissociation energy of NaOH is lower and excess energy is therefore available for further excitation of the Na-atom fragment resulting in additional fluorescence emission for Na, for example at 819 nm as observed in Fig. 2b. As mentioned previously the situation is analogous for the potassium compounds where additional energy available after dissociation of KOH allows for excitation into the 5^2S and 3^2D states.[23] Population of these states would result in fluorescence emission at wavelengths 464, 1174, and 1248 nm. The $3^2D{\rightarrow}4^2S$ transition at 464 nm is, however, rather weak with a coefficient for spontaneous emission five orders of magnitude lower than the $4^2P{\rightarrow}4^2S$ transition.[23] The $3^2D{\rightarrow}4^2P$ and $3^2D{\rightarrow}5^2S$ transitions at 1174 and 1248 nm, respectively, are stronger but are located at wavelengths outside the sensitive range of the employed CCD detector. Thus, implementation of the concept presented by Chadwick et al. would likely be feasible also for KOH using detectors sensitive at near-infrared wavelengths. The energies required for photofragmentation and creation of excited K-atom fragments correspond to threshold wavelengths of 206.8 and 233.1 nm for KCl and KOH, respectively.[10] Thus, a way to induce photofragmentation fluorescence of KOH only, would be

to use a laser wavelength longer than 206.8 nm, for which the 213 nm fifth harmonic of a standard Nd:YAG laser could be an appropriate choice. For NaOH photofragmentation Chadwick et al. have also reported on emission from excited OH-radical fragments, attributed to a multiphoton process as the excess energy after photofragmentation is insufficient for OH excitation.[11] In our investigations of KOH, the fluorescence spectra do show OH lines (cf. Fig. 2c), however no difference were observed between spectra measured in KOH-seeded or unseeded flames. A contribution to the OH signal from a KOH multiphoton process is therefore probably much lower than the OH signal obtained from photodissociation of water in the post-flame region.

The photofragmentation process is influenced by the laser fluence according to Eq. (3) and Fig. 5a presents the photofragmentation fluorescence signal versus laser fluence measured in a KCl-seeded stoichiometric methane-air flame.
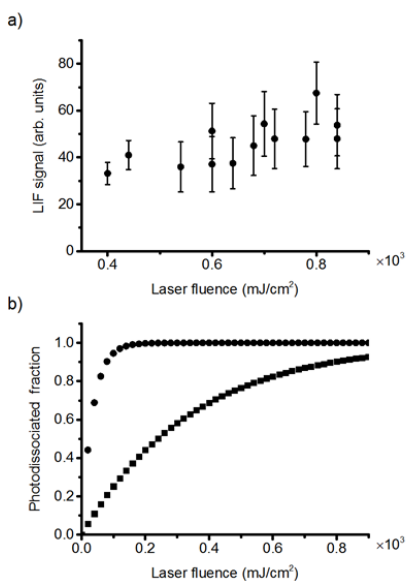

Fig. 5. a) *Photofragmentation fluorescence signal versus laser fluence measured in a stoichiometric methane-air flame seeded with 0.2 M KCl solution. Each measurement point is an average over 300 laser pulses and the error bars represent the standard deviation. The signal shows an essentially saturated trend.* **b)** *Calculated fractions of dissociated molecules versus laser fluence for KCl (circles) and KOH (squares). The experimental conditions for flame measurements correspond to ~800 mJ/cm², which results in complete dissociation for KCl and strong dissociation for KOH.*

The results indicate an essentially saturated signal with some scatter indicated by the error bars. The saturated process is confirmed in Fig. 5b, which presents results from calculations of the fraction of dissociated KCl and KOH molecules versus laser fluence according to Eq. (3). These calculations include the absorption cross section, which for KCl at 193 nm can be estimated to $3 \cdot 10^{-17}$ cm^2 from data presented by Davidovits and Brodhead.[28] Corresponding data for KOH is, however, not available in literature but following the discussion by Sorvajärvi et al.[21] it can be approximated with that of NaOH reported by Self and Plane[29] which gives a value of $5.6 \cdot 10^{-18}$ cm^2 at 300 K. The higher cross section of KCl results in a complete dissociation at lower fluence levels than for KOH, which shows a slower increase in the fraction of dissociated molecules. While these calculations indicate that KOH does not fully reach complete dissociation for the experimental conditions, with laser pulse energies of around 40 mJ in a focused laser sheet resulting in a fluence of 800 mJ/cm^2, the degree of dissociation is above 90% and both species are considered measured under saturated conditions.

Figure 6a shows the photofragmentation fluorescence signals, measured at the edge (open circles) and center (filled circles) of a stoichiometric flame, versus KCl-seeding.
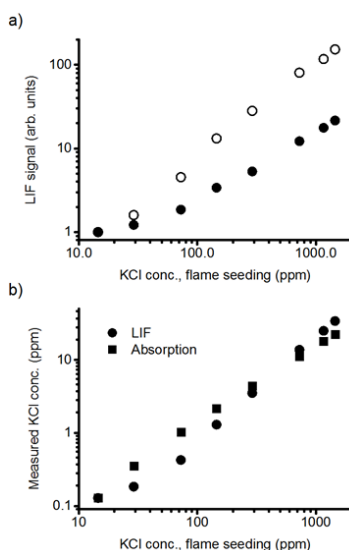

Fig. 6. a) Photofragmentation LIF signals versus KCl-seeding concentration in a stoichiometric methane-air flame. The signal measured at the flame boundary (open circles) is directly proportional to the seeding concentration while that measured in the flame center (filled circles) shows a weaker increasing trend due to signal absorption. b) KCl concentrations measured by LIF (circles) and UV absorption (squares) versus KCl-seeding concentration in stoichiometric flame.

As referred to previously, the signal at the flame edge is directly proportional to the seeding concentration, resulting in a slope close to 1 in Fig. 6a, whereas the signal at the flame center shows a weaker increasing trend with seeding concentration due to fluorescence trapping. Absorption spectroscopy was used to quantify the amount of seeded KCl converted into gas-phase KCl in the flame and post-flame region. Figure 6b shows the KCl-concentrations measured by absorption and photofragmentation fluorescence in the post-flame region of a stoichiometric flame versus KCl-seeding level. Concentrations evaluated from averaged fluorescence data according to Eq. (1), i.e. compensated for fluorescence trapping, for an estimated laser sheet thickness of 200 μm are in good agreement with results from absorption measurements. Note, that both measurements result in concentrations considerably lower than the KCl-seeding input concentrations of the reactant mixture, plotted on the abscissa, indicating losses of KCl-solution via the burner drain as well as due to precipitation and deposits in the burner system. Quantitative measurements are thus feasible and the accuracy is determined by uncertainties in the quantities of Eq. 1. Uncertainties related to calibration of the signal collection and determination of the laser sheet cross section area can be minimized and estimated with thorough experimental design. The laser pulse energy for the Rayleigh scattering and the width of the focused laser sheet can both be determined with accuracies on the order of 5%. The collisional quenching and fluorescence trapping however introduce uncertainties more challenging to assess. Determination of the collisional quenching rate requires knowledge on temperature as well as the concentrations of the major species of the flame and their collisional quenching cross sections. The accuracy of the quenching rate is thus in turn dependent on how accurate these parameters are known, as an example the quenching rate calculated for premixed methane-air flames on the investigated burner configuration varies by 10% for equivalence ratios between $\Phi=0.8$ and $\Phi=1.3$. The fluorescence trapping requires accurate determination of K-atom concentrations, which can be achieved using sensitive absorption techniques. Under the investigated conditions a change in K-atom concentrations of 10% result in a relative change in trapping factor of 5-7%. With experimental uncertainties of these magnitudes the uncertainty of the measured alkali compound concentrations can be estimated to 15-20%.

Imaging measurements are particularly valuable for studies of non-stationary conditions requiring single-shot measurements, exemplified by images measured in KCl- and KOH-seeded flames shown in Fig. 7a and b.
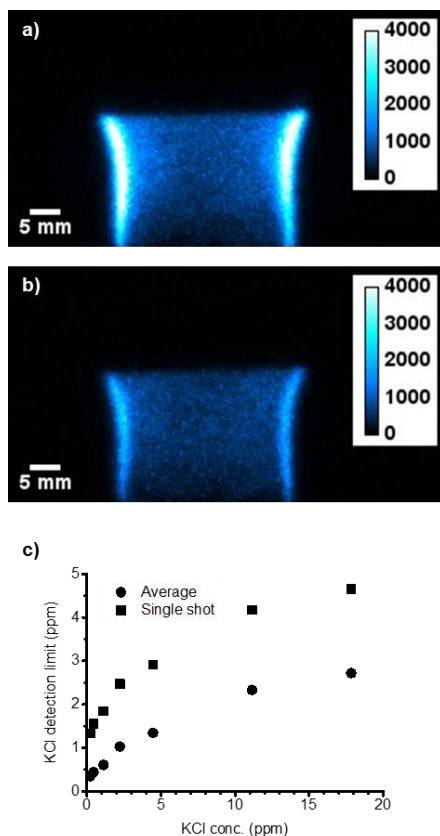
Fig. 7. *Single-shot photofragmentation fluorescence images measured in stoichiometric methane-air flames seeded with potassium compounds **a)** 0.5 M KCl **b)** 0.5 M KOH. **c)** Detection limit determined for a signal-to-background ratio of 3 in KCl-seeded flames for images averaged over 300 pulses (circles) and single-shot images (squares).*

The image of KCl (Fig. 7a) has a signal-to-noise ratio of about 300 while for the KOH image (Fig. 7b) it is about 170. The detection limit is, however, determined by the relation between the fluorescence signal and the background radiation from excited K-atoms formed in the flame. An analysis of the detection limit for a signal-to-background ratio of 3 in KCl-seeded flames and an image spatial resolution of 0.7 mm is shown in Fig. 7c. For measurements at post-flame KCl concentrations of a few ppm and data averaged over 300 laser pulses the lower detection limit is on the order of 0.5 ppm. However, for high seeding levels and a higher background of excited K atoms the detection limit instead approaches 3 ppm. Similar analysis for single-shot data shows detection limits of 1 and 5 ppm, respectively, for measured post-flame concentrations. These detection limits, estimated under conditions with a background

19

consisting of alkali emission, are obviously higher than values of 0.1 ppb reported for NaCl and KCl measured in low-background experiments carried out in cells at lower temperatures than in a flame environment.[10, 11]

Figure 8 demonstrates that it is possible to carry out simultaneous single-shot photofragmentation fluorescence measurements of two relevant alkali components: KCl and NaCl, in a fuel mixture within a context of combustion in biomass and waste-fired boilers.
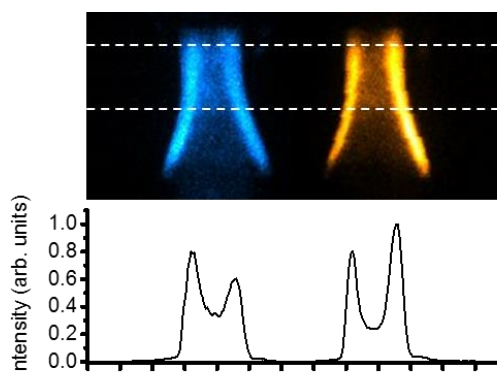

Fig. 8. Fluorescence image (top) with signals from K (left) and Na (right) atoms measured simultaneously using a stereoscope in a stoichiometric premixed methane-air flame with 1.5 M KCl-/NaCl-seeding. An intensity profile, integrated over the region between the horizontal white lines, is shown below.

The fluorescence image was measured in a flame seeded with a mix of 50% 3 M NaCl and 50% 3 M KCl solution utilizing a stereoscope with band-pass filters for detection of K atoms (766 nm) and Na atoms (589 nm). Signals from K (left, blue) and Na (right, orange) atoms both show a shape mimicking the cone of the flame obtained without the stabilizer mounted above the burner. Even though similar in shape, the signals originate from the two different species without cross-talk between the detection channels, which was confirmed by measurements for seeding of KCl and NaCl separately. Gas-phase KCl and NaCl are detected on the inner part of the cone while stronger signals are obtained on the edges due to lower temperature resulting in higher gas density, enhanced formation of chlorides, and possible condensation. While the signals at the edges for the two species are of similar magnitude, KCl shows a signal a factor of ~1.5 stronger inside the cone. The signal is dependent on the concentration N as well as the spontaneous emission coefficient A_{fi} (cf. Eq. 1), which for Na atoms is $1.3 \cdot 10^8$ s^{-1} while the corresponding values for K atoms is $3.8 \cdot 10^7$ s^{-1}.[31, 32] Since signals have been compensated for the detector response at the detection wavelengths, the emission coefficient and the signal ratio

suggest KCl concentrations a factor of ~5 higher than NaCl in the post-flame region under this experimental condition.

The presented imaging technique in combination with the earlier findings from Oldenburg et al.[10] and Chadwick et al.[11] can help in the quantifying and visualizing where the different alkali species are formed in the combustion process. Potentially this could be useful in fundamental investigations to characterize co-combustion of coal and biomass fuels containing sodium and potassium, respectively. The mitigation of alkali-related problems such as high-temperature corrosion, slagging and fouling, that are due to the increased use of biomass fuels of different quality regarding alkali and chlorine[33, 34] demands methods that has the possibility of detecting KCl and NaCl, as demonstrated for this set-up.

CONCLUSIONS

Laser-induced photofragmentation fluorescence can be used for imaging detection of alkali chlorides such as KCl and NaCl and for alkali hydroxides such as KOH with high sensitivity. The application of high-power UV pulses from excimer lasers for photofragmentation allows saturated photodissociation, independent on absorption cross section, to be achieved. Quantitative KCl concentrations up to 20 ppm were evaluated from the fluorescence data and KCl detection limits of 0.5 and 1.0 ppm were determined for averaged and single-shot imaging data, respectively. The method can be employed for detailed studies in laboratory flames to validate chemical kinetic models, and from a fundamental point of view help to increase knowledge and understanding on the fate of alkali-formation from fuel to flue gas in biomass combustion.

ACKNOWLEDGEMENTS

REFERENCES

1. H. Balat. "Prospects of biofuels for a sustainable energy future: A critical assessment". Ener Educ Sci Tech-A. 2010. 24(2): 85-111.

2. A. Demirbas. "Potential applications of renewable energy sources, biomass combustion problems in boiler power systems and combustion related environmental issues[". Prog Energ Combust. 2005. 31(2): 171-192.

3. S. van Loo and J. Koppejan, *The handbook of biomass combustion and co-firing* (Earthscan, UK and USA, 2008).

4. H. P. Nielsen, F. J. Frandsen, K. Dam-Johansen, and L. L. Baxter. "The implications of chlorine-associated corrosion on the operation of biomass-fired boilers". Prog Energ Combust. 2000. 26(3): 283-298.

5. H. Kassman, J. Pettersson, B. M. Steenari, and L. E. Åmand. "Two strategies to reduce gaseous KCl and chlorine in deposits during biomass combustion - injection of ammonium sulphate and co-combustion with peat". Fuel Process Technol. 2013. 105: 170-180.

6. B. Li, Z. W. Sun, Z. S. Li, M. Aldén, J. G. Jakobsen, S. Hansen, and P. Glarborg. "Post-flame gas-phase sulfation of potassium chloride". Combust Flame. 2013. 160(5): 959-969.

7. J. N. Knudsen, P. A. Jensen, and K. Dam-Johansen. "Transformation and release to the gas phase of Cl, K, and S during combustion of annual biomass". Energ Fuel. 2004. 18(5): 1385-1399.

8. J. M. Johansen, J. G. Jakobsen, F. J. Frandsen, and P. Glarborg. "Release of K, Cl, and S during Pyrolysis and Combustion of High-Chlorine Biomass". Energ Fuel. 2011. 25(11): 4961-4971.

9. P. Monkhouse. "On-line spectroscopic and spectrometric methods for the determination of metal species in industrial processes". Prog Energ Combust. 2011. 37(2): 125-171.

10. R. C. Oldenborg and S. L. Baughcum. "Photofragment Fluorescence as an Analytical Technique - Application to Gas-Phase Alkali Chlorides". Anal Chem. 1986. 58(7): 1430-1436.

11. B. L. Chadwick, G. Domazetis, and R. J. S. Morrison. "Multiwavelength Monitoring of Photofragment Fluorescence after 193-Nm Photolysis of Nacl and Naoh - Application to

Measuring the Sodium Species Released from Coal at High-Temperatures". Anal Chem. 1995. 67(4): 710-716.

12. B. L. Chadwick, P. G. Griffin, and R. J. S. Morrison. "Quantitative detection of gas-phase NaOH using 355-nm multiple-photon absorption and photofragment fluorescence". Applied Spectroscopy. 1997. 51(7): 990-993.

13. K. T. Hartinger, S. Nord, and P. B. Monkhouse. "Quenching of fluorescence from Na(3(2)P) and K(4(2)P) atoms following photodissociation of NaCl and KCl at 193 nm". Appl Phys B-Lasers O. 1997. 64(3): 363-367.

14. U. Gottwald and P. Monkhouse. "Single-port optical access for spectroscopic measurements in industrial flue gas ducts". Appl Phys B-Lasers O. 1999. 69(2): 151-154.

15. U. Gottwald, P. Monkhouse, N. Wulgaris, and B. Bonn. "Simultaneous detection of nickel and potassium in the flue gas of a fluidised bed coal combustor by excimer laser-induced fragmentation fluorescence". Fuel Process Technol. 2003. 80(2): 143-153.

16. P. B. Monkhouse, U. A. Gottwald, K. O. Davidsson, B. Lönn, K. Engvall, and J. B. C. Pettersson. "Phase discrimination of alkali species in PCFB combustion flue gas using simultaneous monitoring by surface ionisation and photofragmentation fluorescence". Fuel. 2003. 82(4): 365-371.

17. M. P. Glazer, N. A. Khan, W. de Jong, H. Spliethoff, H. Schurmann, and P. Monkhouse. "Alkali metals in circulating fluidized bed combustion of biomass and coal: Measurements and chemical equilibrium analysis". Energ Fuel. 2005. 19(5): 1889-1897.

18. C. Erbel, M. Mayerhofer, P. Monkhouse, M. Gaderer, and H. Spliethoff. "Continuous in situ measurements of alkali species in the gasification of biomass". P Combust Inst. 2013. 34: 2331-2338.

19. T. Sorvajärvi, J. Saarela, and J. Toivonen. "Optical detection of potassium chloride vapor using collinear photofragmentation and atomic absorption spectroscopy". Opt Lett. 2012. 37(19): 4011-4013.

20. T. Sorvajärvi and J. Toivonen. "Principles and calibration of collinear photofragmentation and atomic absorption spectroscopy". Appl Phys B-Lasers O. 2014. 115(4): 533-539.

21. T. Sorvajärvi, N. DeMartini, J. Rossi, and J. Toivonen. "In Situ Measurement Technique for Simultaneous Detection of K, KCl, and KOH Vapors Released During Combustion of

Solid Biomass Fuel in a Single Particle Reactor". Applied Spectroscopy. 2014. 68(2): 179-184.

22. C. Forsberg, M. Broström, R. Backman, E. Edvardsson, S. Badiei, M. Berg, and H. Kassman. "Principle, calibration, and application of the in situ alkali chloride monitor". Rev Sci Instrum. 2009. 80(2): 023104.

23. D. K. Nandy, Y. Singh, B. P. Shah, and B. K. Sahoo. "Transition properties of a potassium atom". Phys Rev A. 2012. 86(5): 1-12.

24. D. R. Jenkins. "Determination of Cross Sections for Quenching of Resonance Radiation of Metal Atoms .2. Results for Potassium Rubidium and Caesium". Proc R Soc Lon Ser-A. 1968. 303(1475): 453-465.

25. R. B. Miles, W. R. Lempert, and J. N. Forkey. "Laser Rayleigh scattering". Meas Sci Technol. 2001. 12(5): R33-R51.

26. J. Zetterberg. Development of Laser-Spectroscopi Techniques for New Detection Schemes in Combustion Diagnostics. PhD thesis. Lund University: Department of Physics/Combustion Physics, 2008.

27. W. D. Kulatilaka, J. H. Frank, B. D. Patterson, and T. B. Settersten. "Analysis of 205-nm photolytic production of atomic hydrogen in methane flames". Appl Phys B-Lasers O. 2009. 97(1): 227-242.

28. P. Davidovits and D. C. Brodhead. "Ultraviolet Absorption Cross Sections for Alkali Halide Vapors". J Chem Phys. 1967. 46(8): 2968-2973.

29. D. E. Self and J. M. C. Plane. "Absolute photolysis cross-sections for $NaHCO_3$, NaOH, NaO, NaO_2 and NaO_3: implications for sodium chemistry in the upper mesosphere". Phys Chem Chem Phys. 2002. 4(1): 16-23.

30. A. Roine. Outukumpu HSC chemistry for windows version 7.1. Pori, Finland: Outokumpu Research, 2011.

31. J. E. Sansonetti. "Wavelengths, transition probabilities, and energy levels for the spectra of potassium (K I through K XIX)". J Phys Chem Ref Data. 2008. 37(1): 7-96.

32. J. E. Sansonetti. "Wavelengths, Transition Probabilities, and Energy Levels for the Spectra of Sodium (Na I-Na XI)". J Phys Chem Ref Data. 2008. 37(4): 1659-1763.

33. C. J. E. Bajamundi, P. Vainikka, M. Hedman, I. Hyytiainen, J. Silvennoinen, T. Heinanen, R. Taipale, and J. Konttinen. "Towards controlling PCDD/F production in a multi-fuel fired BFB boiler using two sulfur addition strategies. Part I: Experimental campaign and results". Fuel. 2014. 134: 677-687.

34. C. J. E. Bajamundi, P. Vainikka, M. Hedman, J. Silvennoinen, T. Heinanen, R. Taipale, and J. Konttinen. "Searching for a robust strategy for minimizing alkali chlorides in fluidized bed boilers during burning of high SRF-energy-share fuel". Fuel. 2015. 155: 25-36.

Paper IV

Development of an alkali chloride vapour generating apparatus for calibration of ultraviolet absorption measurements

T. Leffler[1,2*], C. Brackmann[2], M. Berg[1], M. Aldén[2], Z. S. Li[2]

[1]*R&D, Strategic Development, Vattenfall AB, 814 26 Älvkarleby, Sweden*

[2]*Division of Combustion Physics, Lund University, Box 118, SE-221 00, Lund, Sweden*

[*]*tomas.leffler@forbrf.lth.se*

ABSTRACT

A novel design of alkali chloride vapour-generating system has been developed, which can serve as a calibration cell for quantitative ultraviolet absorption concentration measurements and meticulous spectral investigations of alkali chloride compounds. The calibration cell was designed to provide alkali vapour of well-controlled concentrations and temperatures and consisted of a sealed quartz cell measuring 0.4 m in length with a temperature-controlled reservoir containing solid alkali salt. The cell was placed in a furnace and the generated alkali vapours have direct access to the measuring chamber. Investigations of potassium chloride (KCl) were made on sublimated vapour at temperatures 650, 700, 750, 780 and 800 °C while the reservoir temperature was kept 50 °C lower to avoid condensation. The cell provides stable KCl vapour pressures and the furnace provides a homogenous temperature profile along the cell. KCl vapour pressures are well characterised and conform the base for determination of the KCl concentration in the cell. The alkali chloride levels matched the concentration range of the absorption setup and indicated a previously employed calibration method to overestimate KCl concentrations. The KCl absorption cross-sections for wavelengths $\lambda = 197.6$ nm and $\lambda = 246.2$ nm were calculated to 3.4×10^{-17} and 2.9×10^{-17} cm^2/molecule, respectively. The absorption cross-section spectra did not show any structural differences with increasing temperature, which could indicate influence of dimers or changes of the population in the KCl

vibrational states. The KCl absorption cross-sections did thus not show any temperature dependence in the temperature region of 700 – 800 °C. Moreover, the applicability of the calibration cell for characterization of other alkali chlorides and hydroxides is discussed.

1. Introduction

Formation of harmful corrosive alkali compounds during combustion makes measurements of alkali chlorides or hydroxides in the flue gas of biomass-fired boilers of strong interest. Such measurements are relevant for fuel-quality assessments in terms of alkali-chloride formation [1], operating conditions adjustments, and also the monitoring of the effects of alkali chloride reduction concepts, e.g. by addition of suitable additives [2, 3]. Measurements can be performed with different optical or spectroscopic techniques and Monkhouse [4] have made a thorough review of online measurements using such methods on alkali metal species. While quantitative species concentrations in principle can be achieved by evaluation of measurements using literature data for necessary physical quantities, e.g. absorption cross sections, for many cases calibration under well-defined experimental conditions is necessary. For example, there might be a lack of data for relevant species such as an absorption cross section for potassium hydroxide as reported by Sorvajärvi et al. [5]. New techniques developed for flue gas measurements, such as the LIDAR concept for KCl detection [6], also require calibration for accurate quantitative measurements. Moreover, extension of instruments based on broadband absorption such as the In-situ Alkali Chloride Monitor (IACM) [7, 8] to incorporate additional alkali species also call for the possibility to measure well-defined reference spectra. There is thus a demand for development of a suitable calibration cell to produce spectra of different alkali compounds under well-controlled conditions that can subsequently be used to carry out reliable quantitative determination of concentrations. This type of calibration cell also facilitates the possibility to carry out detailed spectroscopic studies of how the absorption cross-section of different solid alkali compounds varies due to temperature and formation of dimers. Three different designs of high-temperature calibration cells for alkali compounds at atmospheric (open cell) and lower pressures (sealed cell) from the literature have been studied and are briefly described below. Grosch et al. [9] have developed a high-temperature open flow

cell for reactive gases at temperatures up to 530 °C. This flow cell allows for high-resolution spectroscopic measurements in the ultraviolet (UV) and infrared (IR) spectral regions (190 – 20 000 nm). Vattenfall Research and Development AB has developed and patented an In-situ Alkali Chloride Monitor (IACM) [7] and designed a calibration cell [8] for this instrument. This calibration cell operates at atmospheric pressure where solid potassium chloride is vaporized at 781 °C and the KCl vapour is subsequently diluted with N_2 and transported to a measuring chamber. The diluted KCl vapour is super-heated to 860 °C on its way to the measuring chamber where the concentration is evaluated. Davidovits and Brodhead [10] report on a sealed evacuated cell made of quartz with a diameter of 20 mm and a length of 20 mm where a sealed-off tip functions as a salt reservoir. The cell is placed in a furnace with additional heaters for the cell windows and the temperature of the salt reservoir is controlled by a conduction cooling rod. To avoid condensation, the salt reservoir is kept at a temperature of about 10 °C lower than that of the cell. Measurements were carried out on alkali halide vapours where investigations of potassium- and sodium chloride vapours are relevant for this work [10]. Nevertheless, there is need for a calibration cell that generates vapours from alkali compounds at stable, well-defined concentration levels, and allows for optical measurements at well-controlled temperatures, which has motivated this research. The working hypothesis of this study is to verify that the new design of the calibration cell is fit for purpose.

A novel calibration cell is presented in this paper, which is based on a cold-finger arrangement and offers the possibility to generate sublimated vapour of KCl or other alkali compounds. Vapour is generated from a solid sample located in a small reservoir and the vapour pressure, controlled by the reservoir temperature, determines the concentration of the compound in the cell. The KCl vapour pressure in the cell can in turn be monitored at different pre-defined temperatures.

The outcome from this study is convincing and the design can be used for investigations of other solid chemical components, which are of relevance for, in this particular case, biomass and waste combustion. The calibration cell presented in this paper is stable and robust, which facilitates handling and experimental reproducibility, which in turn result in accurate and reliable calibration data.

2. Experimental
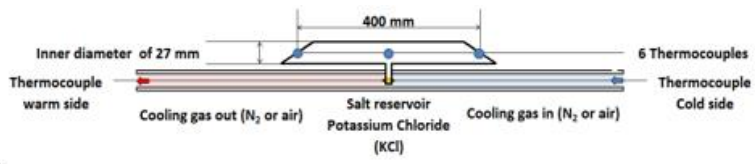
2.1 The calibration cell

The calibration cell, schematically shown in Figure 1a, was made of a quartz tube with outer and inner diameters of 30 and 27 mm, respectively. Windows made of quartz (SILUX® 3) were fused onto each end of the tube at an angle of 45 degrees. The optical path length at the centre line of the cell is 400 mm and a salt reservoir, containing around 2 g of crystalline KCl (EMSURE®, 1.04936.0500), was placed at the centre part of the cell. Before sealing the cell, the pressure inside the cell was brought down to vacuum ($1.33 \cdot 10^{-4}$ Pa) and it was then filled with argon to a pressure of 100 Pa at room temperature. Precise control of the KCl salt temperature is crucial for the performance of the calibration cell and a special design is adopted in this work. In order to achieve precise and independent control of the temperature of the salt reservoir enclosed in the calibration cell, two quartz tubes were fused together to build up a double-jacketed tube structure for cooling. The cooling tube was subsequently fused together with the cell in such a way that the salt reservoir ended up in the centre of the cooling tube (cf. Figure 1a). This permits keeping the salt at a controlled temperature during the experiments by regulating a suitable flow of N_2 through the cooling tube.

Before the cell was placed into the furnace, eight thermocouples (type K) and a Swagelok connector for the cooling gas were mounted onto the cell. Six thermocouples were mounted along the side of the cell with two in the centre (position 2, Figure 1b) and two at each end

(positions 1, 3, Figure 1b). Three of these thermocouples were used to monitor the cell temperature while the remaining three were used by the temperature regulators to control the temperature in the furnace and consequently the cell temperature. Two thermocouples (position 4, Figure 1b) were used to measure the salt (KCl) reservoir temperature, one was mounted together with the Swagelok connector (not shown in Figure 1b) that supplies the cooling gas to the cell, while the other was inserted into the cooling tube from the opposite side.

The thermocouples used for measure cell temperature were connected to a logger system together with the thermocouples connected to the cold and warm side of the salt reservoir. The cold side of the salt reservoir is the wind side (to the right side of the salt reservoir shown in Figure 1a) and the warm side is the lee side (to the left side of the salt reservoir shown in Figure 1a).

The logger system included a standard computer connected to a Hydra data acquisition unit 2620A (Fluke). The calibration cell was equipped with supporting legs to keep its position in the furnace stable, as shown in Figure 1b and in Figure 2.2b presenting the calibration cell in the furnace.


a.
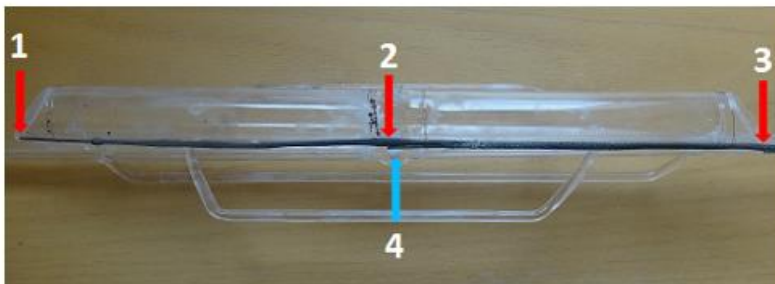
b.

Figure 1a. *Detailed schematic of the calibration cell.* ***b.*** *Photo of the calibration cell with the locations of the thermocouples mounted on the calibration cell.*

2.2 The furnace

Figure 2a shows a principle sketch of the furnace with its temperature-controlling device, optical set-up and calibration cell. Figure 2b shows the calibration cell when it is placed in the furnace. The furnace was constructed as follows: three pieces of Kanthal D wires with an equal length of 15 m and a diameter of 1 mm were cut from a cable reel. The resistivity of the wire was 1.733 Ω/m, which gave a total resistance of 26 Ω in each piece and subsequently total power of 6 kW (3×2 kW) for the furnace at an applied voltage of 230V. The electrical wires were manually wound one by one around a steel rod to form a spring-like heating element. A stainless steel pipe was connected at the wire ends of each heating element to provide a low ohmic connection between the heating wire and the wire from the power supply. The heating elements were evenly distributed around a 670 mm long quartz tube with an internal diameter of 100 mm to create three individually controlled heating zones (Figure 2c). The quartz tube with the heating elements was insulated with a 10 cm thick layer of durablanket (Fiberfrax) and then placed in a box built of 5 cm thick building blocks of duraboard (Fiberfrax). The temperature-controlling device for the furnace was built up with the following components: three-phase residual-current device, three fuses, a safety switch, three solid-state relays, three power controllers, three PID temperature controllers, and three current indicators. The power controllers were included to enable individual adjustment of the current to each heating element since the solid-state relay works on an on-off basis.
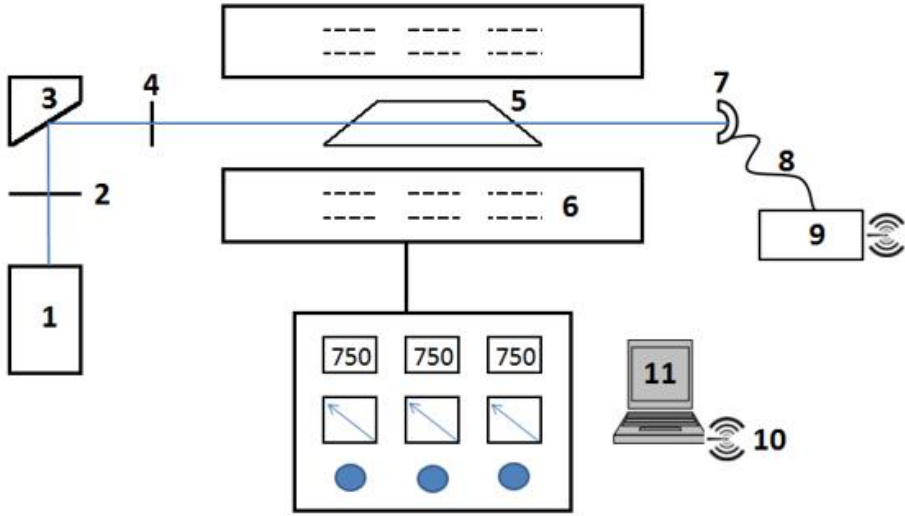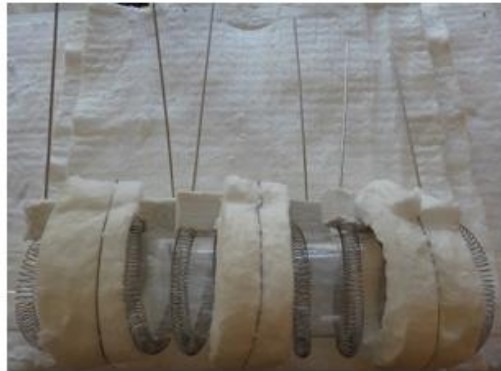
Figure 2a. *Schematic of furnace, temperature control, calibration cell, and equipment for UV absorption spectroscopy. 1. UV light source, 2. Aperture, 3. Parabolic mirror, 4. Aperture, 5. Calibration cell 6. Furnace with temperarure controll equipment, 7. Detector (collimator), 8. Optical fibre, 9. Spectrometer, 10. Blue thooth connection between the spectrometer and the computer, 11. Standard computer **b.** Photo showing the calibration cells location in the furnace. **c.** Photo showing the heating elements wound around the quartz tube forming the furnace chamber.*

2.3 The absorption spectroscopy set-up

Absorption measurements on KCl vapour generated in the calibration cell were performed using an amended version of the IACM instrument [7] arranged in the experimental set-up shown in Figure 2a. The amendments consist of the following changes: the xenon lamp has been replaced by a deuterium lamp; a lens and a spherical mirror have been replaced by two parabolic mirrors, where one of the parabolic mirror (collimator) is equipped with an SMA connector for the optical fibre.

UV light from a high-intensity (150 W) source (1), (L1314, Hamamatsu), was radiated through an aperture (2) and collimated by a 2-inch, 90° off-axis parabolic mirror (3) with UV-enhanced aluminium coating and a reflective focal length of 6 inch (Thorlabs). The collimated UV light beam subsequently passed through another aperture (4) and through the quartz windows on each side of the calibration cell (5), which in turn was located in the furnace (6). The transmitted light was collected in an UV-enhanced aluminium reflective collimator (7) with a diameter of 12 mm and an SMA connector for an optical fibre (Thorlabs). The collected UV light was then transferred through the optical fibre (8) (FC-UV600-0.5-SR, Azpect Photonics) and subsequently dispersed in a spectrometer (9) (AVABENCH-75-2048, Azpect Photonics) with an entrance slit of 50 µm width and a grating with 2400 grooves/mm. A Bluetooth device (10) (WCS-232, SystemBase) was used to transfer the data from the spectrometer to the computer. The collected spectrum was evaluated in a standard computer (11) by means of the Differential Optical Absorption Spectroscopy (DOAS) technique [11] to retrieve the KCl concentration in the calibration cell.

2.4 The calibration of the thermocouples

Prior to the absorption measurements on KCl vapour the thermocouples were calibrated together against a reference thermocouple, which in turn had been calibrated according to EA-4/02 standard. The calculated expanded uncertainty for all calibrated temperatures has been

9

determined to be ± 0.7 °C, which had been carried out earlier at a certified laboratory (Pentronic AB). The experimental system was calibrated for five temperatures: 600, 650, 700, 730 and 750 °C. The calibration started at 750 °C and was progressively lowered down to 600 °C before the calibration process ended. Each temperature was stabilized during a time span of two hours before the reference thermocouple was compared with the other thermocouples in the system.

2.5 Preparation and performance of the experiment

Placement of the cell into the furnace

The cell was placed in a central position in the furnace (cf. Figure 2b) and the hose that supplied the cooling medium was connected. Two insulating end plugs, each with a hole for the UV-beam to pass through the furnace and the cell were placed at the ends of the furnace to minimize heat losses. The optical measurement system consisting of the UV-light source, optical components, and spectrometer was then placed at the respective end of the furnace and as a final step the UV-light beam was aligned through the cell.

Execution of the measurements

Five different saturated vapour pressures of KCl were generated by keeping the salt reservoir at five different temperatures (600, 650, 700, 730 and 750 °C). The trials were randomized to avoid any systematic errors. A measurement was performed in the following steps:

- The experiment was started by setting the selected temperature on each temperature controller. Once the cell temperature had reached the set point value it was kept there for approximately one hour for temperature stabilization while the temperature on the salt reservoir was kept at 300 °C, by regulating the cooling gas flow.

- A reference and a background spectrum was collected after one hour and uploaded into the evaluation software; thereafter, the UV absorption measurements by means of

the IACM instrument were made continuously during a time period of about two hours with spectra measured every 10 s.

- The temperature of the salt reservoir was adjusted by the flow of the cooling medium to the selected temperature and was kept there for two hours to allow the vapour pressure of the KCl inside the cell to reach thermodynamic equilibrium.

- The temperature of the salt reservoir was brought down to 300 °C by cooling the salt reservoir with compressed air. Once the KCl concentration had reached 0 ppm, at 300 °C the experiment was considered completed and a new set point was added to the temperature controllers.

2.6 Determination of the KCl vapour pressure

The partial pressures of the KCl monomer and the K_2Cl_2 dimer in the calibration cell have been determined from measured vapour pressures at different temperatures presented in literature [12] that have been used to fit coefficients *A*, *B* and *C* in the Antoine equation [13] (Eq. 2.1).

$$\ln p = A - \frac{B}{C + T}$$

(2.1)

The coefficients were fitted in Excel using the LINEST function and Eq. (2.1) allows to calculate the vapour pressure at different temperatures, where *p* [Pa] represents the vapour pressure and *T* [K] the temperature. The coefficients were determined as: *A* = 11.35, *B* = 3659.18 and *C* = -581.64.

The same procedure was used to determine the Antoine coefficients A, B and C for K_2Cl_2 vapour pressures using data at corresponding temperatures from literature [12]. The coefficients for K_2Cl_2 were determined as: *A* = 10.96, *B* = 3874.74 and *C* = -600.21.

Vapour pressures thus calculated by Eq. 2.1 have also been compared with vapour pressures calculated with the commercial HSC Chemistry 7.1 software [14] based on extensive compilation of thermochemical data therein.

In addition, the vapour pressure was calculated utilizing the Clausius-Clapeyron equation (Eq. 2.2):

$$p_2 = p_1 exp\left(-\frac{\Delta H_{sub}}{R}\left(\frac{1}{T_2} - \frac{1}{T_1}\right)\right)$$

(2.2)

The Clausius-Clapeyron equation is an approximation where it has been assumed that the vapour volume is much larger than the solid volume, ΔH_{sub} is constant in the measuring temperature region and finally the KCl vapour behaves as an ideal gas [13]. In equation 2.2 ΔH_{sub} represents the sublimation enthalpy, R is the universal gas constant, p_1 and T_1 are the pressure and temperature at state 1, T_2 is the temperature at state 2 and p_2 is the calculated vapour pressure at state 2. The input data for state $T_1 = 900$ K, $p_1 = 1.04$ Pa and the sublimation enthalpy $\Delta H_{sub} = 211716$ J/mol retrieved from literature [15] are based on best fit.

2.7 KCl spectral simulations

The vibrational and rotational energy level structure of the KCl ground state was calculated using the PGOPHER [16] software with molecular constants obtained from Barton et al. [17] Spectral simulations at different temperatures provided energy level population fractions and allowed for analysis of population redistributions between vibrational levels.

3. Results and Discussion

Figure 3 presents salt reservoir temperature kept at 730°C and the calculated KCl vapour pressure in the calibration cell, which was evaluated at a temperature of 780 °C, versus time during the experiment. In the following the used calibration cell temperatures will be presented as salt reservoir temperature/cell temperature (730/780 °C).
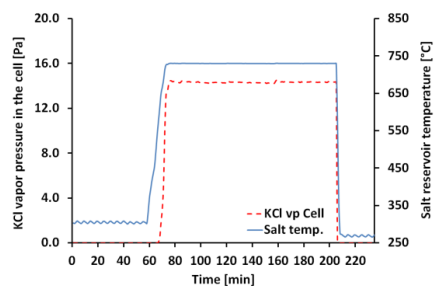
a)
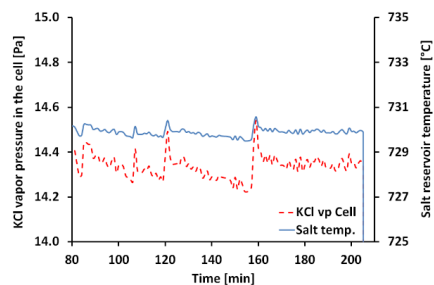
b)

Figure 3 a. *Salt reservoir temperature (solid line) and its corresponding KCl vapour pressure (dashed line) measured in the calibration cell at 730/780 °C.* **b.** *Close-up plot added to clearly show small variations in temperature and KCl vapour pressure in the cell during the measurement. The vapour pressure was calculated every minute and the temperature was measured every minute.*

The salt reservoir temperature between minutes 90 – 200 (cf. Figure 3a) is rather stable at 730 °C, except for three minor adjustments of less than 1 °C, cf. Figure 3b. These three adjustments were made at minutes 105, 120 and 160. The average salt temperature during the experiment was 729.9 °C with a standard deviation of 0.17 °C and a maximum and minimum temperature of 730.4 and 729.6 °C, respectively. The three salt temperature corrections also affected the KCl vapour pressure in the cell, as shown in Figure 3a and more in detail in Figure 3b. The KCl vapour pressure calculated in the cell during the experiment was on average 14.3 Pa with a standard deviation of 0.05 Pa and maximum and minimum vapour pressures of 14.5 and 14.2 Pa, respectively. The oscillations in the salt temperature before (minutes 0 – 60) and after (minutes 205 – 230) the experiment were due to temperature changes in the compressed air used as a cooling medium on these occasions. These oscillations were avoided during the experiment by switching from compressed air to N_2. However, the salt reservoir temperature and subsequently the KCl vapour pressure in the calibration cell could be even better stabilized with an automatic temperature controller instead of manual control (adjusting a needle valve), as was the case for this experiment. This was verified during the last 30 minutes (minutes 175 – 205) of the experiment when very stable operation was achieved (cf. Figure 3b). During minutes 175 to 205 the average salt temperature was 729.9 °C with a standard deviation of 0.07 °C and the difference between the maximum and minimum temperature was 0.3 °C. The average KCl vapour pressure during the same time span was 14.3 Pa with a standard deviation of 0.02 Pa, i.e. on the order of 0.14 %, and a difference between a maximum and minimum concentration of 0.1 Pa. Thus, the cell is able to maintain very stable KCl concentration levels at desired temperature.
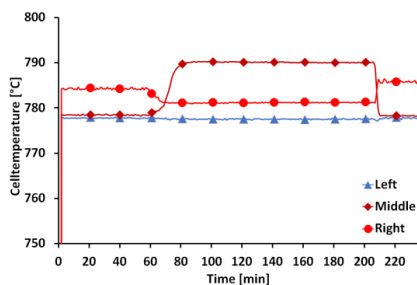
Figure 4. *Temperature on the left side of the cell (line with triangles), in the middle (line with diamonds) and at the right side (line with dots) in the calibration cell during the experiment.*

Figure 4 shows the temperature measured at three locations on the cell: the left end, the middle and the right end when the temperature in the cell was set to 780 °C. Initially, with sufficient cooling flow to maintain the reservoir temperature at temperature 300 °C the temperatures in Figure 4 follow values set by the temperature controllers of the furnace. The experiment started around minutes 60 when the cooling flow was reduced and switched to N_2 to obtain a reservoir temperature of 730 °C, sufficient for generation of detectable vapour but still 50 °C lower than the cell to avoid condensation in the measuring chamber. At this time the temperature at the right end (line with dots) and in the middle (line with diamonds) started to decrease and increase, respectively (cf. Figure 4). This is presumably due to two separate reasons. Firstly, the thermocouples mounted on the cell might be too close to the pipe that cools the salt reservoir since the pipe is not provided with any radiation shield (cf. Figure 1b). This might change the temperature profile in the vicinity of the thermocouples, which control the temperature in the furnace. Radiation from the heating elements heating the furnace in combination with reduced losses from the cooling tube is believed to be the cause for the temperature drop in the right part of the calibration cell at minutes 60 (cf. Figure 4). Secondly, it seems probable that the heating zones in the furnace are close enough to influence each other. During experiments it has been observed that the middle temperature controller of the furnace has not been able to follow the set point. The middle temperature has been around 10 °C too high in each experiment

as can be observed in the corresponding profile at minutes 60 in Figure 4 and is probably due to heating from the surrounding zones.

However, the slight temperature difference of 12 °C between the middle point and the ends is acceptable. This corresponds to a relative difference in absolute temperature on the order of 1% and a corresponding change in gas density and absorbance in the cell. Thus, the cell temperature is sufficiently homogenous for calibration measurements under well-defined conditions.
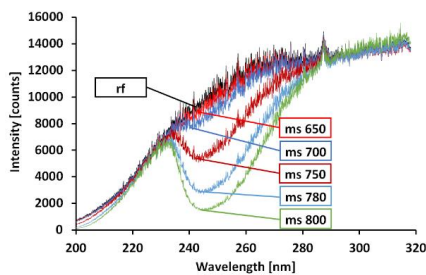
a)
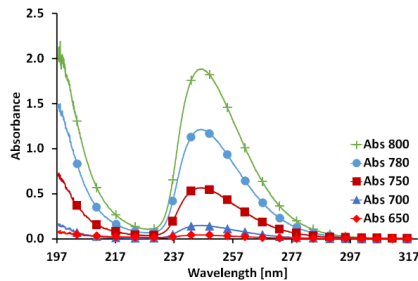
b)

Figure 5a. *Reference- and measured spectra at cell temperatures of 600/650, 650/700, 700/750, 730/780 and 750/800 °C during experiments. Each spectrum is an average of 200 sampled spectra. (rf = reference spectrum and ms = measured spectrum, numbers behind ms indicate the cell temperature).* **b.** *Absorbance spectra for cell temperatures 650 (line with diamonds), 700 (line with triangles), 750 (line with squares), 780 (line with dots) and 800 (line with crosses) °C. The symbols have been inserted to help spectrum identification in the plot.*

Reference spectra were sampled when the salt reservoir was kept at low temperature (about 300 °C) and no absorption was expected. The reference spectrum (rf) in Figure 5a is an average of such spectra sampled at cell temperatures 650, 700, 750, 780 and 800 °C. The measured spectra (ms) shown in Figure 5a were sampled when the salt reservoir temperature was kept at 600 (599.1), 650 (650.0), 700 (700.1), 730 (729.9) and 750 (749.6) °C, i.e. 50 °C below the corresponding cell temperature, resulting in sufficient vapour in the cell for absorption.

The absorbance spectra of KCl in Figure 5b obtained for different salt temperatures have been evaluated in the following way: firstly, a normalized spectrum is obtained by calculating the measured spectrum minus the background spectrum divided by the reference spectrum minus the background spectrum. Secondly, the negative natural logarithm of the resulting spectrum is calculated. The noise appearing in the raw data shown in Figure 5a is mostly caused by the uneven response of the pixels in the CCD detector of the spectrometer. The noise disappears once the measured and reference spectra have been divided with each other, as per the absorbance spectra in Figure 5b. It is shown in Figure 5b that gas-phase KCl has two major absorption regions: region 1, 200 – 220 nm and region 2, 230 – 300 nm as discussed by Davidovits and Brodhead [10]. The absorbance in region 2 at temperatures 650 °C and 800 °C corresponds to ~10% and 85% absorption of light through the cell and the KCl concentration is evaluated in this region by means of differential optical absorption spectroscopy (DOAS) [11]. The absorption measurements performed with this set-up at a cell temperature of 650 °C with the corresponding salt reservoir temperature at 599.8 °C results in a maximum absorbance of 0.04 and sets the lower detection limit for this measurement system (cf. Figure 5b).

The vapour pressures in the calibration cell and subsequently the KCl concentration are based on 38 vapour pressure data points in the temperature region of 576 – 766 °C obtained from

literature [12]. The Antoine equation Eq. 2.1 with its coefficients was derived from the literature data and used to calculate the vapour pressure of KCl at reservoir temperatures: 600 (599.8), 650, 700 (700.2), 730 (729.9), and 750 (749.6) °C. For comparison, vapour pressure calculations were also made with the Clausius-Clapeyron equation and the HSC Chemistry 7.1 software [14]. The results from these calculations are presented in Figure 6 together with the experimental raw data [12] used to fit the Antoine equation coefficients.
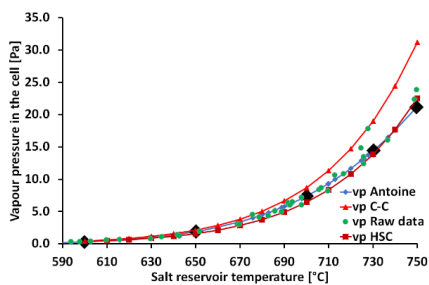

Figure 6. *KCl vapour pressure calculated by the Clausius-Clapeyron equation (vp C-C, triangles), calculated by the Antoine equation determined by the literature data (vp Antoine, diamonds), of the raw data used to determine the Antione constants (vp Raw data, dots) and calculated by a commercial software (vp HSC, squares). Data (5 points) from the performed experiment are marked with black larger diamonds.*

Figure 6 shows that all calculations and the original experimental data of van der Kemp agree well with each other up to temperature 640 °C. At around 660 °C the values obtained from the Clausius-Clapeyron equation start to deviate and appear higher than those of the other calculations. Since the Clausius-Clapeyron equation is an approximation it is reasonable that its values deviate from the rest. When the temperature reaches around 700 °C it can be seen that the experimental data starts to fluctuate more than previously. However, with the exception of the three highest vapour pressure measurements at 730 °C, it can be seen that the calculations

by the Antoine equation and the HSC software follow the experimental data. Thus, KCl vapour pressures in the investigated temperature regime are well characterized.

Nevertheless, thorough vapour pressure measurements in the temperature region of 700 – 750 °C could improve the accuracy of the experimental data further. That would lead to increased accuracy and reliability for the calculated vapour pressure and subsequently the determined KCl concentration in the cell. In the following the Antoine equation, based on experimental data, has been used to calculate the vapour pressures in the cell. From Figure 5b it can be seen that the absorbance measured for cell temperature 600/650 °C indicates the detection limit for the present experimental configuration. From Figure 6 it can be seen that this corresponds to a vapour pressure of less than 1 (0.3) Pa. Improved sensitivity could be achieved using multiple passages through the cell to increase the absorption path length.

Calculated KCl vapour pressures in the cell at the investigated reservoir temperatures are shown with the circle symbols in Figure 7.
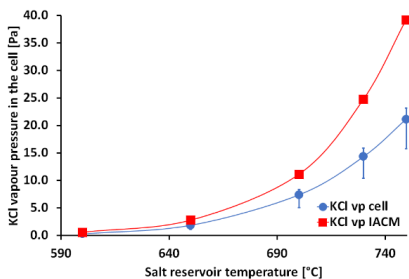

Figure 7. *KCl vapour pressure from all experiments, obtained by IACM (KCl vp IACM, line with squares), and calculated by the Antoine equation, Eq. (2.1) (KCl vp cell, line with dots). Each measurement has been assigned its proper error bar. The error bars for KCl vp IACM are so small that they are covered by their symbol. Details are given in the main text.*

The uncertainty in the salt reservoir temperature directly affects the accuracy of the calculated KCl vapour pressure in the calibration cell and thermocouple calibrations indicate an uncertainty in measured temperatures of 5 °C. In addition, a possible positive temperature offset of 15 °C, caused by the movement of the thermocouple that measured the salt reservoir temperature, was identified. During a set of measurements, it was found that the thermocouple had moved away from the salt reservoir, possibly due to thermal expansion in the thermocouple originating from the randomized trials where the salt reservoir experiences temperature changes between 300 – 450 °C. These temperature changes occur at the beginning of an experiment (increasing the salt reservoir temperature) and at the end of an experiment (decreasing the salt reservoir temperature). The problem was solved by inserting a thin metal wire in the cooling pipe from the opposite side to that of the thermocouple and connect it to the thermocouple. This made it possible to pull the thermocouple back and place it in position before a new experiment was started. On a few occasions it was observed that the reservoir temperature reading dropped about 10 – 15 °C when the thermocouple was pulled back by means of the metal wire. Thus, such shift in thermocouple position could potentially mean that the reading provides an overestimation of the reservoir temperature and vapour pressure. A correct salt reservoir temperature results in a correctly determined vapour pressure, which is subsequently used to produce a calibration spectrum. An overestimated salt reservoir temperature due to the offset in thermocouple position as outlined above results in an overdetermined vapour pressure. The combined effects of thermocouple uncertainties and the temperature offset were investigated in evaluations assuming a salt reservoir temperatures 15 °C lower and 5 °C higher than the thermocouple reading. The results are indicated by the error bars in Figure 7 showing KCl vapour pressures to be either over predicted by 23 – 49% or under predicted by 8 – 23% with the largest relative errors obtained for the lowest temperature.

The IACM instrument has been used to measure KCl concentrations, which have been recalculated to vapour pressures in the calibration cell and the results are shown as square symbols in Figure 7. The measured KCl vapour pressures are about 75 – 100% higher than those determined from calculations with the largest error referring to the lowest temperature/vapour pressure. The differences are significantly higher than the uncertainties estimated for the cell vapour pressures as described above and is probably related to the original calibration procedure on which the absorption evaluation is based [8]. In the evaluation the measured spectrum is fitted to a calibration spectrum measured during continuous evaporation of a certain mass of KCl transported through a calibration cell placed in a furnace [8]. Possible sources of error are salt losses during transport to the cell, a non-uniform temperature profile in the furnace, and pressure build-up in the calibration cell. During operation of this previous calibration equipment it has been noticed that absorption spectra on occasion show traces of previously measured compounds, which indicates that salt vapour can stick to the walls of the tube, which transports a gas-mixture of N_2 and vaporized KCl to the measuring chamber. A temperature gradient in the calibration cell will result in a density gradient of KCl molecules, which introduces a bias in absorption towards low-temperature high-density regions. Even though the calibration cell is built of aluminium oxide, the KCl vapour might induce corrosion in the surrounding steel tubes. Corrosion products could potentially lead to a pressure increase in the cell, which is assumed to have atmospheric pressure during normal conditions, resulting in an excessively high absorption spectrum and in turn a too low concentration value for the calibration spectrum.

Uncertainties due to salt losses, non-uniform temperature profile and pressure build-up in the previous calibration cell have been considered for and are avoided in the newly developed calibration cell presented in this article. Salt losses are avoided in the sealed cell and the salt

reservoir has been made the coldest point of the cell, which determines the vapour pressure. Any wall effects, which result in a pressure drop, will automatically be corrected by the vapour pressure set according to the salt reservoir temperature. In this design, pairs of thermocouples mounted on the cell at the ends and in the middle for combined control and measurements of the temperature ensures that inhomogeneity in cell temperature and accordingly vapour number density is minimized, which then renders a reliable absorption spectrum. The only pressure build-up in the calibration cell originates from the Argon, increased from 100 Pa at room temperature, and the pressure of KCl and K_2Cl_2 vapours at the cell temperature. This avoids unknown pressure build-ups. The new calibration cell has been operated at salt reservoir temperatures of 600, 650, 700, 730 and 750 °C and repeated measurements in randomized orders give reproducible calibration spectra evaluated to the same vapour pressures.

A factor for consideration when comparing calculated and measured KCl vapour pressures in the cell is the formation of the dimer K_2Cl_2. For the investigated temperatures the vapour pressure of this compound is around 20% of that of KCl [12] and the small dimer contribution to the total pressure is thus negligible. The dimer possibly contributes to the UV absorption spectra as suggested by Davidovits and Brodhead [10]. However, this could likely not explain the overestimation of KCl vapour pressures when evaluating the cell spectra using the IACM evaluation procedure since it is based on fit to a calibration spectrum measured on vaporized KCl and which also will contain dimer contributions.

Figure 8 shows KCl UV absorption cross-sections evaluated from measurements at five different KCl vapour pressures generated at the following salt reservoir/cell temperatures: 600/650, 650/700, 700/750, 730/780, and 750/800 °C.
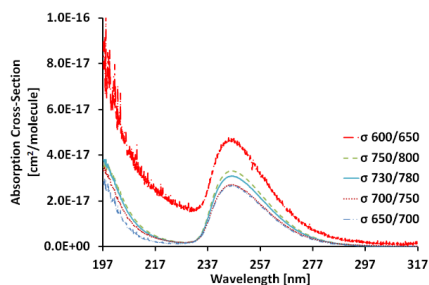
Figure 8. *The absorption cross-sections for gas-phase potassium chloride at different temperatures.*

With the exception of the profile obtained for measurement at temperatures 600/650 °C, for which the uncertainty in KCl vapour pressure is the largest and the absorption in the cell is lowest, the profiles are grouped fairly well together in spite of the large variation in vapour pressures. The absorption from the KCl ground state to the unbound excited state is dependent on the ground state energy level population determined by the temperature-dependent Boltzmann distribution. This would in turn introduce a temperature dependence of the absorption spectral profiles. The absorbance spectra were normalized to investigate if other temperature effects than changes in gas density could be observed as changes in spectral shape and are shown in Fig. 9a.
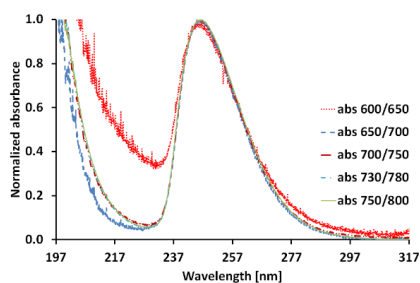
a)
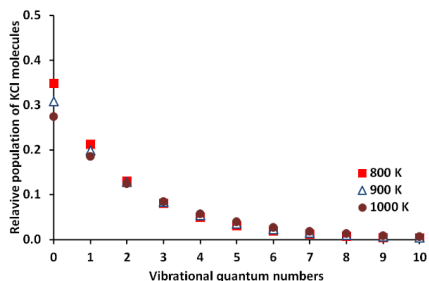
b)

Figure 9a. *Normalized absorbance spectra for cell temperatures of 600/650, 650/700, 700/750, 730/780 and 750/800 °C.* **b.** *The relative population of vibrational levels in the KCl molecules at different temperatures.*

With the exception of the spectrum corresponding to temperature combination 600/650 °C, the spectra show similar shape and do not indicate any temperature effects. Population fractions for vibrational levels of the KCl ground state were calculated for the investigated cell temperatures and are shown in Fig. 9b.

On the order of 6% of the population for vibrational levels of quantum number $v = 0, 1$, and 2 is redistributed to higher vibrational levels when the temperature is increased from 650 to 800 °C. This suggests a weak temperature dependence in agreement with the observations consistent shape of the normalized spectra for temperatures 650/700, 700/750, 730/780, and 750/800 °C in Fig. 9a. The redistributed population for temperature changes between 650 and 700 C is on the order of 2%. The prominent difference in absorption cross sections observed between temperatures 600/650 and 650/700 °C (cf. Fig. 8) is likely due to the previously discussed uncertainties in temperature and KCl vapour pressure at temperature 600/650 °C. For example, assuming an increased salt reservoir temperature of 10 °C would place the absorption cross-section for temperature of 600/650 °C with the others.

Vapour pressures of the KCl monomer and the K_2Cl_2 dimer have different temperature dependencies and even though the monomer pressure remains higher at all temperatures, dimer formation is increasingly favoured at higher temperatures [12]. Significant contributions from both of these components to the absorption spectrum would therefore most likely introduce changes in spectral shape with temperature. The similarity in shape observed for the majority of the normalized absorbance spectra (cf. Fig. 9a) thus suggests that the monomer, dominant at lower temperatures, remains the main contribution to the absorbance spectra.

Figure 10 shows the absorption cross-section for $\lambda = 197.6$ nm, the shortest wavelength of the measurement system, and for $\lambda = 246.2$ nm for gas-phase KCl at elevated temperatures and concentrations. The figure also shows that the absorption cross-sections for the cell temperature of 600/650 °C deviates considerably compared to the rest. This is believed to be due to large uncertainty in the vapour pressure, as earlier discussed. Since the other four vapour pressures at the wavelengths $\lambda = 197.6$ nm and $\lambda = 246.2$ nm, respectively, are scattered around a horizontal line, they indicate that the absorption cross-sections are temperature-independent in the evaluated temperature region of 700 – 800 °C. The average absorption cross-section for these two wavelengths has been calculated to: 3.4×10^{-17} cm^2/molecule with a standard deviation of 4.2×10^{-18} for $\lambda = 197.6$ nm and 2.9×10^{-17} cm^2/molecule with a standard deviation of 3.0×10^{-18} for $\lambda = 246.2$ nm.
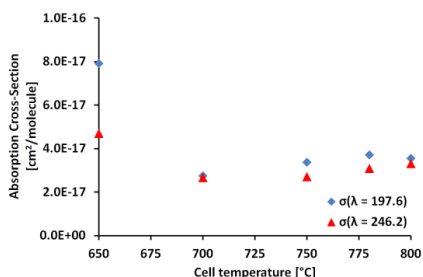
Figure 10. *Absorption cross-sections for λ = 197.6 nm and λ = 246.2 nm of gas-phase potassium chloride at elevated temperatures.*

Short wavelengths approaching the vacuum ultraviolet region below 200 nm can be employed for alkali compound detection by means of laser based photofragmentation fluorescence, for example using Excimer lasers at 193 nm [18, 19]. Thus, KCl absorption cross sections in this wavelength region are of interest for quantitative analysis of laser induced photofragmentation data.

The absorption cross-section at 246 nm determined by Davidovits and Brodhead [10] on vapours of melted KCl in a temperature region of 841 to 951 °C was 2.0×10^{-17} cm²/molecule. The average absorption cross-section determined on sublimated vapour in the calibration cell at the same wavelength was calculated to 2.9×10^{-17} cm²/molecule in a temperature region of 700 – 800 °C. A comparison between the absorption cross-sections shows the value of Davidovits and Brodhead to be about 70% of that determined in the calibration cell. The absorption cross-section determined in the calibration cell for λ = 197.6 nm shows the same pattern, a slightly higher value than for λ = 246.2 nm, which is also reported in Davidovits and Brodhead [10]. Oldenborg and Baughcum [19] determined the absorption cross-section for KCl to be $(4.1 \pm 0.6) \times 10^{-17}$ cm²/molecule at a 193.4 nm which is in good agreement with that determined in the calibration cell for 197.6 nm. However, the difference between those two

values is smaller for those determined in the calibration cell than for those determined by Davidovits and Brodhead [10].

The calibration technique presented in this article can easily be used to generate calibration spectra of other alkali compounds, such as sodium chloride (NaCl), which is of interest in waste and coal combustion. This compound has vapour pressures rather close to those of KCl and the cell could thus be operated under conditions similar to those for the investigations of KCl. There is also a need for calibration data for sodium hydroxide (NaOH) and for potassium hydroxide (KOH) [5]. Previous studies indicate that hydroxides exhibit absorption cross sections about one order of magnitude lower than those of the chlorides [20]. Moreover, since vapour pressures for solid-gas equilibrium for these compounds are rather low [14] the cell needs to be operated above the melting points, 318 °C for NaOH and 406 °C for KOH, to achieve sufficient vapour pressures in the cell. For KOH reservoir temperatures between 600 and 750 °C this result in vapour pressures in the range 5 – 130 Pa, which despite the lower cross section expected for KOH would provide sufficient absorption in the cell for reliable measurements. In contrast, NaOH vapour pressures are lower and temperatures around 900 °C would be required to achieve vapour pressures on the order of 30 – 50 Pa necessary to achieve sufficient absorbance. Alternatively, improved sensitivity and detection at lower vapour pressures can be achieved by arranging dual passages through the cell increasing the absorption path length by a factor of two.

4. Conclusions

The design and performance of a calibration cell based on a cold finger has been demonstrated, which can be employed to generate KCl vapour at stable well-defined concentration and temperature. The cell is suitable for UV absorption measurements to obtain calibration spectra or to perform detailed studies of the absorption cross-section for KCl. Investigations using an instrument for UV absorption measurements of KCl showed that improved calibration and absolute accuracy for the instrument can be obtained compared with previous approaches. In addition, more reliable KCl UV absorption spectral profiles and cross-sections have been measured over different chosen temperatures. The concept of the calibration cell can equally be employed for investigations of other alkali chlorides such as NaCl or hydroxides, i.e. KOH and NaOH. In other words, the cell has potential to be used for detailed spectroscopic studies of high relevance for development of alkali-measuring devices used in biomass combustion to determine alkali concentrations in the flue gas. This research has proven the working hypothesis in that the new design of the calibration cell is fit for this purpose.

5. Acknowledgements

References

1. Leffler, T., C. Brackmann, M. Berg, Z.S. Li, and M. Aldén, *On-line Alkali Measurement for Fuel Quality Control in Biomass-operated Boilers.* Industrial Combustion, 2016.

2. Andersson, C.S., *European Patent EP 1354167 (2006).* VATTENFALL AB PUBL (SE).

3. Kassman, H., J. Pettersson, B.M. Steenari, and L.E. Åmand, *Two strategies to reduce gaseous KCl and chlorine in deposits during biomass combustion - injection of ammonium sulphate and co-combustion with peat.* Fuel Processing Technology, 2013. **105**: p. 170-180.

4. Monkhouse, P., *On-line spectroscopic and spectrometric methods for the determination of metal species in industrial processes.* Progress in Energy and Combustion Science, 2011. **37**(2): p. 125-171.

5. Sorvajärvi, T., N. DeMartini, J. Rossi, and J. Toivonen, *In situ measurement technique for simultaneous detection of K, KCl, and KOH vapors released during combustion of solid biomass fuel in a single particle reactor.* Appl Spectrosc, 2014. **68**(2): p. 179-84.

6. Leffler, T., C. Brackmann, A. Ehn, B. Kaldvee, M. Aldén, M. Berg, and J. Bood, *Range-resolved detection of potassium chloride using picosecond differential absorption light detection and ranging.* Applied Optics, 2015. **54**(5): p. 1058-1064.

7. Andersson, C.S., *European Patent EP 1221036 (2006).* VATTENFALL AB PUBL (SE).

8. Forsberg, C., M. Broström, R. Backman, E. Edvardsson, S. Badiei, M. Berg, and H. Kassman, *Principle, calibration, and application of the in situ alkali chloride monitor.* Review of Scientific Instruments, 2009. **80**(2).

9.   Grosch, A., V. Beushausen, H. Wackerbarth, O. Thiele, and T. Berg, *Temperature- and pressure-dependent midinfrared absorption cross sections of gaseous hydrocarbons.* Applied Optics, 2010. **49**(2): p. 196-203.

10.   Davidovi.P and D.C. Brodhead, *Ultraviolet Absorption Cross Sections for Alkali Halide Vapors.* Journal of Chemical Physics, 1967. **46**(8): p. 2968-&.

11.   Platt, U. and D. Perner, *Measurements of Atmospheric Trace Gases by Long Path Differential UV/Visible Absorption Spectroscopy*, in *Optical and Laser Remote Sensing*, D.K.a.M. Killinger, A., Editor. 1983, Springer-Verla Berlin Heidelberg New York. p. 97-105.

12.   Vanderkemp, W.J.M., L.C. Jacobs, H.A.J. Oonk, and A. Schuijff, *The Vapor Composition and Pressure over Solid Potassium-Chloride - New Mass-Spectrometric Results and Effusion Masses.* Journal of Chemical Thermodynamics, 1991. **23**(6): p. 593-604.

13.   Thomson, G.W., *The Antoine Equation for Vapor-Pressure Data.* Chemical Reviews, 1946. **38**(1): p. 1-39.

14.   Roine, A., *Outukumpu HSC chemistry for windows version 7.1.* 2011, Outokumpu Research: Pori, Finland

15.   Mayer, J.E. and I.H. Wintner, *Measurements of low vapor pressures of alkali halides.* Journal of Chemical Physics, 1938. **6**(6): p. 301-306.

16.   Western, C.M., PGOPHER, a Program for Simulating Rotational Structure, Version 7.1.108, University of Bristol (2010), http://pgopher.chm.bris.ac.uk

17.   Barton, E.J., C. Chiu, S. Golpayegani, S.N. Yurchenko, J. Tennyson, D.J. Frohman, and P.F. Bernath, *ExoMol molecular line lists V: the ro-vibrational spectra of NaCl and KCl.* Monthly Notices of the Royal Astronomical Society, 2014. **442**(2): p. 1821-1829.

18. Chadwick, B.L., G. Domazetis, and R.J.S. Morrison, *Multiwavelength Monitoring of Photofragment Fluorescence after 193-Nm Photolysis of Nacl and Naoh - Application to Measuring the Sodium Species Released from Coal at High-Temperatures.* Analytical Chemistry, 1995. **67**(4): p. 710-716.

19. Oldenborg, R.C. and S.L. Baughcum, *Photofragment Fluorescence as an Analytical Technique - Application to Gas-Phase Alkali Chlorides.* Analytical Chemistry, 1986. **58**(7): p. 1430-1436.

20. Self, D.E. and J.M.C. Plane, *Absolute photolysis cross-sections for NaHCO3, NaOH, NaO, NaO2 and NaO3: implications for sodium chemistry in the upper mesosphere.* Physical Chemistry Chemical Physics, 2002. **4**(1): p. 16-23.

Paper V

Experimental Investigations of Potassium Chemistry
in Premixed Flames

Tomas Leffler[1,2], Christian Brackmann[1,*], Wubin Weng[1],
Qiang Gao[1], Marcus Aldén[1], Zhongshan Li[1]

[1]Division of Combustion Physics, Lund University, Box 118, SE-221 00, Lund, Sweden

[2]Vattenfall Research and Development AB, SE-814 26 Älvkarleby, Sweden

[*]corresponding author: christian.brackmann@forbrf.lth.se

Abstract

Quantitative potassium species concentrations have been measured in alkali-seeded premixed methane-air flames of different stoichiometry. Potassium chloride (KCl) and hydroxide (KOH) were measured by broadband UV absorption and laser-induced photofragmentation fluorescence while atomic potassium was measured using tuneable diode-laser spectroscopy. In addition, laser Rayleigh scattering was employed for temperature measurements. Investigations were made for different alkali-seeding levels and chlorine loads resulting in KCl/KOH concentrations up to ~30 ppm and concentrations of K atoms at ppm levels. Results were compared with predictions from a chemical mechanism used in a homogenous reactor model. Experimentally observed trends, decrease in KCl and KOH concentrations and increase in K-atom concentrations with flame equivalence ratio, were well reproduced in simulations and are compared with results reported in literature. In addition, diagnostics required for further investigations of alkali-related combustion phenomena and detailed model validation of alkali chemistry are discussed.

Introduction

Formation of alkali compounds during combustion remains of high practical importance due to the need for utilization of biomass fuels containing alkali and chlorine contents [1, 2] The tendency of these fuel components to form corrosive alkali chlorides result in severe problems during combustion in boilers and furnaces [3, 4]. Additional problems related to the formation of alkali compounds also include fouling and slagging. Thus, detailed knowledge on the formation process during combustion is crucial for efficient utilization of biomass fuel while also minimizing problems during power plant operation. Moreover, trace-level species, such as alkali and chlorine [5], in the fuel which even though many times neglected in combustion models, have been found to have rather strong impact on the overall combustion process, affecting the fuel oxidation process as well as formation of NO_x [6]. This has mainly been attributed to their ability to participate in chain-branching or chain-terminating chemical reactions resulting in production or consumption of flame radicals such as H, and OH. In combustion chemistry potassium atoms are reported to consume flame radicals such as O and H forming potassium hydroxide (KOH), which in turn establishes rapid equilibrium with KCl [6]. Thus, in addition to forming harmful pollutants the alkali has an overall impact on the combustion chemistry via its consumption of flame radicals. The combustion chemistry of potassium and chlorine is also coupled to that of sulfur via the ability of sulfur to transform potassium chloride to less harmful alkali sulfates [7]. Thus, in addition to understand pollutant formation of alkali species, knowledge on their impact on the overall combustion process and coupling with each other via the flame radical pool is also necessary for development of comprehensive models for biomass fuel combustion.

Detailed studies of alkali chemistry in flames allows for development of chemical mechanisms, which enable predictions of alkali formation under different combustion conditions. Experimental data acquired under well-defined conditions are crucial input for further development and validation of such mechanisms. For example, a study including experiments as well as kinetic modelling of sodium-species in hydrogen flames has been presented by Hynes et al. [8] For potassium, early investigations have included studies on its effect on flame inhibition [9] but also potassium kinetics in premixed methane flames [10]. A rather recent study was made to investigate the effect of sulphur addition on potassium-species formation [11]. In addition to studies of gaseous fuels, detailed characterization of potassium release has also been carried out for single particles of coal [12] and biomass [13].

According to the work presented by Slack et al. [10], when introduced in a flame potassium participates in chemical reactions involving O_2, atomic hydrogen, hydroxyl radical (OH), and water. The potassium species in these reactions are the atomic, potassium hydroxide, potassium oxide (KO), and potassium dioxide (KO_2). Moreover, fuel-rich combustion conditions result in increased formation of atomic potassium via reactions between potassium hydroxide and hydrogen atoms. Conversely the levels of potassium hydroxide are increasing at lean conditions favoured by the availability of oxygen and water. If potassium is introduced together with chlorine in a flame additional reactions will be included involving species such as atomic chlorine, hydrogen chloride, and potassium chloride [14]. Corresponding investigations of combustion in flames burning hydrogen or propane with sodium and chlorine added, show similar trends with decreasing levels of alkali atoms at higher equivalence ratios while chloride and hydroxide concentrations decrease. [14]

This paper presents measurements of potassium species concentrations in alkali-seeded premixed methane-air flames. The methods employed for species concentrations measurements include broadband UV absorption spectroscopy [15], laser-induced photofragmentation fluorescence [15, 16], and diode-laser absorption spectroscopy [15, 17]. While multiple optical diagnostic techniques have been employed for separate measurements in this work due to the large dynamic range of concentrations encountered in the investigated flames, combined measurements of K atoms, KOH, and KCl have been presented previously by Sorvajärvi et al. [18]. Potassium species concentrations measured by the methods used are compared and the dependence on flame equivalence ratio is analysed and discussed in terms of results previously reported in literature. The obtained results can be further employed for future model validation and refinement for alkali flame chemistry.

Experimental

Optical diagnostics

Photofragmentation fluorescence measurements were made using an ArF Excimer laser (Compex 102, Lambda Physik), which provided pulses at wavelength 193 nm with 25 ns pulse duration and output pulse energy of 50 mJ. The laser beam was focused using cylindrical lenses of focal lengths f = 1000 mm and f = 500 mm, which combined with an arrangement of razorblades resulted in a 20 mm vertical sheet. The photofragmentation-induced fluorescence signal was detected with an intensified CCD camera (PI-MAX I, Princeton Instruments) equipped with an f = 50 mm objective (Nikkor f/1.4). A bandpass filter centred at 766 nm (50

mm dia., OD 4, FWHM 10 nm, Edmund Optics) was used for suppression of scattered laser radiation.

The evaluation of alkali species concentrations from the photofragmentation fluorescence signal has been described in detail in a previous publication [19]. In brief, the signal, F, is given by Eq. (1)

$$F = \frac{\Omega}{4\pi} l \varepsilon_F A \frac{A_{fi}}{A_{fi} + Q} TN$$ (1)

where h is Planck's constant, v the fluorescence frequency, Ω the detection solid angle, l the probe volume length, ε_F the detection efficiency for the fluorescence signal, and A is the probe volume cross section area. The fluorescence quantum yield is given by $\frac{A_{fi}}{A_{fi} + Q}$ where A_{fi} is the Einstein coefficient for spontaneous emission and Q the collisional quenching rate. The factor T accounts for fluorescence losses due to absorption, so-called trapping, which in this case is generated by atomic potassium formed in the flame chemistry. The quantity N is the concentration of alkali atoms generated in the excited K-atom 4^2P states by photofragmentation.

Coefficients for spontaneous emission and data on collisional quenching have been obtained from literature. The beam cross section area A, can be estimated from calculations of the width for a focused Gaussian beam, resulting in a beam width of 25 μm, together with the height of the focused laser sheet, which was 20 mm. The solid angle and detection efficiency can be retrieved by calibration using the Rayleigh scattering signal. The concentration of photofragmented potassium compounds is related to the evaluated concentration of K atoms according to Eq. (2)

$$N = N_{KCl} \Phi (1 - e^{\frac{-\sigma E}{h v_{laser} A}})$$ (2)

The factor Φ is the yield of photofragments generated from the parent species and is equal to 1 for the investigated case since dissociation of one KCl molecule results in creation of one K (4^2P) atom. Furthermore, σ is the absorption cross section, E the laser pulse energy, and v_{laser} the laser frequency.

Rayleigh scattering measurements were made using the 532 nm second harmonic of a Nd:YAG laser (Brilliant B, Quantel) with a pulse duration of 7 ns and a pulse energy of 120

mJ. The 532 nm beam was aligned into the beam path and shaped into a laser sheet of 10 mm width using cylindrical lenses of focal lengths f=-40 mm, f=200 mm, and f=500 mm. A half-wave plate positioned in the beam path was adjusted to achieve vertical polarization for optimal Rayleigh scattering. The Rayleigh scattering signal measured at ambient conditions provides the detection solid angle, Ω, and the probe volume length, l, in the concentration evaluation using Eq. (1). In addition, Rayleigh scattering can be utilized for flame temperature measurements by comparison of signals measured in flame and at ambient conditions, taking differences in cross sections into account. Using Rayleigh scattering cross-section data and species concentrations determined from chemical equilibrium calculations, the Rayleigh scattering cross sections of the product gas in the post-flame region of the investigated flames were found to be typically 10% higher than that of ambient air.

Broadband UV absorption measurements of KCl were made using a 150 W UV light source (L1314, Hamamatsu). The light was emitted through an aperture and collimated using a 90° off-axis parabolic mirror with a reflective focal length of f=150 mm (diameter 50 mm, Thorlabs). The collimated UV light beam subsequently passed through another aperture and a plano-convex focusing quartz lens of focal length f=150 mm. The UV beam was guided in five passages across the burner through the flame using UV-enhanced aluminium mirrors (diameter 25.4 mm, Thorlabs) and then collected in an UV-enhanced collimator (250 - 450 nm, diameter 12 mm beam, SMA, Thorlabs). This arrangement gave a total absorption path length of 138 mm. The collected UV light was transferred through an optical fibre (FC-UV600-0.5-SR, Azpect Photonics) to a spectrometer (grating 2400 grooves/mm, slit width 50 μm, AVABENCH-75-2048, Azpect Photonics). KCl concentrations were evaluated from acquired spectra by a least-squares fit to a calibration spectrum measured at temperature 860 °C following the procedure presented by Forsberg et al. [20].

Tuneable diode laser spectroscopy for measurement of potassium atoms was made using a single-mode external cavity laser (DL 100, Toptica Photonics) with output power of 40 mW and a central wavelength of 769.9 nm. A scan control module (SC 110) controls a piezoelectric crystal to change the cavity length and obtain wavelength scanning with a repetition rate of 110 Hz. The laser has excellent tuning ability and can be scanned over a frequency range of 25 GHz without mode-hop, and overlaps perfectly with the D_2 line of potassium. The laser passes through the flame at the centre of the burner path length of 23 mm. A photodiode detector (DTE 210, Thorlabs) was used to receive the laser after absorption by the potassium in the flame. The detector was connected to a data acquisition card (BNC 2110, National Instrument) and an on-

line data processing program based on LabVIEW was employed to monitor the potassium concentration.

Burner

A burner originally made for atomic absorption spectroscopy (Perkin-Elmer), shown in the photo of Fig. 1, was used for measurements in alkali-seeded methane-air flames. The burner has a water-cooled head with a central compartment for the premixed fuel-air blend and an outer channel for a co-flow shielding the flame. The diameter of the inner compartment is 23 mm and the head is topped by a circular honeycomb plate (pore size ~1 mm and length 20 mm). The burner allows for stabilization of flat laminar premixed flames (cf. Fig. 1).

Gases are supplied to the burner through a spray chamber with two connections for air, auxiliary air and nebulizer air, and one connection for the fuel. The nebulizer flow provides seeding of alkali solution, which enters via a capillary tube immersed into the liquid. The alkali-solution from the nebulizer is pre-treated as the droplets collide with a so-called impact bead and a flow spoiler in order to have only finer aerosol droplets to pass through the chamber to the burner head while larger droplets are removed via a drain tube. Methane and auxiliary air are mixed together with the nebulizer air in the spray chamber to get the total correct equivalence ratio of the mix.

A nitrogen co-flow of 10 ln/min was supplied to the burner head to shield the flame. A steel cylinder (cf. Fig. 1) was mounted 30 mm above the burner for flame stabilization required for quantitative signal analysis and to be able to make sequential photofragmentation and Rayleigh scattering measurements under steady-state conditions. The total gas flow of air and fuel to the burner was 5.6 ln/min and individual flows of nitrogen, air to the nebulizer, primary air, and fuel were controlled by four mass flow controllers with maximum flows of 20, 10, 5 and 1 ln/min (Bronkhorst), respectively. Premixed methane-air flames of equivalence ratios 0.8 – 1.3 were investigated and the individual flows are given in Table 1.
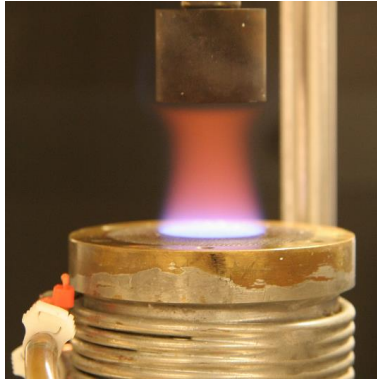
Figure 1. *Methane-air flame of equivalence ratio Φ=1.1 stabilized on porous plug Perkin-Elmer burner with alkali-seeding (KCl) through a nebulizer. Laminar uniform flames were achieved with a stabilizer mounted 30 mm above the burner surface.*

ϕ	CH_4 (L_n/min)	Air (L_n/min)
0.8	0.41	5.19
0.9	0.46	5.14
1	0.51	5.09
1.1	0.55	5.05
1.2	0.60	5.00
1.3	0.64	4.96

Table 1. *Experimental conditions for methane-air flames.*

Chemical Equilibrium Calculations

Post-flame compositions for the investigated flames were obtained through calculations using the PREMIX module in the CHEMKIN software. Conditions of KCl/KOH flame-seeding were then mimicked by introducing atomic species, K and Cl, into the post-flame mixture predicted for each flame. Simulations of these alkali-seeded mixtures were in turn made using the closed homogenous reactor model at temperature 1500 K and atmospheric pressure with a mechanism for alkali-chemistry developed by Hindiyarty et al. [11, 21]. These simulations provided concentrations versus reaction time for KCl, KOH, and K atoms and illustrated the progress towards chemical equilibrium for each condition.

7

Results and Discussion

Temperatures of the investigated flames were measured by means of Rayleigh scattering and the product gas temperatures for two levels of KCl-seeding are shown in Fig. 2. The temperatures reside within the range 1400-1500 K for both conditions and the uncertainty is estimated to be 9% indicated by the error bars. Thus, within the estimated accuracy the two data sets provide similar results. The mean temperature value from two data sets show differences up to 70 K and for both conditions the profiles show the same trend of variations with equivalence ratio with temperature differences less than 50 K. Moreover, the temperatures measured at high KCl-seeding are consistently lower suggesting some additional cooling by the increased KCl concentration.
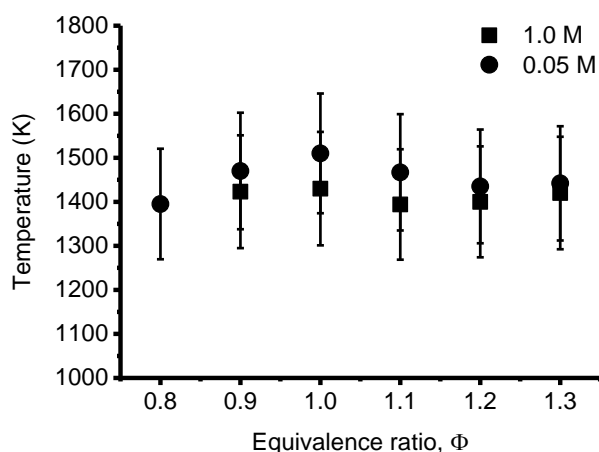

Figure 2. *Average temperature in post-flame region of premixed methane-air flames with two different levels of KCl-seeding to the flame. Circles 0.05 M solution, squares 1.0 M solution. The estimated temperature uncertainty is 9% (error bars), the consistently lower temperatures for the 1.0 M case indicate that high levels of alkali salt may induce some cooling.*

Introducing potassium compounds in the flames result in the formation of atomic potassium as evident from the yellow-red color observed for the seeded flames (cf. Fig. 1). Potassium element concentrations were measured using TDLAS for seeding of KOH and KCl and the results are shown in Fig. 3. The high absorption cross section of atomic potassium D_2 line, on the order of 10^{-12} cm^2, required rather low seeding concentrations to avoid saturation of the absorption line. Experimental data measured for seeding with 0.0025 M solution of KOH and

0.005 M solution of KCl are shown with filled black symbols in Fig. 3a and 3b, respectively. While absorption measurements were unattainable at higher seeding levels, the atomic emission lines in the flame chemiluminescence provide a measure of the K-atom content of the flame. Figure 3c shows flame chemiluminescence versus concentration of the KCl solution used for flame seeding. Two data sets, plotted in the log-log diagram with closed and open symbols, follow a linear trend with a slope of ½, indicating a dependence on $N^{1/2}$ for the chemiluminescence. At high seeding concentrations chemiluminescence is emitted under optically thick conditions where strong absorption at the center of the atomic spectral line result in virtually no transmission of light. However, at the wings of the lineshape absorption is lower allowing for transmission and resulting in the observed $N^{1/2}$ trend. Absorption and emission under optically thick conditions in this type of flames are described more in detail in refs. [22, 23]. This indicates that the K-atom level can be considered proportional to the seeding concentration and that concentrations for higher seeding can be calculated from the quantitative results obtained by TDLAS at low seeding levels. Thus, K atom concentrations calculated through extrapolation for higher seeding levels, corresponding to the experimental conditions for which potassium compounds have been measured, are also plotted in Fig. 3a and 3b with open symbols for the following discussion.

Figure 3d shows chemiluminescence versus height above the burner for three different flame stoichiometries for seeding with 1.0 M KCl solution. All profiles show their highest intensity at lower positions towards the burner and the flame reaction zone. Peak chemiluminescence positions are located at 8-10 mm and indicate high K-atom levels from the flame-front region. Above these positions the profiles show a rapid decrease up to around 15 mm and then a more gradual decrease with height. Rayleigh scattering thermometry indicates temperatures in the range 1300-1500 K for the region 11-18 mm above the burner and a temperature profile for the stoichiometric flame is also shown in Fig. 3d. Thus, the observed decrease in chemiluminescence probably indicates the progress of K-atom concentrations towards levels corresponding to a chemical equilibrium condition. In the vicinity of the flame stabilizer above 25 mm a more rapid decrease, attributed to cooling, is observed.
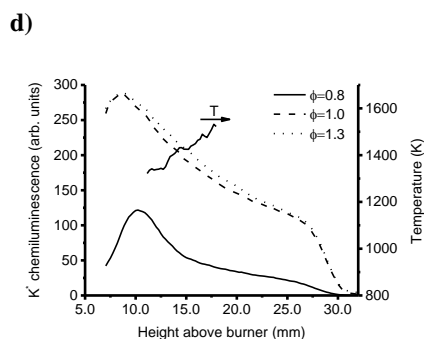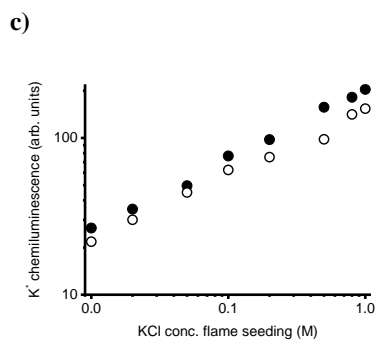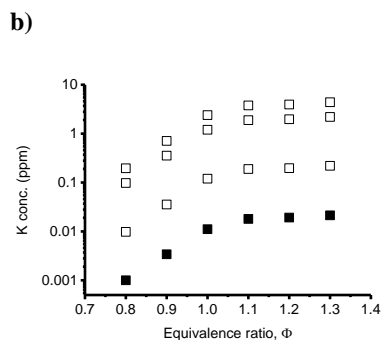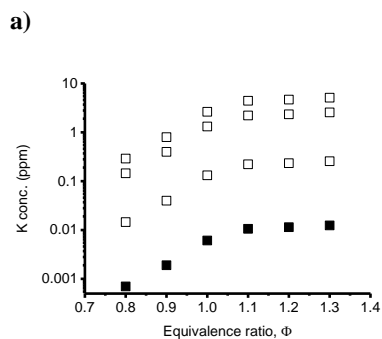
a)

b)

c)

d)

Figure 3. *Post-flame K-atom concentrations versus flame equivalence ratio.* ***a)*** *KOH seeding at solution concentrations of 0.025, 0.05 M, 0.5 M, and 1.0 M.* ***b)*** *KCl seeding at solution concentrations of 0.005, 0.05, 0.5, and 1.0 M. Experimental data are shown in solid symbol for 0.025 M KOH and 0.005 KCl while extrapolated values for higher seeding levels are shown in open symbols.* ***c)*** *Two data sets of K atom chemiluminescence measured at wavelength 766 nm vs. KCl seeding concentration in the stoichiometric flame.* ***d)*** *Flame chemiluminescence profiles measured in lean (Φ=0.8), stoichiometric, and rich (Φ=1.3) flame together with a temperature profile for the stoichiometric flame (plotted on the right axis). Higher K atom levels are observed for the stoichiometric and fuel rich flame. The profile of the lean flame shows a more planar shape in the product zone above 12 mm indicating a condition closer to chemical equilibrium.*

10

The TDLAS results as well as the chemiluminescence profiles show that atomic potassium concentration increase with equivalence ratio, in agreement with observations for sodium in flames burning methane, propane, and hydrogen [8, 14]. This can be attributed to increased levels of atomic and molecular hydrogen at fuel rich conditions. Atomic hydrogen is able to react with potassium hydroxide and/or potassium chloride forming atomic potassium and water or alternatively hydrogen chloride [14]. Equilibrium calculations as outlined above also predict an increase in K atom concentration with equivalence ratio and show a trend similar to experiments. Calculations for seeding of 30 ppm KCl into the flame show that the time to establish chemical equilibrium is 8 and 180 ms for the lean Φ=0.8 and rich Φ=1.3 flame, respectively. However, the time for transport from the burner surface to the region probed in the absorption measurements around 20 mm above the burner surface is 18 ms. Thus, while time to establish chemical equilibrium conditions in the post flame region of the lean flame is shorter than the transport time, it is longer for the fuel-rich flame and chemical equilibrium is not established, in agreement the shapes of the chemiluminescence profiles in Fig. 3d.

K atom concentrations estimated from TDLAS measurements made 21 mm above the burner are 0.2 and 4.4 ppm for the lean and rich flame, respectively. Comparing the calculated transport times with the reaction time profiles obtained from calculations indicate K atom concentrations to be 0.05 and 11 ppm for the lean and rich flame, respectively. As discussed previously the fuel lean condition is expected to be the closest to chemical equilibrium and the higher experimental value of 0.2 ppm may indicate that equilibrium has not been fully established. For the fuel rich flame the K atom concentration from experiments is lower than that predicted by the calculations instead indicating a condition closer towards equilibrium, with K atom concentrations of a few ppm, than estimated from the comparison between reaction and transport times. Nevertheless, it cannot be excluded that experimental K atom concentrations obtained from extrapolation of data measured at low seeding are underestimated even though a linear relation between K atom concentration and flame seeding is indicated in Fig 3c.

Potassium hydroxide and potassium chloride constitute the major alkali compounds formed in the post-flame region when KCl is introduced with the reactants into the flame [14]. The distribution between alkali-chloride and –hydroxide depends on chlorine availability as well as temperature [14]. Equilibrium calculations as well as analysis of KCl-seeded methane flames presented by Li et al. [11] and simulations by Schofield [14] indicate that low temperature favors chloride formation. Figure 4 shows alkali compound concentrations measured by UV absorption spectroscopy at flame equivalence ratios Φ=0.8-1.3.
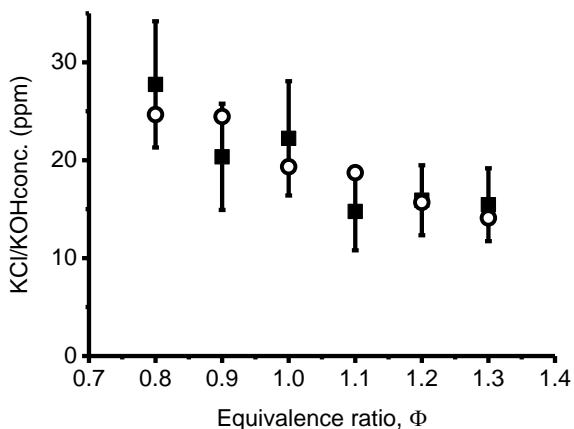
Figure 4. *Average post-flame concentration measured by UV absorption spectroscopy versus flame equivalence ratio for 1.0 M KCl seeding. Lean conditions show higher KCl concentrations. Circle symbols represents the sum KCl+50% KOH of calculated potassium species concentrations.*

Both KCl and KOH show absorption in the wavelength range 230-300 nm probed in the measurements and could contribute to the evaluated absorption spectra. While the peak absorption cross section of KCl at 245 nm has been reported as $2.0 \cdot 10^{-17}$ cm^2 by Davidovits and Brodhead [24] and also determined by the authors of this paper to $2.8 \cdot 10^{-17}$ cm^2, data for KOH are scarce. However, following the discussion by Sorvajärvi et al. [18] and comparing with values presented for NaOH [25] suggest a KOH absorption cross section of $0.5 \cdot 10^{-17}$ cm^2 at 245 nm. Moreover, preliminary investigations by the authors indicate a KOH absorption cross section close to $1.0 \cdot 10^{-17}$ cm^2. With absorption cross sections differing by a factor of two and for equal concentrations of KCl and KOH, the KCl/KOH concentrations would be a factor 2/3 of the evaluated concentration, i.e. the KOH contribution would be 1/3. With chlorine available at the temperatures of the investigated flames, chemistry is expected to promote KCl formation in the post-flame region, in particular under fuel-rich conditions [14]. Since the concentrations of KCl can be expected to be higher than for KOH, the contribution of KOH would be less than 1/3 of the evaluated concentration and the obtained values expected to mainly represent KCl.

Concentrations at lean and stoichiometric conditions are on average higher than values measured at fuel rich conditions. The observed trend is in agreement with the observed increase in K atom concentrations with equivalence ratio, cf. Fig. 3b. For comparison with the results

from absorption measurements, the sum of the calculated KCl concentration and half the calculated KOH concentration are also plotted in Fig. 4. The average concentrations measured by absorption spectroscopy drop from 28 ppm at equivalence ratio $\Phi=0.8$ to typically 15 ppm at fuel-rich conditions. Corresponding values from calculations decrease from 25 to 14 ppm and the trend of the experimental results is thus rather well reproduced by the calculations.

The increase in K-atom concentrations obtained from TDLAS data from 0.2 to 4.4 ppm is lower than the decrease of 13 ppm in KCl/KOH concentration of the absorption spectroscopy data. A possible explanation could be that the absorption spectroscopy data, evaluated assuming KCl only, not fully includes the contribution from KOH. An underestimation of KOH could be a contributing factor to the larger difference observed for concentrations of KCL/KOH compared with those of K-atoms going from lean to fuel-rich conditions. The increase in K-atom concentrations of 4 ppm is lower than results from calculations, resulting in an increase from 0.1 to 11 ppm. An underestimation of experimental K atom concentrations as referred to previously, could also be a possible explanation for the difference between measurements and calculations. Nevertheless, the difference between the trends for KCl/KOH and K-atoms is still within the uncertainty and spread of the absorption data indicated by error bars in Fig. 4, i.e. the lower part of the errorbar at $\Phi=0.8$ is around 22 ppm while the upper part of the errorbar at $\Phi=1.3$ is around 18 ppm corresponding to a difference of 4 ppm.

Detection of both KOH and KCl with better sensitivity than the absorption spectroscopy setup is offered by the laser-induced photofragmentation fluorescence. However, since both species result in fluorescence emission from K-atom fragments the measured signal contains contributions from both species. Figure 5 shows alkali compound concentrations measured by photofragmentation fluorescence at flame equivalence ratios from 0.8 to 1.3 for seeding of KOH (a) and KCl (b) solutions of 0.5 M concentration.
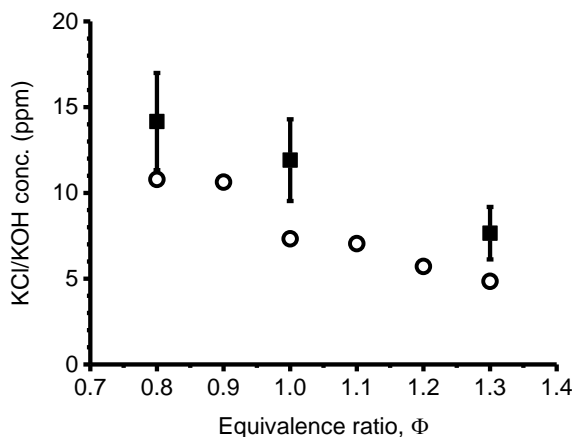
a)
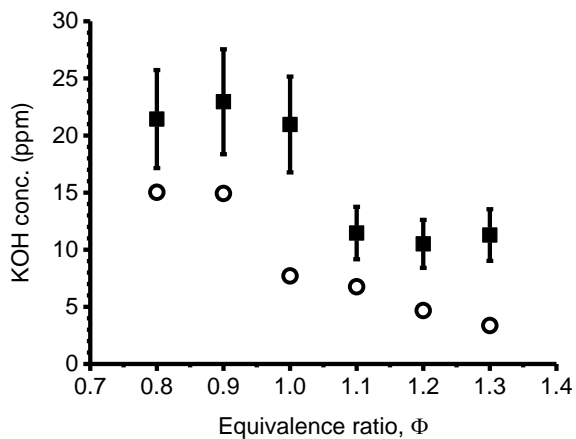
b)

Figure 5. Average post-flame concentration versus flame equivalence ratio measured using laser-induced photofragmentation fluorescence for seeding of a) 0.5 M KOH and b) 0.5 M KCl. Lower KOH/KCl concentrations are measured at fuel-rich conditions due to increased formation of K atoms. Circle symbols represents results from calculations of potassium species concentrations a) KOH and b) the sum KCl+40% KOH.

For the KOH-seeded flame, without chlorine present, the photofragmentation fluorescence signal only arises from KOH. Since seeding concentrations are the same and atomic potassium

levels for both cases are similar (cf. Fig. 3) the sum of KOH and KCl concentrations can be expected to be similar as well. However, the absolute signal obtained for KOH-seeding was lower than that of KCl-seeding by a factor of two and is attributed to differences in KOH/KCl photofragmentation process. While the energy of the 193 nm laser photons is sufficient for photofragmentation and generation of K atoms in the $^2P_{1/2}$ and $^2P_{3/2}$ states for KCl [16], resulting in fluorescence emission at wavelengths 766.5 and 769.9 nm, detected in the photofragmentation setup, the lower energy required for dissociation of KOH allows for formation of K atoms in higher excited states [16] returning to the ground state via transitions not detected. Thus the yield for fluorescence emission at 766.5 and 769.9 nm can be expected to be lower for KOH than for KCl.

In the flames seeded with 0.5 M solutions, KCl-seeding resulted in a signal a factor 2.2 higher than KOH-seeding at equivalence ratio Φ=0.8. Assuming KCl concentrations to be between 50% and 70% of the total KCl and KOH concentration, going from equal distribution to KCl-dominant conditions, the KOH laser-induced photofragmentation fluorescence yield can be estimated to be between 30% and 40% of the KCl yield. Using a value of 40% in the evaluation result in the concentration profile presented in Fig. 5a. Measurements in the KOH-seeded flame shows concentrations decreasing from 21 to 12 ppm when going from equivalence ratio Φ=0.8 to Φ=1.3. Calculations of KOH concentration for 15 ppm KOH seeding show a decrease from 15 to 3 ppm. The atomic potassium concentrations determined for the KOH-seeded flame 21 mm above the burner surface increased from 0.1 ppm to 2.6 ppm. Moreover, chemiluminescence profiles (cf. Fig. 3d) suggest K atom levels in the evaluation region of photofragmentation fluorescence, ~12-18 mm above the burner surface, to be higher than values of the TDLAS measurements by a factor of two, i.e. resulting in K atom levels of ~5 ppm at equivalence ratio Φ=1.3. Thus, the trends of experimental data and calculations are consistent and the potassium species concentrations are balanced within the estimated uncertainties of the experimental data.

Following the discussion above, the evaluated concentration in the KCl-seeded flame thus is expected to represent the concentration of KCl plus 40% of the KOH concentration and the results are presented in Fig. 5b. The concentration evaluated from the photofragmentation fluorescence signal decreases from 14 ppm at Φ=0.8 to 8 ppm at Φ=1.3 while corresponding calculated concentrations drop from 12 to 5 ppm. Measurements of atomic potassium by TDLAS and chemiluminescence as discussed above indicate that the concentration increase from 0.2 ppm to 4.4 ppm at these conditions whereas calculations give an increase from 0.1 to

9 ppm. Thus, the decrease in KOH/KCl concentrations and increase in K-atom concentrations is observed from experimental data as well as calculations.

Figure 6 shows alkali compound concentration versus equivalence ratio for 1.0 M (a) and 0.05 M (b) KCl seeding measured by laser-induced photofragmentation fluorescence.
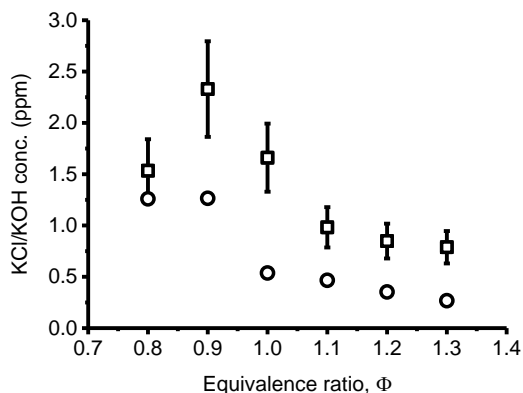
a)
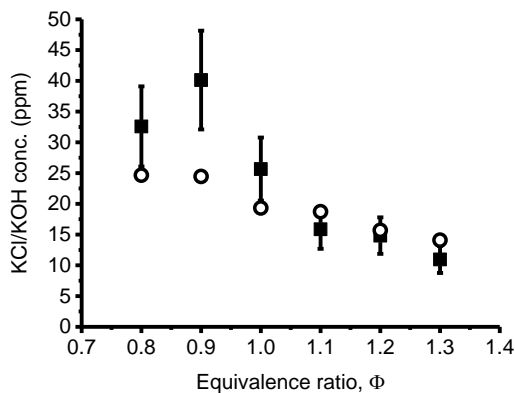
b)

Figure 6. KCl/KOH concentration versus flame equivalence ratio measured using laser-induced photofragmentation fluorescence for seeding with different potassium and chlorine levels. a) 1.0 M KCl seeding b) 0.05 M KCl seeding. Lower KCl/KOH concentrations are obtained under fuel-rich conditions. Circle symbols represents results from calculations of potassium species concentrations a) the sum KCl+40% KOH and b) KOH.

Following the previous discussion related to Fig. 4 and 5, for high KCl-seeding we expect KCl concentrations to be higher than KOH concentrations and KCl therefore the main contribution to the photofragmentation fluorescence signal and the evaluated concentration to mainly represent KCl. Seeding with 1.0 M KCl solution, cf. Fig. 6a, results in post-flame concentrations of 33 ppm at lean conditions decreasing to 15 ppm at $\Phi=1.0$ and 11 ppm at $\Phi=1.3$. The results from calculations, also discussed previously together with Fig. 4, decrease from 25 to 14 ppm. Better overall agreement between experiments and simulations were obtained for the absorption data presented in Fig. 4. For this method experimental data instead show higher values than simulations at lean to stoichiometric conditions, in particular for equivalence ratio $\Phi=0.9$, while agreement within the estimated experimental uncertainty is obtained at fuel-rich conditions. Figure 6a shows a decrease of 22 ppm for the measured potassium species and a corresponding increase is expected for K atom concentrations. Potassium atom concentrations obtained from TDLAS and chemiluminescence profiles, cf. Fig. 3a and 3d, indicate an increase from 0.4 to 9 ppm between equivalence ratios $\Phi=0.8$ and $\Phi=1.3$. The 9 ppm increase in atomic concentration is approaching the uncertainty of the experimental data, represented by the error bars in Fig. 6a, so the balance of potassium species could still be fulfilled. The equilibrium calculations give K atom concentrations increasing from 0.1 ppm to 14 ppm.

At 0.05 M KCl-seeding, resulting in chlorine levels of around 1 ppm, equilibrium calculations as well as previous flame studies indicate KOH to be the dominant post-flame potassium compound. For example, simulations of hydrogen and propane flames seeded with sodium chloride, presented by Schofield [14], indicate negligible amounts of alkali chloride compared with hydroxide and atom levels at chlorine concentrations below 10 ppm. Thus, data measured at this seeding level can be expected to mainly represent KOH. Photofragmentation data measured for 0.05 M KCl-seeding, presented in Fig. 6b, also show a decrease in alkali compound concentration with equivalence ratio from 1.5 to 0.8 ppm. Calculated potassium hydroxide concentrations for 1.5 ppm KCl, mimicking the experimental condition, decrease from 1.3 to 0.3 ppm. For comparison K-atom concentrations derived from experimental data increase from 0.002 to 0.4 ppm, cf. Fig. 3b and 3d, while calculations result in an increase from 0.01 to 1.2 ppm. The experimental results show a 0.7 ppm decrease in KOH concentration and an increase in K atom concentration of 0.4 ppm, However, also in this case these changes are in agreement within the estimated experimental uncertainties indicated by the error bars.

For flame-seeding with KOH as well as KCl, alkali-compound levels decrease with increasing flame equivalence ratio whereas atomic potassium shows an opposite trend. While the transport

times are sufficient for establishing equilibrium conditions in the lean flames this is likely not the case for the stoichiometric and fuel-rich conditions. Nevertheless, also when chemical equilibrium has been established, calculations show lower concentrations of KCl and KOH and correspondingly higher concentrations of K atoms. As mentioned previously, alkali (sodium) concentrations in premixed sodium-seeded propane and hydrogen flames has been presented by Schofield [14], showing trends in agreement with the observations from Figs. 3, 4, and 5.

For the lean flame of 1.0 M seeding the atoms concentration of 0.02 ppm represents a very small fraction of the total alkali content, on the order of 0.05%, whereas the 4.4 ppm at equivalence ratio Φ=1.3 would correspond to 12%. In sodium-seeded propane flames simulated by Schofield [14] atomic sodium constituted around 10% or less of the total alkali content at equivalence ratio Φ=0.8 while at a fuel rich Φ=1.2 condition the Na atom represented around 80% of the total alkali content. The results of Schofield were however, obtained for flame temperatures of around 2000 K, i.e. higher than the temperatures at 1400-1500 K measured for the flames in this study. As high temperature favors atomic species formation and higher equilibrium concentrations approaching the levels from the simulations of Schofield are plausible.

Quantitative measurements of potassium species by optical diagnostics in seeded methane-air show agreement within estimated experimental uncertainties with model predictions. Further studies to validate the mechanism in flame simulations can be pursued, however refined diagnostics is required to obtain more accurate data for detailed investigations. This would include methods to clearly distinguish between KCl and KOH, for example by means of absorption spectroscopy extended to wavelengths above 280 nm where KCl shows negligible absorption [18]. Alternatively, photofragmentation laser-induced fluorescence using different dissociation wavelengths could allow for selective measurements of KOH and KCl [16]. The high concentrations of K-atoms result in saturated absorption when probing the strong potassium D_2 line and measurements instead probing weaker transitions, for example at 405 nm would enable atomic measurements also at high levels of flame seeding. Detailed validation would also benefit from more accurate temperature measurements using either Coherent anti-Stokes Raman Spectroscopy or two-line atomic fluorescence.

Conclusion

Quantitative data on potassium species concentrations obtained from non-intrusive measurements in potassium-seeded premixed methane-air flames have been presented. Observed potassium species concentrations at different equivalence ratios can be compared with results from calculations using a mechanism for potassium chemistry in a homogeneous reactor model. The burner and diagnostic methods employed thus present an experimental configuration for further detailed studies for validation of alkali combustion chemistry models as well as investigations of phenomena related to alkali in combustion, such as sulphation and catalytic effects.

Acknowledgements

Appendix A

Scanned spectra from tuneable diode laser absorption measurements in the flames, showed the potassium D_1 line at 769.9 to be fitted by a Voigt profile with a Gaussian width of 0.11 cm^{-1} and a Lorenzian width of 0.05 cm^{-1}. An average integrated absorption cross section for the two 4^2P transitions was determined to be $8.36 \cdot 10^{-6}$ cm^{2}s^{-1} which distributed over the measured line profile resulted in a peak absorption cross section of $1.6 \cdot 10^{-11}$ cm^2. Using this quantity, a trapping factor, T, for the photofragmentation fluorescence signal fraction of intensity absorbed is given by Eq. A1

$$T = \frac{\int I_t d\nu}{\int I_0 d\nu} = \frac{\int I_0(\nu) e^{-\sigma(\nu) N_K l} d\nu}{\int I_0 d\nu} \qquad \text{(A1)}$$

In Eq. A1 I_0 represents the input intensity and I_t the transmitted intensity, both integrated over frequency ν to obtain total intensity values. The left-hand ratio thus represents the fraction of intensity absorbed, which is determined by the Beer-Lambert law introduced in the nominator of the right-hand ratio. The exponential factor includes the absorption cross section, σ, the potassium atom concentration N_K, and the absorption path length l.

Figure A1 shows the transmitted intensity I_t for the K-atom emission at three conditions. For the case of negligible absorption, the intensity shows a single-peak profile plotted as solid curve and representing the unaffected K atom lineshape. At moderate absorption, represented by the dashed intensity profile, the intensity is attenuated while the shape of the spectral line is preserved. At strong absorption, the transmitted intensity at the center of the spectral line is stronger attenuated resulting in symmetric dual-peak lineshape. Under such conditions transmission of light is mainly obtained at the wings of the line profile which at high concentrations in the flame eventually results in a dependence of $N^{1/2}$ for the K atom flame chemiluminescence [22, 23].

Using potassium atom concentrations determined from TDLAS measurements and extrapolation as values for N_K together with an assumed path length l of 1 cm for passage to the detector in the central region of the flame, trapping of the photofragmentation fluorescence signal was calculated by integration over the attenuated line profile.
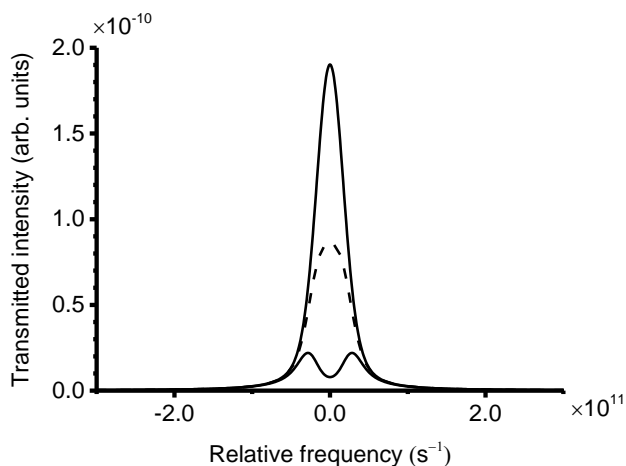

Figure A1. *Calculated transmitted intensity for 4^2P K atom emission at negligible absorption (solid single peak), moderate absorption (dashed single peak), and strong absorption, (low dual peak). The strong attenuation at the line center confines emission the wings of the spectral line resulting in a sub-linear dependence on K-atom concentration for the flame chemi-luminescence.*

References

[1] F.J. Frandsen, Utilizing biomass and waste for power production - a decade of contributing to the understanding, interpretation and analysis of deposits and corrosion products, Fuel, 84 (2005) 1277-1294.

[2] J.M. Johansen, J.G. Jakobsen, F.J. Frandsen, P. Glarborg, Release of K, Cl, and S during Pyrolysis and Combustion of High-Chlorine Biomass, Energ Fuel, 25 (2011) 4961-4971.

[3] H.P. Nielsen, F.J. Frandsen, K. Dam-Johansen, L.L. Baxter, The implications of chlorine-associated corrosion on the operation of biomass-fired boilers, Prog Energ Combust, 26 (2000) 283-298.

[4] S. van Loo, J. Koppejan, The handbook of biomass combustion and co-firing, Earthscan, UK and USA, 2008.

[5] J.N. Knudsen, P.A. Jensen, K. Dam-Johansen, Transformation and release to the gas phase of Cl, K, and S during combustion of annual biomass, Energ Fuel, 18 (2004) 1385-1399.

[6] P. Glarborg, Hidden interactions - Trace species governing combustion and emissions, P Combust Inst, 31 (2007) 77-98.

[7] H. Kassman, J. Pettersson, B.M. Steenari, L.E. Åmand, Two strategies to reduce gaseous KCl and chlorine in deposits during biomass combustion - injection of ammonium sulphate and co-combustion with peat, Fuel Process Technol, 105 (2013) 170-180.

[8] A.J. Hynes, M. Steinberg, K. Schofield, The Chemical-Kinetics and Thermodynamics of Sodium Species in Oxygen-Rich Hydrogen Flames, J Chem Phys, 80 (1984) 2585-2597.

[9] W.A. Rosser, S.H. Inami, H. Wise, The Effect of Metal Salts on Premixed Hydrocarbon Air Flames, Combust Flame, 7 (1963) 107-119.

[10] M. Slack, J.W. Cox, A. Grillo, R. Ryan, O. Smith, Potassium Kinetics in Heavily Seeded Atmospheric-Pressure Laminar Methane Flames, Combust Flame, 77 (1989) 311-320.

[11] B. Li, Z.W. Sun, Z.S. Li, M. Aldén, J.G. Jakobsen, S. Hansen, P. Glarborg, Post-flame gas-phase sulfation of potassium chloride, Combust Flame, 160 (2013) 959-969.

[12] W.Q. Li, L.Y. Wang, Y. Qiao, J.Y. Lin, M.J. Wang, L.P. Chang, Effect of atmosphere on the release behavior of alkali and alkaline earth metals during coal oxy-fuel combustion, Fuel, 139 (2015) 164-170.

[13] P.E. Mason, L.I. Darvell, J.M. Jones, A. Williams, Observations on the release of gas-phase potassium during the combustion of single particles of biomass, Fuel, 182 (2016) 110-117.

[14] K. Schofield, The chemical nature of combustion deposition and corrosion: The case of alkali chlorides, Combust Flame, 159 (2012) 1987-1996.

[15] P. Monkhouse, On-line spectroscopic and spectrometric methods for the determination of metal species in industrial processes, Prog Energ Combust, 37 (2011) 125-171.

[16] R.C. Oldenborg, S.L. Baughcum, Photofragment Fluorescence as an Analytical Technique - Application to Gas-Phase Alkali Chlorides, Anal Chem, 58 (1986) 1430-1436.

[17] Z.C. Qu, E. Steinvall, R. Ghorbani, F.M. Schmidt, Tunable Diode Laser Atomic Absorption Spectroscopy for Detection of Potassium under Optically Thick Conditions, Anal Chem, 88 (2016) 3754-3760.

[18] T. Sorvajärvi, N. DeMartini, J. Rossi, J. Toivonen, In Situ Measurement Technique for Simultaneous Detection of K, KCl, and KOH Vapors Released During Combustion of Solid Biomass Fuel in a Single Particle Reactor, Appl Spectrosc, 68 (2014) 179-184.

[19] T. Leffler, C. Brackmann, M. Aldén, Z.S. Li, Laser-induced Photofragmentation Fluorescence Imaging of Alkali Compounds in Flames Applied Spectroscopy (accepted for publication), (2016).

[20] C. Forsberg, M. Broström, R. Backman, E. Edvardsson, S. Badiei, M. Berg, H. Kassman, Principle, calibration, and application of the in situ alkali chloride monitor, Rev Sci Instrum, 80 (2009).

[21] L. Hindiyarti, F. Frandsen, H. Livbjerg, P. Glarborg, P. Marshall, An exploratory study of alkali sulfate aerosol formation during biomass combustion, Fuel, 87 (2008) 1591-1600.

[22] C. van Trigt, T.J. Hollander, C.T.J. Alkemade, Determination of the a′-parameter of resonance lines in flames, Journal of Quantitative Spectroscopy and Radiative Transfer, 5 (1965) 813-833.

[23]   C.T.J. Alkemade, R. Herrmann, Fundamentals of Analytical Flame Spectroscopy, Adam Hilger Ltd., Bristol, U.K., 1979.

[24]   P. Davidovits, D.C. Brodhead, Ultraviolet Absorption Cross Sections for Alkali Halide Vapors, J Chem Phys, 46 (1967) 2968-2973.

[25]   D.E. Self, J.M.C. Plane, Absolute photolysis cross-sections for $NaHCO_3$, $NaOH$, NaO, NaO_2 and NaO_3: implications for sodium chemistry in the upper mesosphere, Phys Chem Chem Phys, 4 (2002) 16-23.

LUND
UNIVERSITY